Use of Micro-Mechanical Models to Study the Mastic Level Structure of Asphalt Concretes Containing Reclaimed Asphalt Pavement

by

Akshay Gundla

A Thesis Presented in Partial Fulfillment
of the Requirements for the Degree
Masters in Science

Approved November 2014 by the
Graduate Supervisory Committee:

B. Shane Underwood, Chair
Kamil Kaloush
Michael Mamlouk

ARIZONA STATE UNIVERSITY

December 2014

ABSTRACT

This study investigates the mastic level structure of asphalt concrete containing RAP materials. Locally sourced RAP material was screened and sieved to separate the coated fines (passing #200) from the remaining sizes. These binder coated fines were mixed with virgin filler at proportions commensurate with 0%, 10%, 30%, 50% and 100% RAP dosage levels. Mastics were prepared with these blended fillers and a PG 64-22 binder at a filler content of 27% by volume. Rheological experiments were conducted on the resulting composites as well as the constituents, virgin binder, solvent extracted RAP binder. The results from the dynamic modulus experiments showed an expected increase in stiffness with increase in dosage levels. These results were used to model the hypothesized structure of the composite. The study presented discusses the different micromechanical models employed, their applicability and suitability to correctly predict the blended mastic composite. The percentage of blending between virgin and RAP binder estimated using Herve and Zaoui model decreased with increase in RAP content.

DEDICATION

This thesis is dedicated to my parents, Revathi Gundla and Yoganand Gundla, who have taken innumerable sacrifices in every phase of my life and have provided me with moral support and guidance throughout my academic career. Without their love, affection and support I would not be here.

ACKNOWLEDGMENTS

First and foremost, I would like to express my gratitude to my advisor, Dr. Shane Underwood for providing me the opportunity to work with him. I am grateful to him for his valuable lessons on the fundamentals of asphalt rheology and teaching me how to operate the Dynamic Shear Rheometer. Dr. Underwood has shown me the importance of attending to details while performing experiments and analyzing the test data. His emphasis on minute details and consistency has helped me become an able researcher. His encouragement and support throughout the course of my masters has been a major driving force.

Secondly, I would like to thank the rest of my thesis committee, Dr. Kamil Kaloush and Dr. Michael Mamlouk for teaching me the important aspects of pavement engineering through my graduate studies.

I would like to acknowledge Dr. Waleed Zeiada for his valuable inputs throughout the course of my study.

I would to like thank Mr. Peter Goguen and Mr. Kenneth Witzcak for helping me with the logistics and setup of the test machinery in the laboratory.

I would like to explicitly thank Mr. Joe Phillips from AMEC for helping us conduct RAP binder extraction at their research facility. I would also like to thank Holly Frontier and FNF Construction for donating the materials for the present study.

I'd like to thank all my co-researchers in the Advanced Pavement Laboratory at Arizona State University for their support and assistance throughout this research. I'm

greatly appreciative of Padmini Gudipudi for her inputs on mix design and volumetric calculations for the non-RAP mixtures.

I would also like to thank my dear friend, Sneha Prabha Narra who has been a great source of inspiration and whose grit and determination I only hope to match someday.

Finally, I'd like to thank my family and my friends here and in India for their love and support especially during the difficult times.

TABLE OF CONTENTS

Page

LIST OF FIGURES viii

LIST OF TABLES xiii

CHAPTER

1 INTRODUCTION 1

1.1 Background 1

1.2 Study Objective 2

1.3 Scope of Work 2

1.4 Organization of Thesis 3

2 LITERATURE REVIEW 4

2.1 RAP Background 4

2.1.1 State of the Practice 5

2.1.2 NCHRP 9-12: Blending Study 7

2.1.3 RAP in Mix Design 8

2.1.4 Performance of Asphalt Concrete Mixtures Containing RAP 10

2.2 Physicochemical Interactions 18

2.3 Asphalt Mastics and their Importance 28

3 EXPERIMENTAL PROGRAM 33

3.1 Summary of Study Materials 33

CHAPTER Page

3.2 Phase I: Separation, Sampling and Characterization of RAP Stockpiles 36

3.2.1 Sampling and Separation 36

3.2.2 Material Characterization Tests 39

3.3 Phase II: Binder and Mastic Sample Preparation 43

3.3.1 Binder Sampling and Separation 43

3.3.2 Mastic Sample Preparation 44

3.4 Phase III: Rheological Tests on Binders and Prepared Mastics 50

3.4.1 Temperature and Frequency Sweep Tests 52

3.4.2 Controlled Strain Fatigue Tests 55

3.4.3 Repeated Stress Sweep (RSS) Tests 56

4 MICROMECHANICAL BASED EVALUATION OF RAP BLENDING 58

4.1 Introduction 58

4.2 Experimental Results 59

4.2.1 Temperature-Frequency Sweep 59

4.2.2 Controlled Strain Fatigue Tests 62

4.3 Micromechanical Modeling of Non-Modified and RAP Modified Mastics 85

4.3.1 Dilute and Empirical Models 85

4.3.2 Micromechanical Models 87

CHAPTER Page

4.3.3 Applications of Micromechanical Models to Non-Modified and RAP Modified Asphalt Mastics 95

4.4 Modeling of RAP Mastics using Herve and Zaoui Model 116

4.4.1 Hypothesized RAP Mastic Structure 117

4.4.2 Methodology for Model Implementation 120

4.4.3 Modulus Predictions from Herve and Zaoui Model 125

5 SUMMARY AND CONCLUSIONS 135

5.1 Summary and Conclusions 135

5.2 Future Work 138

REFERENCES 139

APPENDIX

A VOLUMETRIC CALCULATIONS FOR RAP MASTICS 145

B CALCULATION OF PERCENTAGE UNCOATED FILLER IN RAP FILLER 151

C CALCULATION OF PERCENTAGE VM AND RAP 100 in RAP 10, RAP 30, and RAP 50 153

LIST OF FIGURES

Figure Page

2-1: (a) RAP Aggregate and (b) Virgin Aggregate 4

2-2: Schematic of a Blending Chart Using Method A as Outlined in [5]. 24

2-3: Schematic of a Blending Chart Using Method B as Outlined in [5]. 25

3-1: Schematic of Study Materials and Experimental Matrix 33

3-2: Fillers Used in the Present Study 34

3-3: RAP Stockpile Bags as Procured From Field 37

3-4: Fine and Coarse RAP Millings. 38

3-5: Separation and Partitioning of Fine Millings RAP Stockpile. 38

3-6: Agglomerated RAP Aggregate Along with Virgin Aggregate of Similar Size 39

3-7: Schematic of Agglomerated RAP Aggregate Along With its Finer Constituents 40

3-8: Asphalt Binder/Mastic Sample in a 8mm Silicon Mold 44

3-9: AR 2000 EX Dynamic Shear Rheometer 52

3-10: Graphical Representation of Thermal Equilibrium Results at 10°C 54

3-11: Graphical representation of Thermal Equilibrium Results at 20°C. 55

3-12: Repeated Stress Sweep Loading History [32]. 57

4-1: Modulus Mastercurves of the Study Materials in log-log Space. 60

4-2: Modulus Mastercurves of the Study Materials in semi-log space. 61

4-3: Phase Angle Data for the Study Materials 61

4-4: An Example of Phase Angle Drop: RAP 30 at 5% Strain Level 63

4-5: Number of Cycles to Failure at 1.25% Strain Level. 65

Figure Page

4-6: Number of Cycles to Failure at 2.5% Strain Level. 65

4-7: Number of Cycles to Failure at 5% Strain Level. 66

4-8: Variation of |G*| and Phase Angle for RB at 1.25% Strain Level. 67

4-9: Typical Modulus Response of RSS Loading Group. 72

4-10: NLVE Response of the Study Materials (semi-log). 76

4-11: NLVE Response of Study Materials. 76

4-12: Damage Characteristic Curves for VM: (a) Linear Based; (b) Non- Linear Based. 78

4-13: Damage Characteristic Curve for RAM: (a) Linear Based; (b) Non-Linear Based. 79

4-14: Damage Characteristic Curve for RAP 10: (a) Linear Based; (b) Non-Linear Based.

..... 80

4-15: Damage Characteristic Curve for RAP 30: (a) Linear Based; (b) Non-Linear Based.

..... 81

4-16: Damage Characteristic Curve for RAP 50: (a) Linear Based; (b) Non-Linear Based.

..... 82

4-17: Damage Characteristic Curve for RAP 100: (a) Linear Based; (b) Non-Linear

Based. 83

4-18: Damage Characteristic Curve for RB: (a) Linear Based; (b) Non-Linear Based. ... 84

4-19: Series Spring Analog. 88

4-20: Parallel Spring Analog. 88

4-21: Generalized Self Consistent Scheme Model Schematic. 92

Figure Page

4-22: Predictions for RAP Modified Mastics at High Frequency Using Paul's Rule of Mixtures. 97

4-23: Predictions for RAP Modified Mastics at Moderate Frequency Using Paul's Rule of Mixtures. 98

4-24: Predictions for RAP Modified Mastics at Low Frequency Using Paul's Rule of Mixtures. 98

4-25: Predictions for VM and RAM at High Frequency Using Paul's Rule of Mixtures. 99

4-26: Predictions for VM and RAM at Moderate Frequency Using Paul's Rule of Mixtures. 99

4-27: Predictions for VM and RAM at Low Frequency Using Paul's Rule of Mixtures. 100

4-28: Verification of Hashin's Model for VM: (a) log-log space; (b) arithmetic space 102

4-29: Verification of Hashin's Model for RAM: (a) log-log space; (b) arithmetic space. 103

4-30: Verification of Hashin's Model for RAP 10: (a) log-log space; (b) arithmetic space. 104

4-31: Verification of Hashin's Model for RAP 30: (a) log-log space; (b) arithmetic space. 105

4-32: Verification of Hashin's Model for RAP 50: (a) log-log space; (b) arithmetic space. 106

Figure Page

4-33: Predictions for RAP Modified Mastics at High Frequency Using Hashin and Shtrikman's APG Model. 108

4-34: Predictions for RAP Modified Mastics at Moderate Frequency Using Hashin and Shtrikman's APG Model. 109

4-35: Predictions for RAP Modified Mastics at Low Frequency Using Hashin and Shtrikman's APG Model. 109

4-36: Verification of Christensen and Lo GSCS Model for VM: (a) log-log space; (b) arithmetic space. 111

4-37: Verification of Christensen and Lo GSCS Model for RAM: (a) log-log space; (b) arithmetic space. 112

4-38: Verification of Christensen and Lo GSCS Model for RAP 10: (a) log-log space; (b) arithmetic space. 113

4-39: Verification of Christensen and Lo GSCS Model for RAP 30: (a) log-log space; (b) arithmetic space. 114

4-40: Verification of Christensen and Lo GSCS Model for RAP 50: (a) log-log space; (b) arithmetic space. 115

4-41: Hypothesized Blended Structure of RAP Mastics, Applicable to RAP 10, RAP 30, and RAP 50. 119

4-42: Hypothesized Blended Structure of RAP 100. 120

4-43: Stage 1: Procedure for Calculation of Adsorbed and Non-Adsorbed Binder Stiffness and the Stiffness of Four Phase Asphalt Mastic [43]. 124

Figure Page

4-44: Stage 2: Procedure for Calculation of Composite Modulus of RAP Mastics and the Percentage of Blending. 125

4-45: Predictions for VM Using Herve and Zaoui model: (a) Adsorbed modulus fit; (b) VM fit..... 128

4-46: Predictions for RAM Using Herve and Zaoui Model: (a) Adsorbed modulus fit; (b) VM fit..... 129

4-47: Predictions for RAP 10 at Pb = 50% using Herve and Zaoui Model: (a) semi-log scale; (b) log-log scale. 130

4-48: Predictions for RAP 30 at Pb = 27% Using Herve and Zaoui model: (a) semi-log scale; (b) log-log scale. 131

4-49: Predictions for RAP 50 at Pb = 20% Using Herve and Zaoui model: (a) semi-log scale; (b) log-log scale. 132

4-50: Predictions for RAP 100 at Pb = 15% Using Herve and Zaoui model: (a) semi-log scale; (b) log-log scale. 133

4-51: Variation of Blending for Different RAP Mastic Dosages. 134

LIST OF TABLES

Table Page

2-1: Refined Virgin Binder Selection Criteria for RAP Mixes as Given in NCHRP 9-12 [5]..... 9

3-1: Schematic Showing the Mastic Type and Materials Present in Them. 36

3-2: Gradation of RAP Stockpiles. 40

3-3: Gradation of Burnt Fine and Coarse RAP Stockpiles. 41

3-4: Maximum and Minimum Stress Levels for the Loading Groups in RSS Test..... 56

4-1: Number of Cycles to Failure, for Test Materials at 1.25% Strain Level..... 64

4-2: Number of Cycles to Failure, for Test Materials at 2.5% Strain Level..... 64

4-3: Number of Cycles to Failure, for Test Materials at 5% Strain Level..... 64

4-4: The Values of C for block G-2 B-5 for the Study Materials. 74

4-5: The Proportions of VM and RAP 100 in RAP 10, RAP 30 and RAP 50..... 96

Chapter 1 Introduction

1.1 Background

Over 90% of U.S highways and roads are constructed using hot mix asphalt (HMA) [1]. As the country's infrastructure ages, these roads and highways have to be maintained and rehabilitated. Reclaimed asphalt pavement (RAP) is the term given to asphalt pavement materials that have been removed from an existing pavement structure during re-construction, re-surfacing and/or other utility/maintenance works and processed so that they can be incorporated into new asphalt concrete or be used as a granular base, subbase, embankment material, or fill material [1]. When properly crushed and screened the final product consists of high quality well graded asphalt coated aggregates. Pavement recycling became popular in the 1970's due to the high crude oil prices during the Arab oil embargo [1]. However, depleting raw materials, coupled with increased demand and limited supply and emphasis on sustainable infrastructure has necessitated use of RAP more now than ever before. Traditionally, the use of RAP in pavements has been restricted to a maximum of 15% [1]. The main concern among the contractors and the states with using higher dosage rates is the increase in stiffness of the mix that comes with the addition of RAP. This increase in stiffness makes the pavement rut resistant but also makes it more brittle and prone to cracking [1]. Past research [2] has emphasized the importance and influence of physicochemical interaction on the behavior of regular asphalt concrete mixtures. These influences are likely present in RAP mixtures as well albeit in a more complicated way. Recent research has supported this hypothesis and suggests that the difference in performance of non-modified and RAP modified asphalt

concrete mixtures to the possible difference in physicochemical interactions due to presence of RAP [3]. The hypothesis behind this thesis is that a better understanding of physicochemical interactions of RAP modified mixtures will provide more insight into the performance of these mixtures. The present research seeks to study these physicochemical interactions at the mastic scale due to relatively simpler interactions present in mastics when compared to the mixtures [4].

1.2 Study Objective

The main objective of the present study is to compare and model the mastic level structure of un-modified and RAP modified asphalt concretes using multiple phase micro mechanical models. Better understanding of the mastic level structures of these materials provides more insight into physicochemical interactions which contribute significantly to the performance of these mixtures [2], [4] .

1.3 Scope of Work

At the outset of this research no experimentally supported theory with quantified characterization existed for the structure of RAP modified mastics. Indeed the objective of the present work has been to develop such a theory. In light of the lack of a substantial preceding methodology to accomplish this objective, the present study focuses on a single asphalt binder, filler type and RAP source. Five RAP dosage levels, 0%, 10%, 30%, 50% and 100% were employed in the present study. A PG 64-22 binder obtained from Holly Frontier Refinery, Phoenix was used. The RAP materials were obtained from SR 87. Volumetric calculations were carried out and mastics were prepared commensurate with the RAP dosage level. Rheological experiments such as temperature

and frequency sweep tests, constant strain time sweep tests, and repeated stress sweep tests were carried out on these mastics. The same set of experiments were carried out on PG 64-22 asphalt binder and on binder extracted from RAP stockpile. Using the test results from temperature-frequency sweeps and the principle of time–temperature superposition, modulus mastercurves were developed. These results were employed to develop the proposed structural theory of RAP mastics. The results from time sweep and repeated stress sweep tests were finally used to assess the fatigue and nonlinear viscoelastic responses of these materials.

1.4 Organization of Thesis

This thesis is divided into five chapters. Chapter 1 provides the background and brief description of the work done in this research including the research objective and scope of work. Chapter 2 summarizes the literature review conducted in support of the current research study, which covers the topics of RAP modified asphalt concretes, physicochemical interactions, and mastics. Chapter 3 provides information about the materials used, sample preparation, and the rheological experiments and their procedures. Chapter 4 presents the experimental results and analysis, introduction to micro-mechanical modeling, and results from the different models developed. Chapter 5 presents a summary of main findings and conclusions of this research as well as the potential for future research.

Chapter 2 Literature Review

2.1 RAP Background

Researchers in the late 1960's found that materials present in old asphalt pavements, which were at the end of their life may still have some value and could be reused even when the pavements are at the end of their service life. These old pavements when removed by grinding and stored for later use became known as reclaimed asphalt pavements, or RAP. All RAP materials contain two valuable components: (a) aggregate and (b) the aged binder that coats these aggregates [1]. Samples of RAP and virgin aggregate are shown in Figure 2-1.

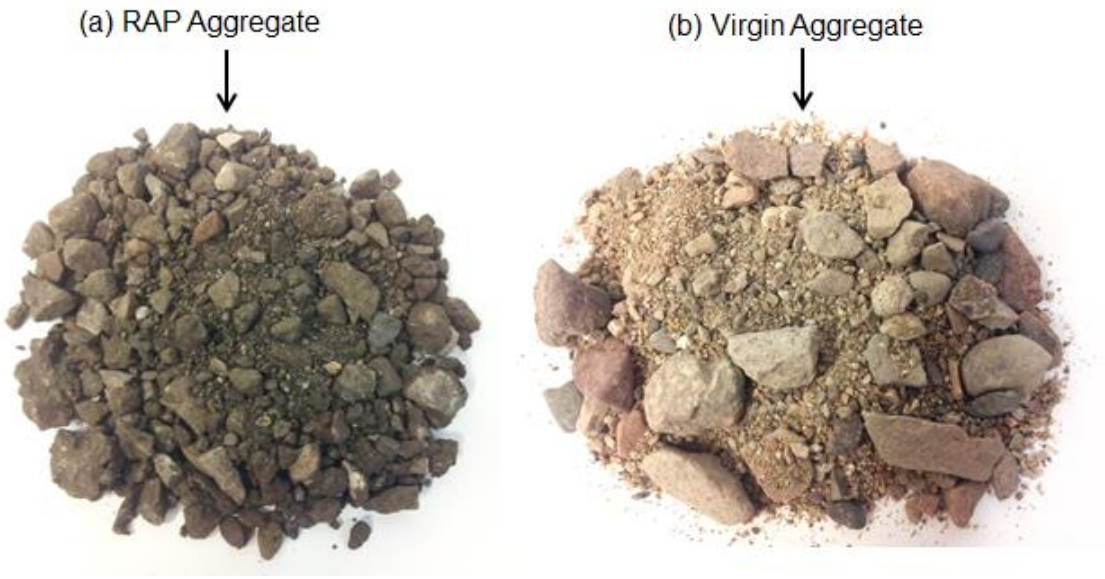

Figure 2-1: (a) RAP Aggregate and (b) Virgin Aggregate

Recognizing the value of RAP materials, contractors and agencies have made extensive use of these materials for decades. RAP has proven to be an environmental friendly and economically viable option [1] , [5] . In light of absence of guidelines for use of RAP in asphalt concrete pavements, FHWA formed an expert task group (ETG) in the

late 1990's to formulated interim guidelines for the use of RAP in Superpave mix design method [6]. The notable contribution of the ETG was its proposal of modification to virgin binder grade in RAP modified mixtures. These guidelines were further refined and developed under NCHRP project 09-12 by McDaniel et al. [5].

2.1.1 State of the Practice

In the early 1990's U.S Environmental Protection Agency in partnership with FHWA estimated that more than 90 million tons of asphalt pavements were reclaimed every year, of which 80% i.e. 72 million tons was used in construction related activities, including pavements. The remaining 20% i.e. 18 million tons was simply disposed by traditional means (landfilling, stockpiling etc.) [7]. As of 2007, the total yearly usage of RAP was estimated to be around 100 million tons, which was up from 72 million tons in the early 1990's. This statistic made asphalt binder the most frequently recycled material [1]. Of the 100 million tons used every year, about 40% goes into pavement related applications [1].

The amount of RAP to be incorporated in the mixes has always been a debatable issue. Historically, the percentage of RAP in mixes was limited to 10-15% owing to the high stiffness of aged binder in RAP mixes. Many authors have evaluated the aged binder properties and high PG grades for the extracted RAP binder, which confirms the high stiffness of RAP binder. Huang et al. [8] evaluated properties of RAP binder from two RAP sources in Manitoba and South Carolina. The authors reported that the continuous PG grades of the extracted binders were PG 91-28 and PG 95-18 respectively. McDaniel et al. [5] in their study, reported PG grades of binder extracted from three RAP sources as

PG 82-25, PG 82-24 and PG 89-15. Li and Gibson [9] reported that the high temperatures grade of two sources aged for 94 months(7.8 years) at the Federal Highway Administration's Accelerated Load Facility as 94.5 and 94.6°C. Similar high PG grade of PG 82 was found by Basueny et al [10]. Adding higher percentages of RAP in the mix increases overall stiffness of the mix [5],[9] and makes it more brittle, thus raising concerns of its adequacy to resist thermal and fatigue cracking [11]. As of 2011, the national average for the RAP content of mixes containing RAP was 19% (Source: Asphalt Recycling and Reclaiming Association) which was 7% higher than the national average of 12% in 2007 [1].

In 2007, a nationwide survey by the North Carolina Department of Transportation asked the following questions regarding RAP use: 1. How much RAP is permitted in the mixtures? 2. How much RAP is actually used? 3. What are the main roadblocks for greater usage of RAP? [1] Forty states responded to the survey.

The results showed that 40 states use up to 10% RAP in intermediate and surface layers. Thirty one states use up to 20% RAP in the surface layers and only two states would use up to 30% RAP in surface layers. The number is slightly higher for the intermediate layer, where about 25% of the respondents allowed up to 30% RAP. It is worth noting that even though very few states use a higher percentage of RAP, many have notified of the potential to use higher percentage of RAP. It is understood from the survey that many states are not willing to use higher percentages of RAP unless the blending mechanism or the physicochemical interactions between virgin and RAP binders are well understood.

Initial insight into the blending mechanism was provided by McDaniel et al.[5], as part of NCHRP 9-12, who investigated three blending theories namely, black rock theory, total blending theory, and partial blending theory. Black rock theory proposed that there is no interaction that takes place between virgin and RAP binder. Total blending theory suggests that the virgin asphalt and the RAP binder from the RAP aggregates blend completely. The partial blending theory is a hybrid of the two other cases and is a method in which RAP material is added to virgin aggregates at the plant. More information regarding the three theories is presented in the following section.

2.1.2 NCHRP 9-12: Blending Study

Before preliminary guidelines were developed for inclusion of RAP in the mixtures, RAP was added on the premise that all of the aged RAP binder would blend with the virgin binder. This theory is known today as the total blending theory. The extreme opposite hypothesis, known as the black rock theory, supposes that the RAP and virgin binders do not blend at all. Many questions have arisen over the years as to the accuracy of either of the theories and the precise factors that control the existence of any one situation between these two extremes.

To answer this question McDaniel et al. [5] performed comprehensive testing on mixtures, simulating the black rock case, total blending case and actual practice case. The black rock case was simulated by extracting the binder from the RAP aggregates and blending the recovered aggregates with virgin aggregates in proper proportion and then before mixing with virgin binder. The actual practice case samples were prepared as usual by adding the RAP with its coating intact to virgin aggregate and virgin binder. The

total blending samples, which assumed that RAP binder completely blends with virgin binder, were prepared by extracting RAP binder and blending it with virgin binder and then mixing the blended binder with recovered aggregates (aggregates recovered from RAP stockpiles by first extracting the reclaimed asphalt binder from the RAP materials) and virgin aggregates.

McDaniel et al. carried out experiments to evaluate the relative and absolute performance of each study case. At intermediate and high temperatures, samples were tested with frequency sweep tests in simple shear at constant height. At low temperature, indirect tensile creep and indirect tensile strength tests were performed. The authors concluded that at lower RAP content no significant differences among different cases of blending were observed. However, at higher RAP contents, the results from the black rock case were significantly different from the other two cases. No statistically significant difference was found between many of the actual practice and total blending results. This study also showed that RAP aggregate does not act as a black rock and that there exists some interaction between virgin and RAP binder. The extent of interaction is of primary importance and is not yet clearly understood.

2.1.3 RAP in Mix Design

As explained in previous sections RAP binder consists of two material components, aggregate and the aged binder that coats these aggregates. These two components must be considered while designing an asphalt mix containing RAP. The new Superpave mix design protocol developed as part of the NCHRP 9-12 [5]

incorporates RAP and its properties into mix design. The protocol recommends use of a tiered approach to incorporate RAP into the mixtures.

Earlier, the Superpave expert task group [6] developed draft guidelines for the use of RAP wherein they introduced the concept of grade bumping. The concept involves reduction of virgin binder grade to a grade softer that would be normally used for asphalt concrete mixes containing high RAP content. This bumping process was done to negate the negative impacts due to increased stiffness that is observed in high RAP mixes. Based on those draft guidelines, RAP can be used up to 15% without altering the virgin binder grade selected for a particular project location. The guidelines also suggest that at RAP contents of between 16 to 25% by total mix weight, the virgin binder grade should be reduced by one grade on the low and high temperatures. If more than 25% RAP is to be used, then blend charts are to be developed to determine the percentage of RAP to be used for a given virgin binder grade. The concept was refined in NCHRP 9-12 and is as presented in Table 2-1.

Table 2-1: Refined Virgin Binder Selection Criteria for RAP Mixes as Given in NCHRP 9-12 [5].

	RAP Percentage		
	Recovered RAP Grade		
Recommended Asphalt Binder Grade	**PG XX-22 or lower**	**PG XX-16**	**PG XX-10 or higher**
No change in binder selection	<20%	<15%	<10%
Select virgin binder one grade softer than normal (e.g., select a PG 58-28 if a PG 64-22 would normally be used)	20-30%	15-25%	10-15%
Follow recommendations from blending charts	>30%	>25%	>15%

The interpretation of the table is explained with the following example. For the recovered RAP binder, whose grade is PG XX-16, <15% RAP can be used without change in virgin binder grade, 15-25% RAP can be used by selecting a virgin binder one grade softer than normal and to use >25% RAP, blend charts must be developed to calculate the permissible percentage of RAP for a given virgin binder grade.

2.1.4 Performance of Asphalt Concrete Mixtures Containing RAP

In this section studies related to the performance aspects of RAP modified asphalt concrete mixtures are presented. The studies presented here evaluated the RAP mixtures for their modulus, fatigue performance, rutting potential and resistance to thermal cracking.

Shah et al. [12] investigated performance related properties of plant produced RAP mixtures. The authors conducted temperature-frequency sweep tests to study the influence of RAP on dynamic modulus. Indirect tensile strength (IDT) tests were conducted to determine the tensile strength of the samples at 0, -10, and -20°C. Subsequently the strength values at -10°C were used to calculate the critical cracking temperature of the mixtures. RAP dosage levels of 0%, 15%, 25% and 40% were added to virgin aggregate along with a virgin PG 64-22 binder. The results from temperature-frequency sweep tests indicate that addition of 15% RAP does not increase the dynamic modulus of the mix in comparison to control mix. In fact the modulus was about 26% lower than the control mixture. However, the addition of 25% and 40% RAP resulted in an increase of dynamic modulus compared to the control mixture. The largest increase in modulus was observed from the 40% RAP case. The authors also conducted two sample

t-tests to evaluate statistical significance among different RAP dosage levels. The authors found statistically significant difference in at least two of the three testing temperatures in all comparisons except for between the control and 25% RAP case. In this comparison, no significant difference was found at any of the three test temperatures.

The indirect tensile strength of the mixtures had a similar pattern as dynamic modulus test results. RAP dosage level of 40% had the highest strength followed by 25% RAP, control, and finally 15% RAP. Even in this case the 15% RAP case had a lower strength compared to the control mixture. Critical cracking temperature (*Tc*) was calculated for these mixes. Mixture with 40% RAP had the highest critical cracking temperature (-22.8°C) followed by 15% RAP (-23.3°C), 25% RAP (-25.6°C) and control (-28.9°C). The *Tc* values of 15% RAP and 25% RAP are surprising as we would expect the stiffer mix, 25% RAP to have a warmer *Tc* value.

Huang et al. [13] evaluated the laboratory fatigue characteristics of HMA mixtures containing RAP. The mixtures were evaluated at 0%, 10%, 20% and 30% of No.4 sieve screened RAP materials. One virgin aggregate (limestone) and two virgin binders (PG 64-22 and PG 76-22) were used in the study. The fatigue characteristics were evaluated through IDT tests, semi-circular beam (SCB) fatigue tests, and beam fatigue tests. Also, the authors evaluated the effect of long term aging on the performance of RAP modified asphalt concrete samples. In this regard, half of the test samples were long term aged before performance testing.

Results from the IDT test showed that an increase in the percentage of RAP resulted in an increase in the tensile strength for both aged and un-aged mixtures. Apart

from the tensile strength and tensile strain, toughness index (TI), a parameter used to describe the toughening characteristics in the post-peak region of the IDT test, was also employed to evaluate the fatigue behavior of the mixture. For a brittle material TI is zero and for a perfectly elastic material TI is equal to one. The author suggested that recycled mixtures would have a higher fatigue life based on the facts that increase in percentage of RAP resulted in more tensile strength gains, less tensile strength loss at failure and less decrease in post-failure toughness index (TI).

Results from SCB fatigue test also indicated that fatigue life increased with increase in RAP percentage for both un-aged and long term aged cases in most cases. The exception being 30% RAP in long term aged case, where the fatigue life decreased at lower stress levels.

Results from strain controlled bending beam fatigue tests also in general indicated a higher fatigue life for RAP modified mixtures for both un-aged and long term aged cases. However, for the un-aged mixtures, made with PG 76-22, the control mixture had the highest fatigue life. Overall, it can it concluded that the inclusion of RAP increases the stiffness, tensile strength and fatigue resistance of the mixtures.

A similar study [14] evaluated fatigue resistance by performing strain controlled beam fatigue tests. The authors used the ratio of dissipated energy change, RDEC, method to determine failure. The RDEC is the ratio of the change in dissipated energy between two neighboring cycles divided by the dissipated energy of the first cycle. A plateau value (PV), which is a nearly constant value of RDEC, is determined. This value represents the period in the test where there is a constant percent of input energy that is

being turned into damage. The authors used this value of PV to characterize fatigue life of HMA mixtures. For a given mixture type a lower PV corresponds to longer fatigue life. The authors also used the traditional fatigue characterization method, wherein a 50% reduction in initial stiffness is defined as failure.

The authors observed that when failure was characterized using the traditional method, the mixture containing higher RAP percentages showed more number of cycles to failure. However, when failure was characterized using RDEC method, it was observed that addition of RAP resulted in higher PV values, which corresponds to lower fatigue life. The authors concluded that based on this characterization method the addition of RAP reduces the fatigue life of the mixtures.

Recent research [9], has employed the simplified viscoelastic continuum damage (S-VECD) models to evaluate RAP fatigue performance. Li and Gibson [9] have employed the above stated S-VECD methodology to evaluate the influence of RAP, with known source history, on fatigue performance of RAP modified HMA mixtures. The RAP materials were milled from FHWA accelerated loading facility site after 94 months. Mixtures were prepared with 0, 20, and 40% RAP. The authors found that 0% RAP had the lowest dynamic modulus whereas 40% RAP had the highest. The modulus values for 20% RAP were between 0% and 40% RAP. The authors reported that the increase in modulus due to addition of 20% RAP ranged from 8% at coldest temperature/highest frequency to 125% at the warmest temperature/lowest frequency tested. The increase in modulus due to addition of 40% RAP ranged from 9% at coldest temperature/fastest frequency to 247% at warmest temperature/lowest frequency tested.

The fatigue testing was carried out in axial mode in an AMPT following the S-VECD direct tension cyclic fatigue test protocol. The authors developed the damage characteristic curve (C vs. S curve), which can be used to evaluate fatigue cracking even at conditions where the material was not directly tested. The failure for 0%, 20% and 40% RAP mixtures occurred when the pseudo stiffness reached 0.13, 0.18, and 0.21 respectively. A pseudo stiffness of 0.13 as in 0% RAP indicates that the material has resisted damage until its modulus reduced to 13% of its original value and failed subsequently after. The results obtained by the author follow an expected trend where stiffer materials are expected to show higher pseudo stiffness at failure. After obtaining the damage characteristic curve the authors simulated a pure strain control fatigue test using a strain range of 50 to 700 micro strains. The results from the simulations show that fatigue life decreases with increase in RAP dosage. The authors also calculated the endurance limit for the mixtures, and reported that increasing the RAP percentage from 0% to 20% to 40% reduces the endurance limit from 246 με to 191 με to 121 με respectively.

Apeagyei et al. [15] performed laboratory evaluation of rutting resistance of asphalt concrete mixes containing RAP. The mixtures were plant produced and contained 0, 10, 15, 20 and 25% RAP. Dynamic modulus and flow number tests were carried out to characterize the material viscoelastic response and rutting resistance of the mixtures. A total of 19 mixtures were tested of which, eight were surface mixtures with nominal maximum size of aggregate, NMSA, of 9.5mm, another eight were base mixtures with NMSA of 25mm and three stone matrix asphalt mixtures with NMSA of 12.5mm. The

authors used Virginia DOT specifications for the selection of binder grade. A PG 70-22 binder was specified for mixtures that contain less than 20% RAP and for mixtures that contain more than 20% RAP, PG 64-22 binder was specified.

Based on the dynamic modulus results, the authors reported that the increase in stiffness as observed in 10% and 15% RAP when compared 0% RAP was on expected lines. However, mixtures with 25% RAP showed modulus values similar to that from the with 0% RAP mixtures. The authors attributed this unexpected behavior to the softer binder grade that was used in the 25% RAP mixtures. The results from the flow number test indicated that mixtures with 10% and 15% RAP had significantly higher flow number than 25% RAP. This unexpected behavior is again attributed to the softer PG 64-22 binder used in 25% RAP mixtures and also to the observed decrease in effective binder content. The authors theorized that mixtures with lower effective binder content will have less asphalt binder for aggregate-aggregate binding and therefore will have less resistance to rutting.

Loria et al. [11] evaluated the moisture damage and thermal cracking resistance of HMA mixtures with high recycled asphalt pavement content (50%) at a field section in Manitoba, Canada. The study also included a comparative analysis in mix properties and performance between mixtures produced in laboratory and field produced mixtures. The moisture sensitivity of the control and 50% RAP mixtures was evaluated by performing unconditioned and moisture conditioned indirect tensile strength tests along with tensile strength ratio test at multiple freeze-thaw cycles. The authors evaluated mechanical properties of the mixtures by performing dynamic modulus tests and their resistance to

thermal cracking was assessed using thermal stress restrained specimen test (TSRST) after multiple freeze-thaw cycles.

Based on the dynamic modulus results, the authors reported that at a given freeze-thaw cycle the stiffness of the mixtures increased with increase in RAP content. Also it is noticed that stiffness of the mixtures reduced as they were subjected to freeze-thaw cycles. The authors reported that incorporation of 50% RAP increased the tensile strength of the mixtures, while similar strengths as control mixtures were obtained for mixtures with 15% RAP. Also, in general the tensile strength of laboratory produced mixtures had tensile strengths that were either similar or higher than the field produced mixtures. This, the author says is an indication of laboratory produced mixtures being stronger and more durable than corresponding field mixtures.

The results from TSRST test indicate that the fracture temperatures for mixtures with 50% RAP was greater than that from 0% and 15% RAP. Also, the authors reported that plant produced mixtures with 50% RAP content had higher fracture stress in both unconditioned and moisture conditioned scenarios, whereas lab produced mixtures had similar stresses as control mixtures. The authors believe that the fracture stress controls the spacing of thermal cracks once they occur and higher fracture stress corresponds to longer spacing of transverse cracks in the field. Based on author's theory it can be said that though the transverse cracks first appear in RAP modified mixtures, the spacing of cracks will be longer than control mixtures.

Huo et al. [16] conducted fatigue performance prediction for various North Carolina mixtures using the simplified continuum damage. Six mixtures as per NCDOT

specifications [17] were evaluated. Of these six mixtures, five of them also had their corresponding RAP mixtures. So, in total 11 mixtures were evaluated. The RAP content in each mixture was 15%. Tension-compression dynamic modulus tests with rest periods were performed on the mixtures at five temperatures (-10°, 5°, 20°, 40° and 54°C) and six frequencies (25, 10, 5, 1, 0.5 and 0.1 Hz). In general it was observed that the RAP mixtures show higher modulus than the corresponding non-RAP mixtures.

In addition, a controlled crosshead (CX) cyclic test was used for fatigue performance characterization. In this test the actuator displacement of the machine is programmed to reach a constant peak level at the end of each loading cycle. All CX tests were conducted at 10Hz frequency and fixed temperature. The test was performed at different strain levels and temperature conditions and the viscoelastic damage characterization was carried out. Damage characteristic curves were then developed for all the eleven mixture types. The authors opined that the fatigue performance of the mixtures cannot be compared just by looking at the positions in the damage characteristic curve as this would not account for the material's resistance to damage. In order to achieve such a comparison, the authors conducted fatigue test simulations for all eleven mixture types in both strain and stress controlled modes at 10Hz and 19°C. The relative vertical position of the fatigue simulation lines was then used to rank the fatigue performance of the mixtures. From, strain controlled simulations it was observed that the non-RAP mixtures had better fatigue performance than corresponding RAP mixtures. The authors also found that the mixtures with smaller NMAS performed better than the mixtures with a larger NMAS.

Presented below are the basic conclusions that can be drawn from the above described performance studies on RAP and non-RAP asphalt mixtures:

1. All studies show that the dynamic modulus of mixtures increases with increase in RAP content. The magnitude of increase is less at lower RAP percentages and increases with increase in RAP percentage.
2. The mixtures containing RAP have a higher tensile strength ratio than non-RAP mixtures and the magnitude of TSR increases with increase in RAP content.
3. The mixtures containing a higher percentage of RAP have warmer critical temperature, making them most susceptible to low temperature thermal cracking.
4. Fatigue characterization performed on mixtures subjected to strain controlled tests using traditional definition for failure i.e. failure at 50% reduction in initial modulus resulted in RAP improving the fatigue performance of the mixtures.
5. However, employing advanced fatigue characterization techniques such like simplified viscoelastic continuum damage method showed that in strain controlled tests the addition of RAP is detrimental to the fatigue performance of the mixtures.

2.2 Physicochemical Interactions

When discussing the addition of RAP into asphalt pavements, it is important to have an understanding of how the aged binder in RAP interacts with the virgin binder. Since the interacting mediums are different in structure as well as composition, the interaction between the two materials is both physically and chemically driven. Such interactions are called physicochemical interactions. The importance of these interactions

is underlined by the fact that the differences in performance between RAP modified and un-modified asphalt mixtures might be a result of these interactions [3].

The process of blending between virgin and RAP binders is an outcome of physicochemical interactions between virgin binders and the aged binder coating on the RAP materials [8]. Recognizing the importance of blending between RAP and virgin binders, research reports and papers have been published to understand the level of interaction between the two binders.

Until the late 1990's, RAP was used under the assumption that RAP binder interacts completely with the virgin binder. In other words, there exists 100% blending between RAP and virgin binder. However, as described previously NCHRP 9-12 [5], proved the assumption to be wrong and concluded that what actually exists a partial blending between the old and new asphalts.

Oliver [18] investigated the blending process by creating artificial RAP and by performing mechanical testing. In order to represent the field, a virgin HMA was aged, compacted and broken into pieces. This artificial RAP was blended with new virgin HMA and compacted again. The virgin and RAP modified mixtures were tested for laboratory fatigue and rutting performance. The results of laboratory testing showed that the RAP mixtures performed better than the virgin mixes in both fatigue and rutting. The improvement in rutting performance was expected, given the high stiffness of the artificial RAP but the improvement in fatigue behavior is against the general belief that higher stiffness leads to lower fatigue life. The author postulated that the unexpected results might be a consequence of improper blending between virgin and aged binder

which in turn might have occurred due to the formation of agglomerates of aggregates and filler, which makes virgin binder difficult to penetrate through.

Stephens et al. [19] developed an extensive testing program to evaluate the effects of blending. A total of 12 mixes, 11 RAP based mixes at 15% RAP content and one virgin mix were evaluated. The virgin mix consisted of virgin binder and aggregates recovered from RAP after burning in ignition oven. The main difference among the various RAP mixes was the difference in RAP preheating time prior to mixing. The times varied from zero to 540 minutes. Indirect tensile strength and unconfined compression were the tests used to evaluate blending. The authors observed that increase in preheating time increases the mix strength, which the authors believed to be an indication of blending.

Huang et al. [20] presented a study in which blending between virgin and RAP materials were studied through a process of staged extraction. RAP material used in the study was screened on No. 4 sieve and the material passing was added in three different RAP percentages 10%, 20% and 30%. In order to better distinguish between the RAP and the virgin aggregates after mixing, the virgin aggregates chosen were coarser than the RAP aggregates (retained on No. 4 sieve). RAP was mixed with virgin aggregates at 190℃ for 3 min, followed by a process of a four staged solvent extraction, representing four different layers of asphalt. The RAP particles thus formed a three layer composite in the blended mixture. The asphalt was recovered from the solvent using Abson recovery technique. The stiffness of the binder increased from outside layers to the inside. The results indicated that about 60% of total layer thickness, the inner layers, had properties

close to pure RAP binder, whereas the outer 40% of the binder blended with the virgin binder.

Al Qadi et al. [3] sought to determine the amount of residual binder in RAP. The authors conducted performance related tests on three mixes corresponding to 0%, 20% and 40% RAP. Four different blend theories were evaluated. Apart from the three blend theories mentioned in NCHRP 9-12 [5] , an additional case called (partial blending) was incorporated. This case is somewhat similar to the total blending case. The only difference being that in the present case 50% RAP binder is mobilized, compared to 100% mobilization in total blending case. The results from the study, confirmed the findings of McDaniel et al. [5].

The authors found that at low RAP contents, results from performance tests of all the blend theories were statistically similar but at high concentrations results of black rock theory was statistically different from other blend theories. This study essentially confirms the presence of partial blending between RAP and virgin binders. The author also found that no additional total binder was needed by RAP modified mixes to achieve densities similar to no RAP mixes. The author opined that this might be because the RAP binder has combined with the virgin binder to a high extent.

This study went on to check this theory by performing dynamic modulus tests on the mixtures. Based on the above mix design results, it would be expected that the dynamic modulus values for actual practice case would be similar to the total blending case (100% working binder). If less than 100% blending occurs then the modulus values for actual practice would be lower than those have 100% working binder. But the author

found that dynamic modulus values of actual practice samples were higher than 100% working binder case. The author theorized that the asphalt-aggregate interface in the actual practice samples is not well defined. Due to this the asphalt material at the aggregate interface is stiffer than the remaining binder. The author attributed this increased stiffness to the selective absorption of binder into the aggregate which forms a stiff layer of binder on the aggregate surface. Aged RAP in actual practice case already contains this stiff layer of binder which is absent in mix prepared under 100% working binder case. The explanation provided by the author emphasizes the importance asphalt-aggregate interface in RAP modified asphalt concretes and provides a basis for studying the mastic level structure as a means to better understand interactions between virgin and RAP binder.

Many authors have also looked into interaction properties of virgin and RAP materials by evaluating pure virgin binder- RAP binder blending [5],[8],[21]-[23]. Presented below are the studies which are distinct and convey the importance of knowing the properties of the blended binder.

One of the most significant contributions of the NCHRP 9-12 project by McDaniel et al. [5] was their development of blend charts. It should be recalled that development of blend charts were necessitated to incorporate high percentage of RAP into the mixtures. The primary purpose of the blend charts was to arrive at a relationship between PG grade of virgin binder and the percentage of RAP to be used in the mixture. McDaniel et al. proposed two methods for the development of blend charts.

- Method A : Blending at a known RAP percentage (virgin binder grade unknown)

- Method B : Blending with a known virgin binder (RAP percentage unknown)

Both methods first require an assumption of the required blended binder grade. Method A requires determination of the properties of recovered RAP binder at high, intermediate and low critical temperatures. High, intermediate and low temperatures here refer to those in the SHRP binder performance grading protocol. Since the percentage of RAP is known, the critical temperature of virgin binder at all the three above mentioned temperatures can be known using Equation (2.1) . Use the high and low temperature grade to determine the virgin binder grade to be used. An example of the blend chart using method A is presented in Figure 2-2.

In this example outlined in [5], the percentage of RAP to be used is known as 30% and the desired blended binder grade is PG 64-22. The critical high temperature of RAP binder is known as 86.6°C. Based on these values, the blend chart is constructed and extrapolated to 0% to find the virgin binder grade. The $T_{critical}$ value at 0% is 54.4°C, so the virgin binder to be used should have a high temperature grade of 58. Similar analysis should be carried out at critical low temperature to find the low temperature grade of the virgin binder.

$$T_{Virgin} = \frac{T_{Blend} - (\%RAP \times T_{RAP})}{(1 - \%RAP)} \tag{2.1}$$

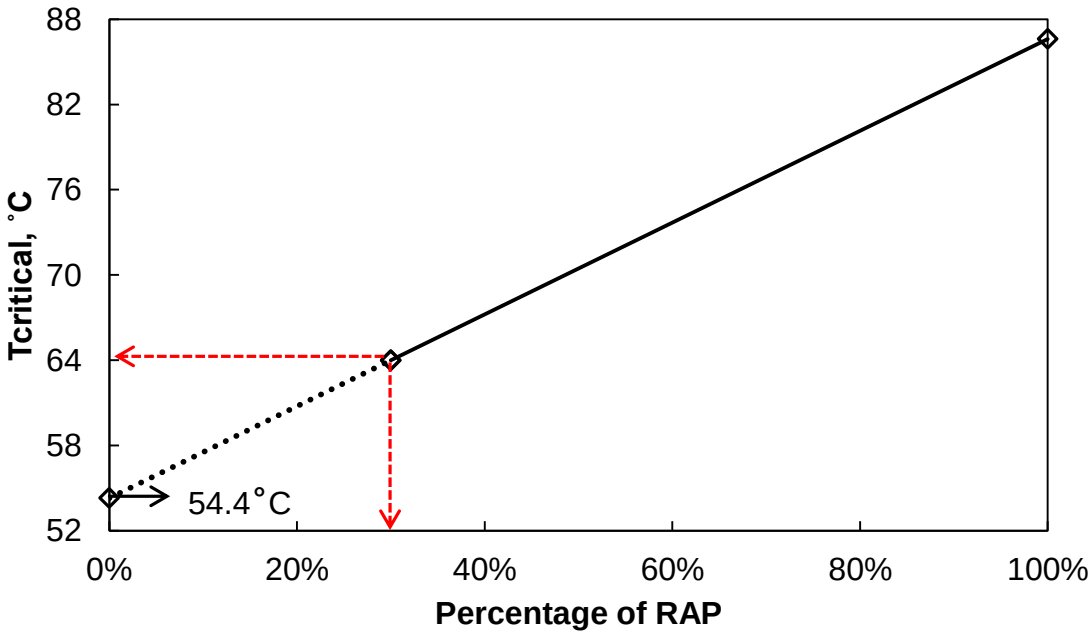

Figure 2-2: Schematic of a Blending Chart Using Method A as Outlined in [5].

Method B requires determination of properties of both virgin binder and recovered RAP binder at high, intermediate and low temperatures. The amount of RAP to be added can be calculated using Equation (2.2). It should be remembered that the RAP percentage obtained here is the minimum percentage of RAP that can be used based on assumption of blended binder grade. In order to arrive at the maximum percentage of RAP that satisfies the assumed blended binder grade, we have to find the RAP percentage at one PG grade higher than the assumed blended PG grade. This now gives the range for the percentage of RAP to be incorporated in the mix. An example of the same is presented in Figure 2-3. In this method, the virgin and RAP binder critical high temperatures are known as 60.5˚C and 86.6˚C respectively. It is desired to have blended binder which is PG 64-XX (i.e. $T_{critical}$ between 64˚C and 70˚C). Using this info, the

range of RAP binder to be used in order to achieve a blend which is PG 64-XX is estimated as 14% to 36%.

$$\%RAP = \frac{T_{Blend} - T_{Virgin}}{T_{RAP} - T_{Virgin}} \tag{2.2}$$

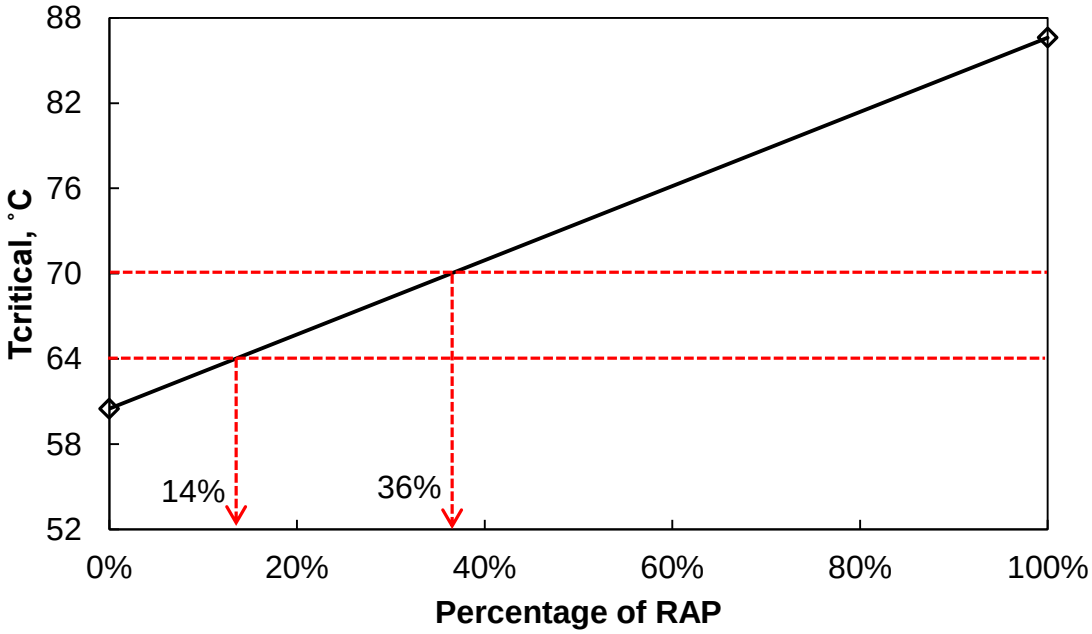

Figure 2-3: Schematic of a Blending Chart Using Method B as Outlined in [5].

In order to determine the presence and amount of RAP material in asphalt concrete mixture Buttlar et al. [23] used a micromechanics based approach. The authors theorized that if there was any RAP material present in the mixture then the binder recovered from this mixture would have a modulus value in between RTFO aged virgin binder and RAP binder recovered from the same RAP material.

The hypothesized procedure for determination of RAP binder depends on the complex modulus values of RTFO aged virgin binder, recovered binder from the RAP modified mixture and the recovered RAP binder from the RAP material used in the

mixture. The basis of the procedure was that if the trend followed by virgin binder- RAP binder blends at varying RAP binder concentrations can be predicted then the RAP binder concentration in the mixture can be back calculated from the trend established.

Various micromechanical models were evaluated to establish this trend in order to back calculate the RAP amount in the mixture. Virgin binder- RAP binder blends at 0%, 15%, 30%, 45% and 100% RAP binder concentrations were prepared and their corresponding modulus values were calculated. Using the same concentrations, trends were developed using the micromechanical models. The model that closely matches the experimental and the simulated data was selected for further evaluation. A single point calibration was then carried out by using the modulus value of a blended binder prepared in laboratory at a known RAP binder concentration. Binders from different RAP mixtures were then extracted and the model was used to predict the RAP binder amount. The authors reported that any prediction within +/- 10% of the actual RAP binder amount that was present in the mixture is considered acceptable for QA purposes. It should be noted that the RAP binder concentration obtained through this procedure is based on total binder amount. The conversion of the same into percentage RAP used in the mixture can be done using simple mathematical calculations.

Huang et al. [8] carried out a study on virgin binder-RAP binder blends in order to evaluate the compatibility between RAP and virgin binders. SHRP asphalts, AAA-1 and AAC-1 which are both chemically and physically different were used as virgin binders for the study. The binders had a continuous PG grade of PG 61-33 and PG 69-33 respectively. These binders were mixed with extracted RAP binders at 15% and 50%

dosage levels. The authors evaluated physico chemical characteristics of these RAP binder blends. The author's objective was to investigate the interaction between virgin and RAP binders and how RAP binders influence physical properties of virgin binders. Authors extracted RAP binders belonging two different sources namely Manitoba and South Carolina which had continuous PG grades of PG 91-28 and PG 95-18.

The rheological properties of the all the binders in the study were measured at -20, 0, 20, 40, 60 and 80°C using 25 mm, 8 mm and 4 mm parallel plates in the Dynamic Shear Rheometer (DSR). Using the results obtained from the DSR tests at low and high temperature grades for RTFO aged AAA-1, AAC-1 and their blends. The authors found that addition of 15% Manitoba RAP binder to AAA-1 increase its PG high temperature grade from 61°C to 70°C and addition of 50% increased the grade to 78°C. The authors found a linear relationship between RAP binder percentage and measured high temperature grade for the blends. Upon addition of 50% Manitoba RAP binder the blend now has a PG grade that is 3 grades apart from the virgin AAA-1 grade. The authors reported similar trends with AAC-1 binder. But with AAC-1, 50% Manitoba RAP blend was only one PG grade apart from virgin binder. The authors do not present the blend results with South Carolina RAP binder but claim that the PG grade of 50% blend with this binder was four PG grades apart from virgin binder. Based on these results the authors report that different virgin binders will interact differently with different RAP binders.

The authors also provided experimental proof for the above statement by calculating the glass transition temperatures for the RAP binder blends and also

performing temperature modulated differential scanning calorimetry (TMDSC). The compatibility of virgin binders to Rap binders was established based on glass transition broadening. No significant glass transition broadening was found for RTFO aged AAA-1/South Carolina or AAA-1/Manitoba RAP blends. However, 75% blend of RTFO aged AAC-1/ Manitoba RAP and AAC-1/South Carolina RAP have glass transition broadening similar to RAP binder. This indicates that compatibility of RTFO aged AAC-1 with Manitoba or South Carolina RAP is not as good as RTFO aged AAA-1 with Manitoba or South Carolina RAP.

2.3 Asphalt Mastics and their Importance

Asphalt mastic is a composite made up of two components: (i) asphalt binder and (ii) aggregates smaller than 75 μm. These aggregate particles are commonly referred to as filler particles [24]. Historical data suggests that, there is no formal manner on how filler and mastic are defined. However, it is widely accepted that mastic is one characteristic scale larger than the pure asphalt binder [4]. It is regarded that asphalt mastic is the real binding agent in the bituminous mixture [24].

Filler particles play a major role in determining the properties and behavior of the asphalt mixture [2]. In general, the role of filler in asphalt mixture is known to be complex, having both physical and chemical significances. Filler, on one hand serves as an inert material for filling the voids between larger aggregates in the asphalt mixture [2]. On the other hand, because of its high surface area, other physical and chemical aspects such as surface texture, angularity, adsorption intensity, it behaves as an active material. Craus et al. [2] pointed out that these properties can in a significant way influence the

optimum binder content, durability, workability of the asphalt mixture. Craus et al. also pointed out that the geometric irregularities of the filler particles provide a potential to intensify the adsorption capacity of the filler at the filler-binder interface. The authors opined that this capacity is mainly a function of chemical properties and mineralogical composition and geometrical characteristics of the filler. Fillers with same mineral composition but different geometric characteristics such as roughness and angularity will have different adsorption capacities. Also, the fillers greater surface irregularity will have greater adsorption potential.

Anderson and Goetz [25] suggested that the reinforcement of asphalt binder by filler inclusions is a result of two factors (i) volume filling and (ii) physicochemical interactions between aggregate and the binder. The reinforcement in other terms refers to the observed stiffening from the binder scale to mastic scale. Researchers have also pointed out that the potential for stiffening depends upon various factors such as type of filler, size of the particles and concentration [25]-[26]. These factors along with other physicochemical properties at the filler bitumen interface such as geometric properties, surface characteristics, adsorption, and adhesion can have a direct influence on the stiffening potential, thereby the behavior of asphalt mixture [2].

Some of the early work on predicting the stiffening potential of the fillers was carried out by Rigden [27]. The author evaluated the effect of four different fillers and two binders. Rigden expressed filler concentration as a ratio of filler to binder by weight and established a relationship between viscosity of the mastic and the filler concentration. Due to the enormous change in viscosities from low to high concentration, the values

were expressed in logarithmic scale. The author found that log-viscosity increased at a fast rate with increase in concentration of the filler and finally reaches a stage when it is at a maximum and any further increase in concentration yielded variable results, which were lower than the maximum value. This decline in viscosity can occur because at higher concentrations, the inter particle contact will dominate any potential physicochemical interactions between filler and mastic. Also, the flow properties of the mastic will reduce and the material tends to transition from a viscous state to a plastic state. Due to this the overall viscosity will come down. The binder content at which maximum viscosity is achieved is termed as optimum binder content.

Although the results obtained for both binder types tar and bitumen were similar, the results were unique for each type of the filler. This can be attributed to the unique surface properties of the fillers. So in order to eliminate these differences, Rigden proposed to plot the relationships on volumetric basis. The concept of fractional compaction, which considered the packing properties of the fillers was introduced along with a method to measure the densely compacted volume and associated void content. . These voids now, are better known as Rigden voids [28] and are considered as an important parameter in predicting filler behavior. The test is used even today to account for the differences in filler characteristics and was most recently employed in NCHRP 09-45 [29]. The studies presented above underline the importance of filler and its characteristics and the impacts they have on the performance of asphalt mixtures.

From the above studies it can be concluded that the differences in behavior of mastics of various fillers is not just a function of its physical properties (shape, size etc.)

but also of the resulting filler-bitumen interactions (physicochemical). Researchers have hypothesized that the interaction between filler and asphalt binder changes the properties of the binder around the filler [30]. This adsorbed layer of binder around the filler will have the highest stiffness and its value will reduce as the distance increases and finally becomes equal to that of free asphalt when the influence of the filler reduces completely [31]. Similar observations were made by Underwood [32], who explained the concept in terms of increased stress levels in the proximity of the filler particle and its gradual reduction with increase in distance. Underwood also evaluated the effect of interaction of stress levels of two different particles as a way to predict the behavior of the mastics at high filler concentrations. The adsorbed layer of binder around the filler can have a significant impact on the rheological properties of the mastic.

From Section 2.2 it is known that blending between RAP binder and virgin asphalt binder is a physicochemical process. This binder based blending is known to occur at the surface of the RAP aggregates. Also, Delaporte [24] reported that the true material that coats the larger aggregates is not the binder but a combination of binder and filler i.e., mastic. So, it is important to understand the behavior of the mastic present on the surface of the RAP material in order to fully understand the physicochemical process of blending.

The studies [3], [5],[18]-[20] evaluate the process of blending on a mixture scale. In order to better capture the process of blending, the material being characterized should be isolated from any external effects that might have a diminishing influence on the process. In the case of mixtures, these external effects can be the effects of aggregate

interlock and air voids. Also research by Underwood and Kim [4] has shown that experiments with asphalt mastics can isolate the effects of physicochemical interactions in an asphalt concrete mixture from those of air void and aggregate interlock.

The present study looks into the mastic level structure of RAP and its interaction with virgin materials, binder and filler are studied. The methodology employed and the materials used in the study will be explained in the following chapter.

Chapter 3 Experimental Program

In this chapter the material sampling techniques, sample preparation methods and rheological testing procedures on the study materials are clearly explained. The study materials consisted of binders and mastics which include both non-RAP modified and RAP modified mastics. The rheological tests performed include, temperature-frequency sweeps, strain controlled time sweeps and repeated stress sweep tests. Figure 3-1 provides an overview of the experimental matrix and study materials. More details on this plan are presented in the following sections.

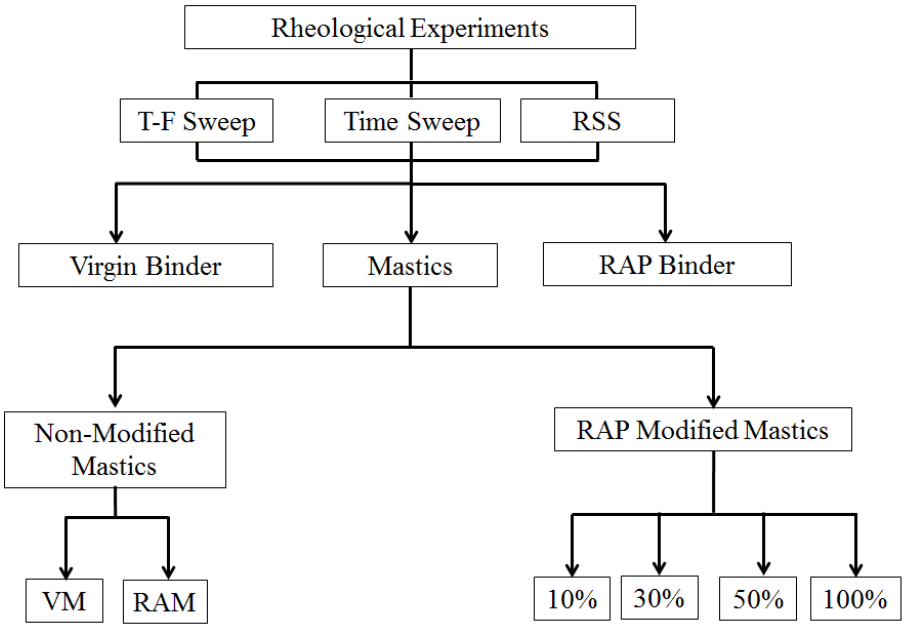

Figure 3-1: Schematic of Study Materials and Experimental Matrix

3.1 Summary of Study Materials

In order to evaluate the mastic level structure of RAP, mastics were prepared in the laboratory at different dosages of RAP. As mentioned in the previous chapter, mastics contain aggregate filler and binder. For this study three different types of filler have been included; virgin filler is obtained from a regular aggregate stockpile, RAP filler is the

passing #200 sieve material, obtained by sieving the RAP stockpiles, and recovered filler is the filler obtained by burning RAP material in an ignition oven and subsequently sieving it to obtain the passing #200 material. Recovered filler in the present study is used to represent the filler that might have lost its coating during the RAP handling process. The fillers used in the present study are shown in Figure 3-2.

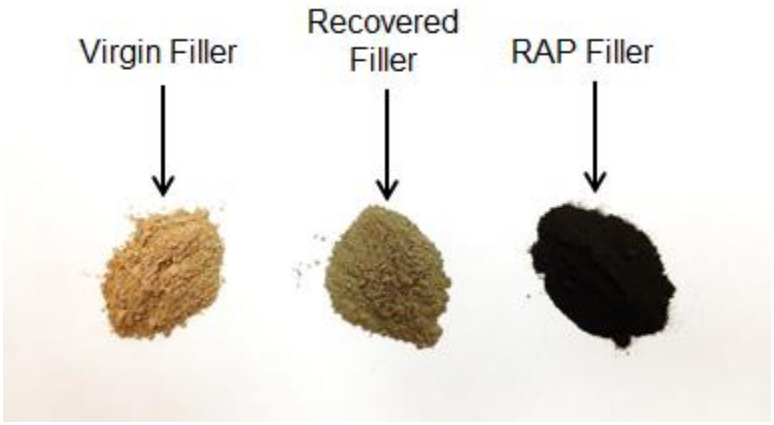

Figure 3-2: Fillers Used in the Present Study

For the present study all the materials used were locally sourced. The mix design used as the basis for the mastics is a 19mm NMSA typical to Arizona. The percentage filler content in the aggregate blend was 4.9%. The total binder content in the designed mix was 6%. The aggregate blend was modified to include RAP in accordance with test method ARIZ 833 as in the material testing manual [33]. The state of Arizona specifies its RAP as the percentage of the total aggregate in the mixture. As detailed below, the RAP aggregate was received in presorted fine and coarse millings and both were processed in the ignition oven before determining their gradation. It was also known from RAP supplier that the coarse and fine RAP stockpiles were to be blended at an overall ratio of 1 coarse to 2 fine. This RAP aggregate blend was incorporated into the total

blend and proportioned accordingly in order to arrive at 10%, 30%, 50% and 100% RAP aggregate blends. From the aggregate blend it is possible to know the individual contribution from each virgin, fine RAP and coarse RAP stockpiles in each mastic. It is seen that the filler contribution to the mastics from the coarse and fine RAP stockpiles are in a ratio 1:2.7. The blended aggregate gradations are presented in APPENDIX A.

In order to prepare material for the mastics the RAP filler material was blended with virgin filler and virgin binder at different RAP dosages. The RAP dosages used in the present study were selected to approximate 0, 10, 30, 50 and 100% RAP composition of a regular mixture. The mastic that represents a zero percent RAP dosage is referred to as the virgin mastic (VM), since there is only virgin filler and virgin binder and no RAP. The dosages 10% RAP (RAP 10) and 30% RAP (RAP 30) represent the minimum and maximum RAP dosages adopted by many states [1]. The dosage of 50% RAP (RAP 50) represents high RAP dosage and 100% RAP (RAP 100) represents full replacement of virgin aggregate. Volumetric calculations were carried out to estimate the proportion of virgin filler, RAP filler and virgin binder for each blend. These volumetric calculations, while not overly complex are somewhat involved and are presented in detail in APPENDIX A. As it will be discussed later, an important component of the overall RAP mastic system was found to be RAP filler that were initially uncoated. It was surmised that these particles were created during the crushing and recovery process. In order to study the behavior of this uncoated RAP filler, an additional case, called recovered aggregate mastic (RAM), was added to the test matrix. In addition to the mastics, virgin

binder and RAP binders were also tested. RAP binder (RB) for the study was recovered from the RAP aggregate using the rotavapor recovery process (AASHTO T 319) [34].

Table 3-1: Schematic Showing the Mastic Type and Materials Present in Them.

Mastic Blend Type	**Materials Contained**			
	Virgin Binder	Virgin Filler	Recovered Filler	RAP Filler
Virgin Mastic (VM)	✓	✓	×	×
Recovered Agg. Mastic (RAM)	✓	×	✓	×
10% RAP (RAP 10)	✓	✓	×	✓
30% RAP (RAP 30)	✓	✓	×	✓
50% RAP (RAP 50)	✓	✓	×	✓
100% RAP (RAP 100)	✓	×	×	✓

The experimental study presented in this document was divided into three distinct phases:

1. Separation, sampling and characterization of RAP stockpiles
2. Mastic sample preparation
3. Rheological tests on binders and the prepared mastics

3.2 Phase I: Separation, Sampling and Characterization of RAP Stockpiles

3.2.1 Sampling and Separation

RAP stockpiles received from the field were separated and sampled for better ease of handling in the laboratory and also to reduce the material to test size. The RAP materials for the study were provided by FNF construction. The material was sampled from SR 87 in Arizona. The material was procured in bags as shown in Figure 3-3. In the field the material was sieved over a ½" sieve and was separated into two stockpiles namely, fine millings and coarse millings as shown in Figure 3-4.

Figure 3-3: RAP Stockpile Bags as Procured From Field.

The coarse and fine millings were separately emptied onto large trays and were air dried in a controlled laboratory environment until the material reached a constant mass. Upon drying, all the fine millings RAP material was collected and mixed thoroughly to obtain homogeneity. The material was then partitioned into 10 parts and separated as shown in Figure 3-5.

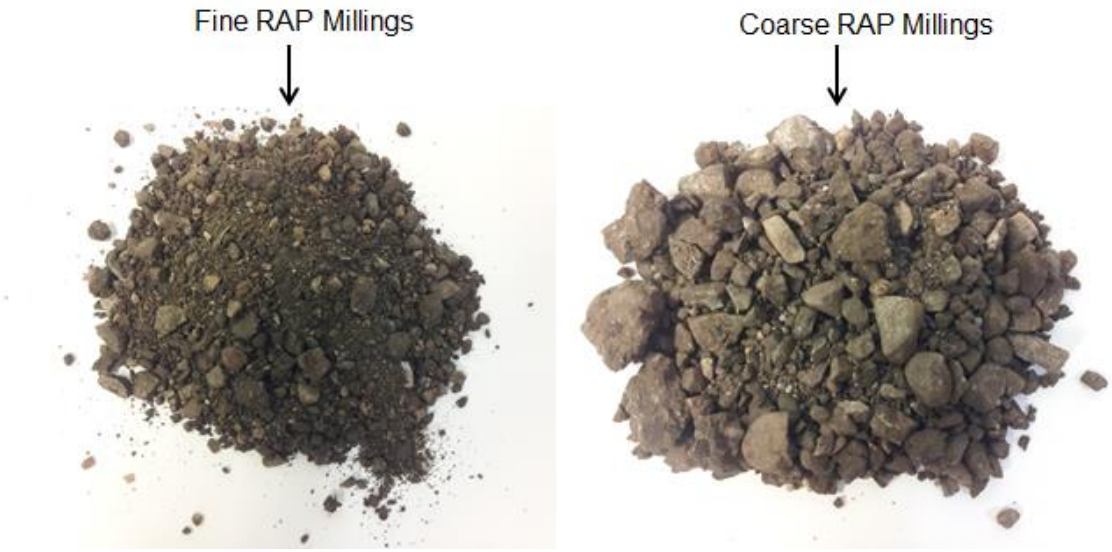

Figure 3-4: Fine and Coarse RAP Millings.

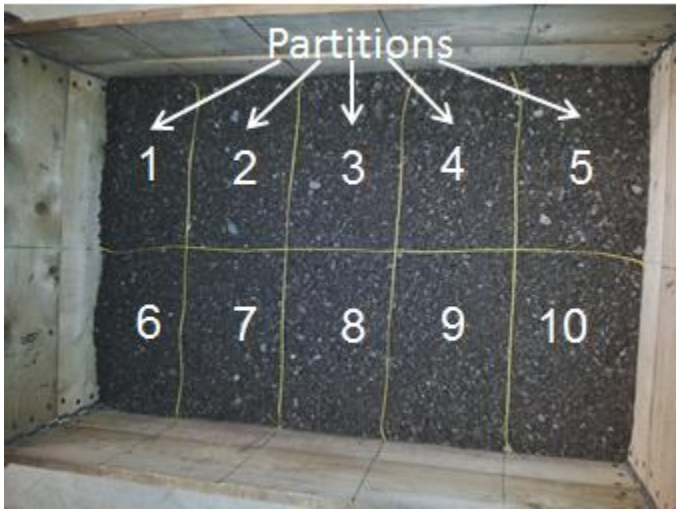

Figure 3-5: Separation and Partitioning of Fine Millings RAP Stockpile.

Subsequently the material in each portion was placed into 10 buckets. A similar process was carried out for the sampling of coarse millings. The material in the bucket was then split using a sample splitter into test sizes in accordance with AASHTO T 248 [35].

3.2.2 Material Characterization Tests

After reducing RAP aggregate to test size, the asphalt content was determined using the ignition oven method, AASHTO T 308 [36]. The asphalt content of the coarse and fine millings were 6.15% and 8.05% respectively. The RAP stockpiles, both coarse and fine were sieved to determine their respective gradations. However, this gradation should not be considered as the true gradation because RAP materials reclaimed from the field are agglomerates of aggregate with different sizes, as shown in Figure 3-6. For example in Figure 3-7, a RAP aggregate retained on ¾" sieve might actually be an agglomeration of several finer aggregates. In order to determine the true gradation of the aggregates, the RAP samples were subjected to burning in the ignition oven after which sieve analysis was conducted on these samples.

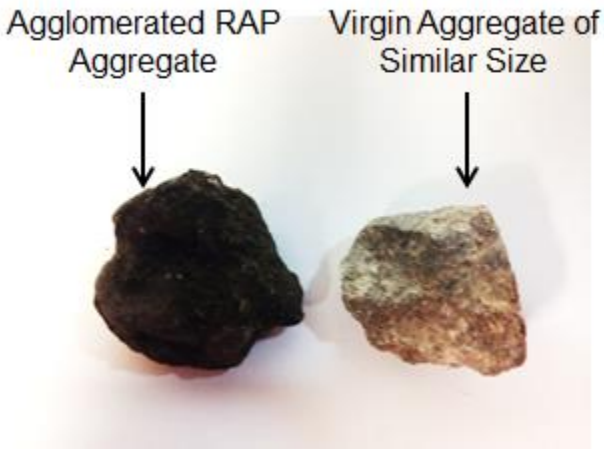

Figure 3-6: Agglomerated RAP Aggregate Along with Virgin Aggregate of Similar Size

Figure 3-7: Schematic of Agglomerated RAP Aggregate Along With its Finer Constituents

The stockpile wise gradation of both RAP and burnt RAP samples are presented in Table 3-2 and Table 3-3 respectively.

Table 3-2: Gradation of RAP Stockpiles.

Fine RAP Millings		Coarse RAP Millings	
Sieve Size	% Passing	Sieve Size	% Passing
1"	100.0	1"	98.6
3/4"	100.0	3/4"	94.6
1/2"	99.0	1/2"	78.7
3/8"	96.5	3/8"	63.3
#4	59.9	#4	28.4
#8	37.0	#8	16.1
#16	24.3	#16	10.6
#30	15.6	#30	7.3
#50	8.2	#50	4.3
#100	3.7	#100	2.1
#200	1.5	#200	0.9

Table 3-3: Gradation of Burnt Fine and Coarse RAP Stockpiles.

Burnt Fine RAP		Burnt Coarse RAP	
Sieve Size	%Passing	Sieve Size	%Passing
1"	100.0	1"	100.0
3/4"	99.8	3/4"	98.2
1/2"	99.3	1/2"	89.6
3/8"	98.3	3/8"	77.7
#4	73.8	#4	48.8
#8	52.7	#8	35.0
#16	40.8	#16	27.5
#30	31.4	#30	22.2
#50	21.3	#50	16.2
#100	13.3	#100	10.2
#200	8.8	#200	6.5

As the current study involves with mastics, the percentage of burnt RAP material passing #200 sieve (filler) was of prime importance. The percentage of filler in burnt coarse and fine stockpiles was 6.5% and 8.8% respectively. These values for filler contents were used as inputs in the volumetric calculations of the mastics which are presented in APPENDIX A.

RAP filler to be used for the preparation of the RAP mastics was obtained by sieving the RAP stockpiles and retaining the material passing #200 sieve. The asphalt binder content for the fillers in both the fine and coarse millings were determined by subjecting the fillers to a burn and measuring the mass before and afterwards. It would be difficult to determine the asphalt content of the fillers in the ignition oven as there is heavy air circulation with in the oven and particles might fly away. Instead, a one gram sample of coarse/fine RAP filler was measured and placed in a crucible, which was in turn placed into a conduction oven with no air flow. Trials were performed to determine

the temperature at which the burn had to be carried out. It was important to keep the burn temperature at a minimum as well as to completely burn the sample within a short period of time. It was observed that a temperature of 550°C-600°C was sufficient to burn the RAP filler sample within 30-35 min. At such high temperatures there is a possibility of loss of aggregate due to burning. In order, to account for this loss, one gram of virgin filler was placed in a crucible and was burned at similar conditions as the RAP filler. The observed loss in the virgin filler was about 1.43%. This loss was added to the burnt RAP filler in order to account for any loss of aggregate that might have occurred. The asphalt contents for coarse and fine RAP fillers after making this correction were 18.27% and 19.02% respectively. These numbers seem low knowing that the regular mix has approximately 50% binder in the mastic. It was hypothesized that this lower asphalt content might actually be a consequence of uncoated particles being present in the RAP filler which was burnt in the crucible. A trial and error method was followed to estimate the amount of these uncoated particles. The method is outlined in the APPENDIX B, and suggested that approximately 73.8% by weight of the RAP filler was uncoated.

As mentioned earlier in the chapter, recovered aggregate mastic was included in the test matrix to simulate the mastic that is formed from the uncoated filler in the RAP filler. This uncoated filler might be generated due to the agitation and crushing of RAP aggregates, which occurs during sieving. In order to build up material for this particular case, RAP stockpiles, both coarse and fine were burnt in the ignition oven and material was sieved to recover filler. The recovered fillers both coarse and fine were then blended

in a ratio of 1:2.7 as per the aggregate blend presented in the APPENDIX A. The blended aggregate was then used to prepare recovered aggregate mastic.

3.3 Phase II: Binder and Mastic Sample Preparation

3.3.1 Binder Sampling and Separation

The virgin binder for the present study was a PG 64-22 conventional binder sourced from Phoenix, AZ and was supplied by Holly Frontier Corporation. The binder was received in 5 gallon buckets. It was reduced to test size by heating the binder bucket at a temperature of 140°C and subsequently pouring into smaller quarter gallon containers. Prior to all testing, the sampling process was evaluated to ensure that it did not introduce substantial changes in the study materials. At various stages of the pouring process, binder was sampled into smaller 60 ml tins. The collected samples were subjected to temperature-frequency sweep tests in the DSR to make sure that the sampling process did not introduce any artificial aging. It was found that very minimal to no aging has occurred during the process. The virgin binder sample for mechanical testing was prepared by heating the quarter gallon tin to mixing temperature of 160°C and pouring into smaller 60 ml tins. The binder was heated to 160°C to maintain consistency with the mastic preparations for which the mixing temperature is 160°C. The sample tins were then stored in a cool and dry environment. Prior to testing, the sample tins were heated to a temperature of 135°C and poured into 8 mm silicon molds for DSR testing. It was found that a heating time of 20-25 minutes with a stir after 10 minutes is sufficient to make the sample fluidic. The sample tin was stirred once again immediately

prior to pouring into the silicon mold to ensure that all particles were in suspension while pouring into the mold.

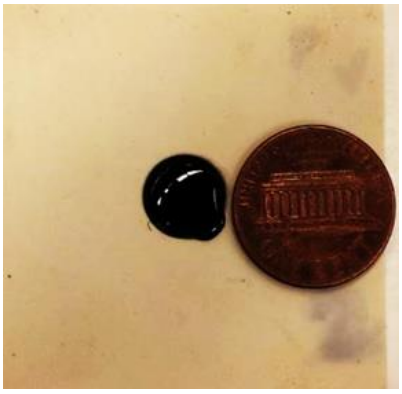

Figure 3-8: Asphalt Binder/Mastic Sample in a 8mm Silicon Mold

The RAP binder for the present study was recovered from the RAP aggregate using the process mentioned in AASHTO T 319 [34]. Tricholoroethylene (TCE) soaked RAP material was centrifuged to separate asphalt binder from the aggregates and then the solvent obtained from the centrifuge which contains both RAP binder and TCE was subjected to rotavapor binder recovery process to recover asphalt binder. In order to reduce the recovered RAP binder to test size, the binder had to be heated to temperatures as high as 170°C. This was expected, as the extracted RAP binder was really stiff and 170°C was sufficient to make the binder workable enough to pour into the DSR molds.

3.3.2 Mastic Sample Preparation

The mastic sample preparation can be classified into three categories based on the type of mastics being prepared:

a. Virgin Mastic (VM) and Recovered Aggregate Mastic (RAM)
b. Blended Mastics: 10%, 30% and 50% RAP mastics

c. Full aggregate replacement: 100% RAP mastic

3.3.2.1 Virgin Mastic (VM) and Recovered Aggregate Mastic (RAM)

The virgin filler for the virgin mastic was obtained from the aggregate blend that was locally sourced. As mentioned earlier, the mix design developed for the present study is a 19 mm NMAS typical to the state of Arizona. A brief description of the process and the steps and equations as shown by Underwood [32] are replicated below. From this mix design the volumetric concentration of the mastic could be calculated. Knowing the mixture gradation, the total mass of the absorbed binder can be calculated using Equation (3.1).

$$M_{ba} = \sum_{i=1}^{N} M_{ba,i} = \sum_{i=1}^{N} \left[\left(P_{i+1} - P_i \right) \left[\frac{1}{G_{sb,i}} - \frac{1}{G_{se,i}} \right] G_b \right] \tag{3.1}$$

where

M_{ba} = total mass of absorbed binder in mixture (grams),

$M_{ba,i}$ = mass of absorbed binder for aggregate retained on sieve i (grams),

P_{i+1} = percentage passing the sieve size immediately larger than the current sieve size,

P_i = percentage passing the current sieve size,

$G_{sb,i}$ = bulk-specific gravity of aggregate size i,

$G_{se,i}$ = effective specific gravity of aggregate size i, and

G_b = specific gravity of binder.

Usually the G_{sb} values are reported by stockpile type and not size, so it is assumed that all sizes within a given aggregate stockpile have the same specific gravity. The value of G_{se} is known for the entire aggregate blend and not for individual stockpiles. Here it is

assumed that the ratio of the volume of binder absorbed by the aggregate, V_{ba}, to the volume of total voids in the aggregate, V_v, is constant for all aggregate sizes. Absorption varies from size to size and is a function of the total voids in the aggregate. A smaller sized aggregate will absorb more binder but at the same time, the volume of voids relative to the total volume will also be high. Consequently, a larger sized aggregate will absorb relatively less amount of binder and at the same time the volume of voids relative to the total volume is also less. So, the assumption is reasonable.

The total aggregate in the mixture is assumed to be 100 grams. Since the asphalt content used in the mixture is known, the mass of binder can be calculated using Equation (3.2)

$$M_b = \frac{100 * \%AC}{100 - \%AC} \tag{3.2}$$

where

M_b = total binder mass (grams), and

$\%AC$ = asphalt content by total mixture mass (known).

Using Equation (3.1) and Equation (3.2), the total effective binder mass, M_{be} can be calculated by Equation (3.3) , and the effective binder volume, V_{be}, can be calculated by Equation (3.4).

$$M_{be} = M_b - M_{ba} \tag{3.3}$$

$$V_{be} = \frac{M_{be}}{G_b * \rho_{water}} \tag{3.4}$$

Since the percentage passing the #200 sieve and the mass of the aggregate blend is known, the mass of filler, M_{filler}, can be calculated. In this case since the mass of the aggregate blend is 100 grams, M_{filler} is equal to percentage passing as shown in Equation (3.5);

$$M_{filler} = P_{filler} \tag{3.5}$$

The volume of filler, as shown in Equation (3.6), can be calculated by dividing their mass by bulk density of filler

$$V_{filler} = \frac{M_{filler}}{G_{sb,\,filler} * \rho_{water}} \tag{3.6}$$

Combining Equations (3.4) and (3.6), the volume of mastics in the mixture can be determined. The volumetric concentration of filler in mastic can found using Equation (3.7). For the present mix design this value was determined as 27%.

$$V_{filler,mastic} = \frac{V_{filler}}{V_{filler} + V_{be}} \tag{3.7}$$

In order to determine the mass percentage of the filler to be added to the mastic, it was necessary to know the effective specific gravity of the filler. Its value for virgin filler was 2.63. Based on this value, the calculations were carried out and the mass percentages of filler and binder in mastic were 48.6% and 51.4% respectively. For preparation of the mastic the mixing temperature was 160°C. Accordingly, the filler was heated at 160°C for a minimum of 6 hours and binder was heated until it attained the mixing temperature of 160°C. The binder was then added to the filler in appropriate proportions and mixed

thoroughly using a mechanical blender. To be consistent with the process, a mixing time of 90 seconds was adopted across all the mastics. The prepared mastic was then poured into smaller 60 ml tins for future testing purpose. At the time of testing, the material in the 60 ml tins was heated to suitable temperature until fluidic enough to pour into the 8 mm silicon molds. The material was stirred half way through the heating process in order keep the particles in suspension. This heating temperature for virgin mastic was 135°C and the heating time was between 25 to 30 minutes. The material in the tins was stirred again immediately prior to pouring into the molds.

The RAM was prepared similar to the virgin mastic, but in this case recovered RAP filler was used instead of the virgin filler. The aggregate for RAM was obtained by burning RAP in the ignition oven. Both coarse and fine RAP stockpiles were burnt in the ignition oven and subsequently filler was sieved out from both of them and blended in a ratio of 1:2.7. The volumetric concentration of filler in RAM was maintained the same as virgin mastic i.e. 27%. In order to determine the mass proportions it was necessary to know the effective specific gravity of the recovered filler. In the case of virgin filler, the value was readily available from a previous study. So, in order to determine the effective specific gravity of the recovered filler, the following assumption, as shown in Equation (3.8), regarding the specific gravity of fillers was made.

$$\frac{\left(G_{se}\right)_{virgin}}{\left(G_{sa}\right)_{virgin}} = \frac{\left(G_{se}\right)_{recovered}}{\left(G_{sa}\right)_{recovered}} \tag{3.8}$$

The apparent specific gravities of both virgin and recovered fillers were determined by ASTM D854 to be 2.71 and 2.72 respectively. The G_{se} of the virgin filler was 2.63, and

so the G_{se} of the recovered filler was estimated to be 2.64. The mass proportions of filler and binder were then calculated for the preparation of the mastic. The mass percentages of filler and binder in mastic were 48.7% and 51.3% respectively. The mastic preparation was conducted in same way as the virgin mastic.

3.3.2.2 Blended Mastics

The blended mastics 10%, 30% and 50% RAP were prepared by blending virgin filler, RAP filler and virgin binder. The RAP filler here refers to the blend of coarse and fine RAP fillers which were blended in a ratio of 1:2.7. The proportion of each component was determined through volumetric calculations. The methodology of the calculations is presented in . In the blended mastics too, the volume of filler was maintained at 27%. The filler in the present case refers to virgin filler plus any filler from the RAP stockpiles. The weight of virgin binder and virgin filler were suitably adjusted to account for the aggregate and binder contribution from RAP filler. The preparation of mastics was mostly similar to the virgin mastic case, the only difference being the addition of RAP filler.

The pre-mixing conditions of virgin filler and virgin binder of blended mastics were similar to virgin mastic where the mixing temperature was 160°C. The RAP filler was heated for two hours prior to mixing in a forced draft oven set at 110°C. The temperature of 110°C was selected as it was the temperature at which RAP samples were conditioned for the actual practice case in NCHRP 9-12 project [5]. At the time of mixing, RAP filler was first added to virgin filler and mixed to achieve homogeneity. Subsequently virgin binder, accounted for the binder contribution from RAP filler, was

added and the material was blended using a hand held mechanical blender. The prepared mastic was then poured into smaller 60 ml sample tins for future testing. The addition of RAP filler to virgin filler and mixing of the two was conducted as soon as possible in order to minimize any temperature loss.

3.3.2.3 Full Aggregate Replacement

The mastic of 100% RAP was intended to represent the portion of material in RAP modified asphalt concretes where the RAP material is coated with asphalt binder. The present mastic case isolates the interaction of RAP material (filler in this case) and virgin binder and will help to better understand the behavior of the material. The mastic case of 100% RAP is an important component for modeling and studying the mastic level structure of RAP modified asphalt concretes. More details regarding the same will be presented in Chapter 4. The preparation of 100% RAP mastic consisted of heating the RAP filler at 110°C, two hours prior to mixing and heating the virgin binder at a mixing temperature of 160°C. The binder temperature was always monitored using a thermocouple. Upon reaching the mixing temperature, virgin binder was added to the RAP filler and mixed for 90 seconds using a hand held mechanical blender. The added virgin binder, was accounted for with the binder contribution from RAP filler. The prepared mastic was then poured into smaller 60ml sample tins for future testing.

3.4 Phase III: Rheological Tests on Binders and Prepared Mastics

In order to determine the mechanical properties of the test materials mentioned in Section 3.3, rheological tests were performed on dynamic shear rheometer. The rheometer used for the present study is TA Instruments AR 2000 EX. Trios, the data

analysis software provided by the manufacturer, was used to collect and analyze the data. In addition, a separate and standalone data acquisition program was used to log the time, torque, and angular displacement data during testing. The materials were tested using 8 mm parallel plate geometry at a testing gap of 2 mm. In parallel plate testing it is important to have proper adhesion between the plates and the test sample. The samples were seated at a gap larger than the testing gap and allowed to rest for 2 minutes at 64°C. This allowed for the development of adequate adhesion between the test sample and the parallel plates. After this equilibrium time, the sample was trimmed and the chamber was set to test temperature. The final gap was set as the temperature inside the chamber reached the test temperature. The following mechanical tests were performed on the binder and mastic test samples:

1. Temperature and Frequency Sweep Tests (Dynamic Modulus)
2. Controlled Strain Fatigue Tests
3. Repeated Stress Sweep Tests

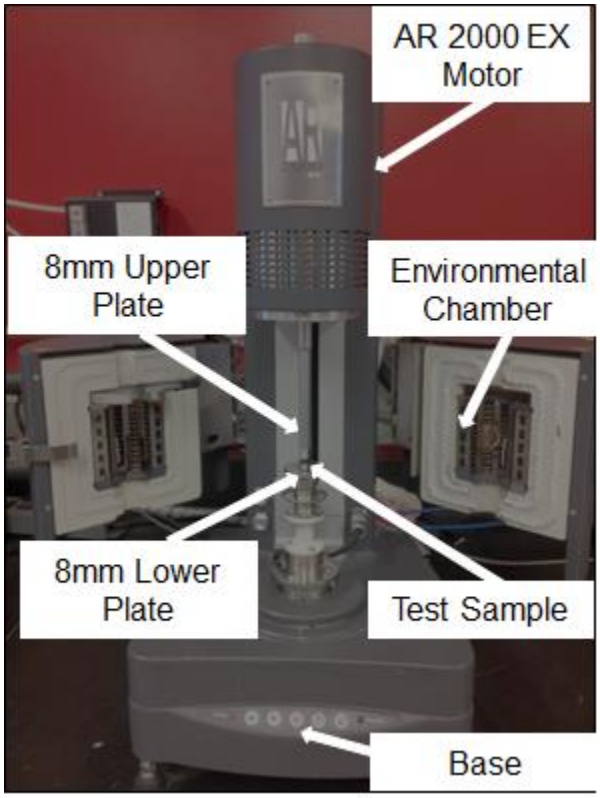

Figure 3-9: AR 2000 EX Dynamic Shear Rheometer

3.4.1 Temperature and Frequency Sweep Tests

Temperature and frequency tests on mastics and binders were conducted to assess their respective linear viscoelastic (LVE) properties. The test temperatures and frequencies are same for all materials and are as shown below. The material response functions of interest are complex shear modulus ($|G^*|$) and phase angle (δ).

- Temperatures: 10˚, 20˚, 30˚, 40˚, and 54˚C
- Frequencies: 30, 14, 6.5, 3, 1.4, 0.65, 0.3, 0.14, 0.1Hz

Strain levels at each temperature were determined by performing strain sweeps on separate samples. The strain levels varied from 100-250 με zero to peak for all

temperatures except for 54°C low frequencies where strain level of 500 με was needed to achieve quality data.

Prior to commencing with the experiments for this study, a pilot experiment was performed to determine the time for temperature conditioning, i.e. the time required for the sample to reach the test temperature. Strain controlled time sweeps were performed on the sample at the test temperatures and 10Hz frequency. Low strain amplitude of about 50 με was applied and the response of the samples, modulus in this case, was monitored over time. The desired outcome of the test was to find the time at which the modulus of the material equalizes, which indicates that the material has attained thermal equilibrium. The limits for modulus difference were set as +/- 1%. The temperature was evaluated in a band of +/- 0.1°C

The test sample was trimmed at 64°C and the chamber was subsequently set to 10°C. After setting the final gap, the test was started. The test steps were set up to run for a period of 35 minutes. As shown in Figure 3-10, at 10°C it was observed that the sample takes about 1500 seconds (25 minutes) to reach thermal equilibrium. However, for the experiments performed in this study the time for equilibrium at 10°C was set at 30 minutes.

Similar experimentation was carried out at 20°C. The temperature was brought down similarly from 64°C to 20°C. As shown in Figure 3-11, it was observed that a period of about 8 minutes was sufficient to achieve thermal equilibrium. However, for the experiments performed in this study the time for equilibrium at 10°C was set at 20 minutes. This temperature was done to estimate the conditioning time for the fatigue

tests. For the dynamic modulus tests, the temperature was ramped from 10˚C to 20˚C. The time for thermal equilibrium here would be less than what was observed for 64˚C to 20˚C. However, 20 minutes was used in this case too. Similar experimentation was performed at remaining test temperatures and it was observed thermal equilibration time of 20 minutes sufficed for all.

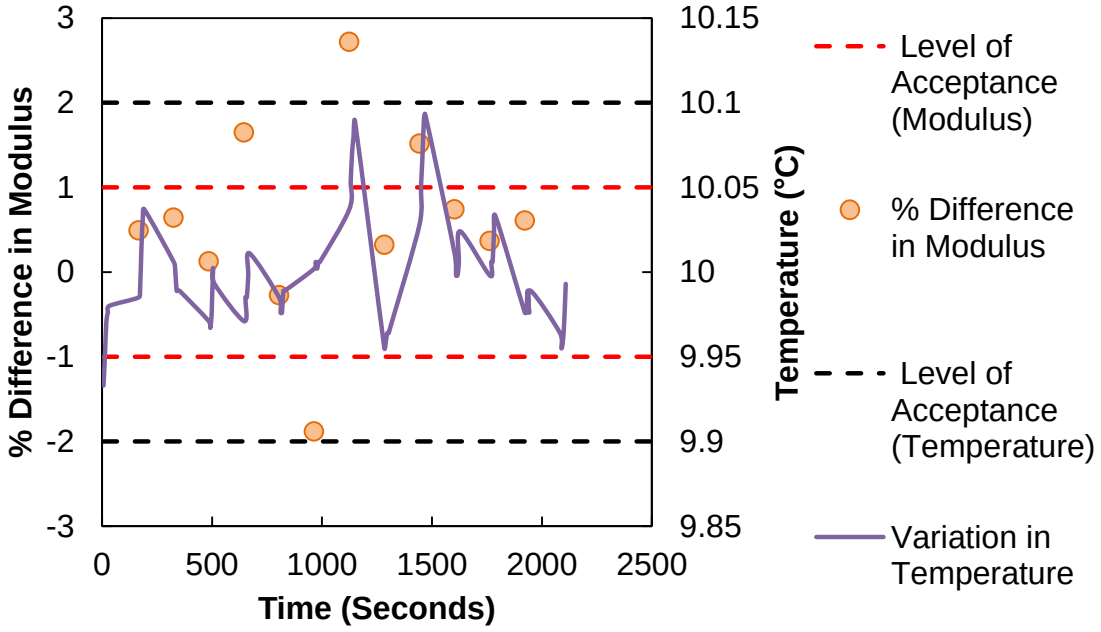

Figure 3-10: Graphical Representation of Thermal Equilibrium Results at 10˚C.

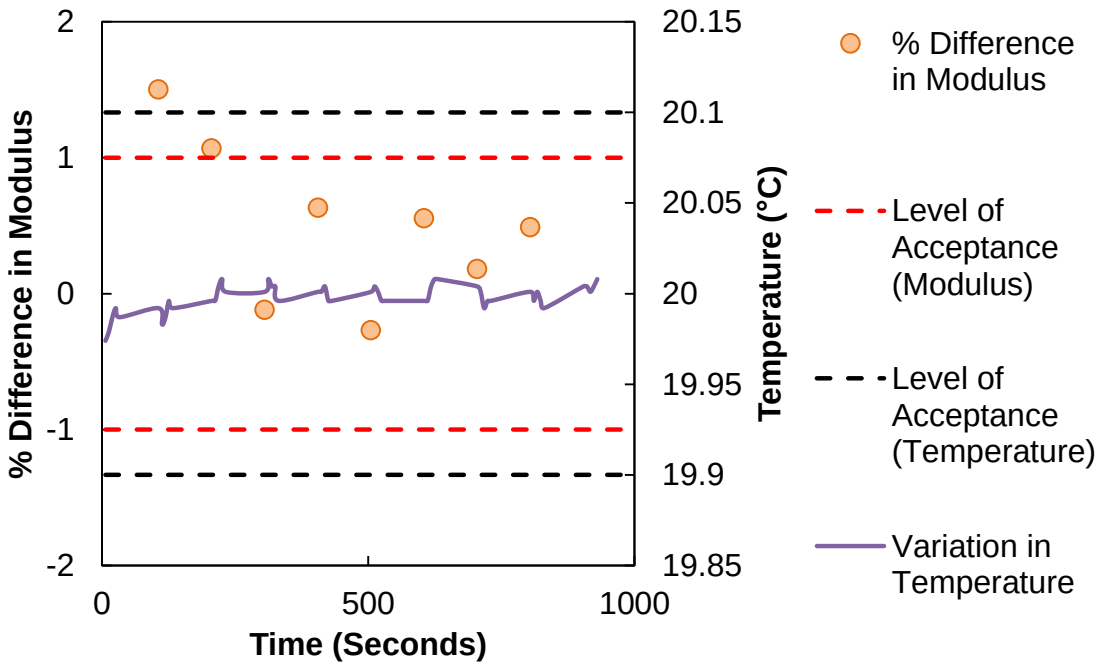

Figure 3-11: Graphical representation of Thermal Equilibrium Results at 20°C.

3.4.2 Controlled Strain Fatigue Tests

Controlled strain fatigue tests were performed to assess the fatigue properties of the binders and mastics and to characterize the continuum damage model. The samples were subjected to a continuous constant shear strain sinusoidal loading. The tests were conducted at 20°C, a frequency of 10 Hz, and three different zero to peak strain magnitudes of 1.25%, 2.5% and 5%. For these tests the raw data was acquired using an independent program setup on LabVIEW. The acquired data is used for data analysis. The signal obtained by the LabVIEW program is corrected for inertia and bearing friction during the data analysis process. The values of calibrated inertia and bearing friction can be obtained from the calibration tab of the Trios test file. The modulus values used in the analysis were calculated by the internal algorithm in Trios.

3.4.3 Repeated Stress Sweep (RSS) Tests

Repeated stress sweep tests are used in the present study to assess the strain level non-linearity of binders and mastics [32]. An alternative way of determining the same would be to perform a temperature frequency sweep test at high strain levels, but this test will smear the effect of damage in to the responses, hence it is not used [32].

A stress sweep is a test where the test sample is loaded at fixed temperature and frequency but with incrementally increasing stress levels. The stress increments follow a logarithmic increase. In RSS test, a given stress increment block is repeated multiple times. After the final loading block, the stress magnitudes are refigured and the process is repeated again. Each subsequent refiguring of stress increment constitutes a unique loading group [32]. In the present study, two loading groups are employed. Loading group 1 constitutes of two repetitions and loading group 2 constitutes of five repetitions. A schematic of the test as depicted by Underwood [32] is shown in Figure 3-12. The maximum and minimum stress levels are presented in Table 3-4

Table 3-4: Maximum and Minimum Stress Levels for the Loading Groups in RSS Test

Material	Loading Group 1		Loading Group 2	
	Minimum Stress (Pa)	Maximum Stress (Pa)	Minimum Stress (Pa)	Maximum Stress (Pa)
VM	5.5E+02	5.5E+04	5.5E+02	5.5E+05
RAM	7.0E+02	7.0E+04	7.0E+02	7.0E+05
RAP 10	6.0E+02	6.0E+04	6.0E+02	6.0E+05
RAP 30	8.0E+02	8.0E+04	8.0E+02	8.0E+05
RAP 50	8.0E+02	8.5E+04	8.0E+02	8.5E+05
RAP 100	1.5E+03	1.5E+05	1.5E+03	1.5E+06
RB	1.9E+03	1.9E+05	1.9E+03	1.9E+06

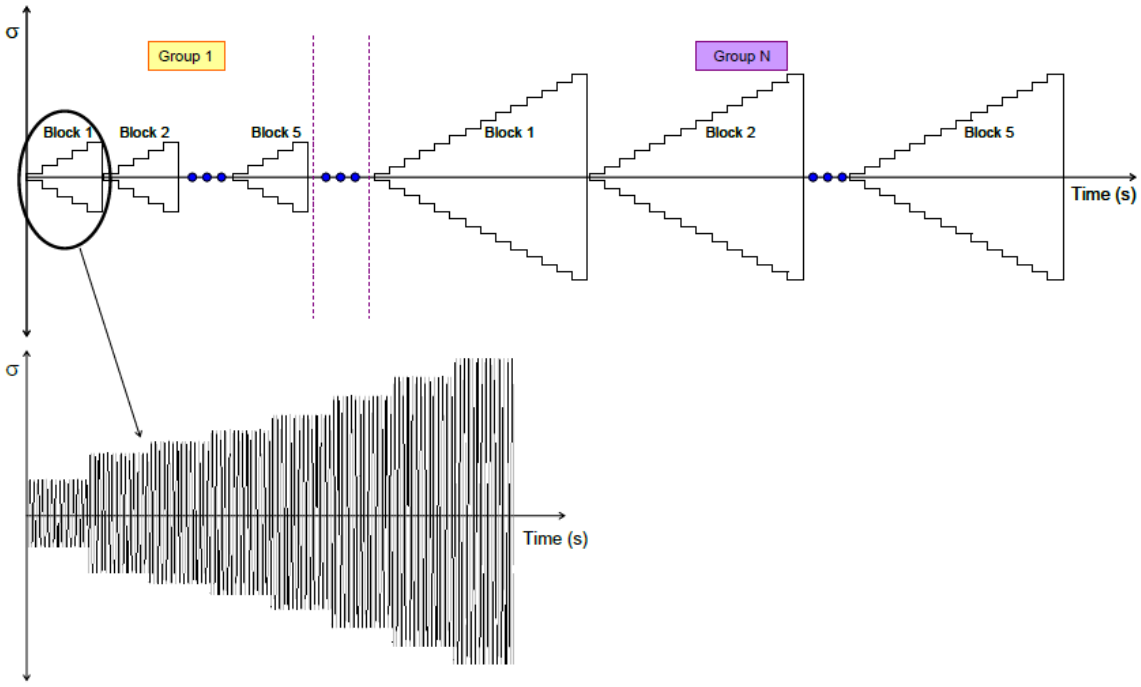

Figure 3-12: Repeated Stress Sweep Loading History [32].

Chapter 4 Micromechanical Based Evaluation of RAP Blending

4.1 Introduction

The term micromechanical model implies the use of a model, based on the principles of micromechanics, which can predict the behavior of a composite material, when the properties and the proportions of the constituents in the composite are known. Any composite material consists of two basic phases, (i) matrix and (ii) inclusions. Thereby the term micromechanics can be envisioned as the mechanics involved in the explicit interactions that occur at matrix and inclusion level [38].

Micromechanical models can predict the fundamental characteristics of the composite based upon the properties of the individual constituents [39] . The applications of micromechanical models are diversified and can be found in the fields of polymer composites, asphalt concrete, solid composites with reinforced matrices, and portland cement concrete [43]. In the present study its applications to asphalt mastics, both virgin and RAP modified mastics is studied. These micromechanical models are developed based on the idealization of microstructure using regular particle geometries. Also, the models treat the matrix as an inert and elastic medium. But, often materials contain well graded and irregularly shaped particles and a matrix that is physico-chemically active and viscoelastic. Asphalt mastics are one of the prime examples for such a difference. The authors were still able to successfully apply these models to asphalt mastics. Notable studies being Buttlar et al.[44] , Shashidhar and Shenoy [45], Kim [46], Yin et al [47], Underwood [43], and Faheem and Bahia [48]. A detailed description of the models and the studies involving asphalt mastics are presented later in the chapter.

In the first part of the chapter, the results from temperature-frequency sweeps, time sweep and repeated stress sweep are presented. In the second part of the chapter, a detailed discussion on the micromechanical models being employed in the present study is presented. The final part of the chapter would include two subparts. Subpart 1 will explain the mastic structure idealization developed as part of the present study. Subpart 2 will include predictions of the micromechanical models for both non-modified and RAP modified mastics to match the hypothesized mastic structure. The model predictions will be carried out based on the modulus values generated from the temperature frequency tests.

4.2 Experimental Results

4.2.1 Temperature-Frequency Sweep

It should be recalled that for all the materials tested as part of this study, the materials responses were evaluated at five temperatures, 10°, 20°, 30°, 40°, and 54°C and nine frequencies, 30, 14, 6.5, 3, 1.4, 0.65, 0.3, 0.14, 0.1Hz. All mastics in the study were tested at single filler concentration of 27% . A form of the Christensen-Anderson-Marasteanu (CAM) model in Equation (4.1) was used to develop the mastercurves. A second order quadratic equation, Equation (4.2) was used to estimate the shift factor a_T.

$$\left|G^*\right| = \frac{10^g}{\left(1+\left(\frac{\omega_c}{\omega_R}\right)^k\right)^{\frac{m_e}{k}}} \tag{4.1}$$

$$\log\left(a_T\right) = \alpha_1\left(T-T_R\right)^2 + \alpha_2\left(T-T_R\right) \tag{4.2}$$

where

$|G^*|$ = dynamic shear modulus (Pa),

10^g = binder glassy modulus, determined through optimization (Pa),

ω_c = crossover frequency (rad/s), a fitting coefficient,

ω_R = reduced frequency (rad/s),

m_e, k = fitting coefficients,

T = temperature (°C),

T_R = reference temperature (°C), and

α_1, α_2 = fitting coefficients.

The modulus and the phase angle data for the study materials are presented in Figure 4-1 and Figure 4-3 respectively.

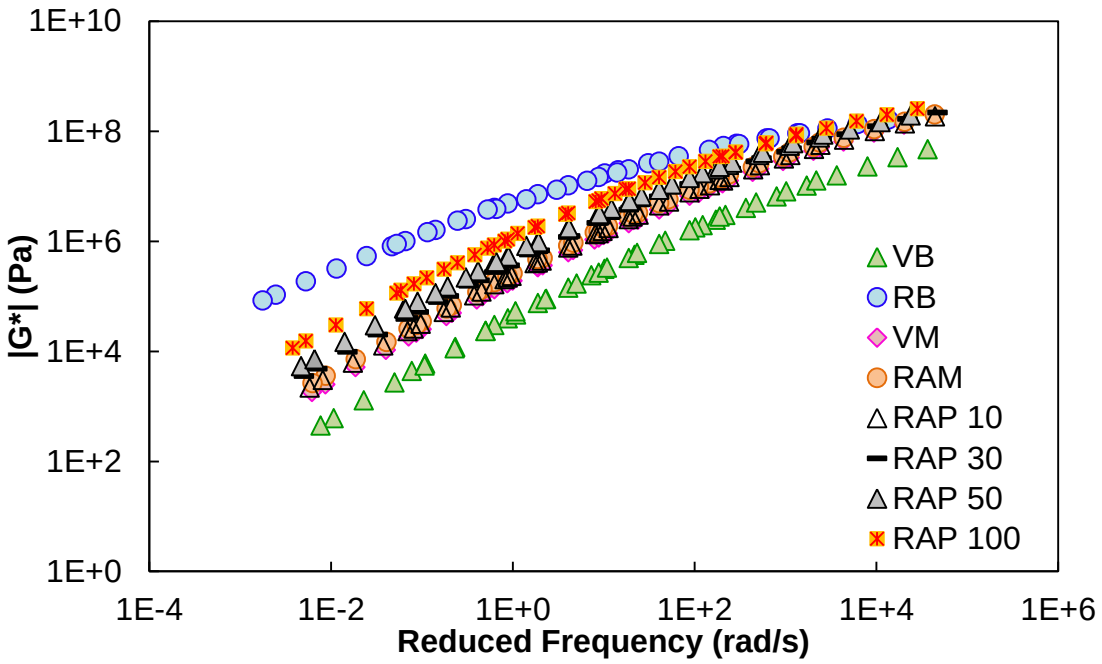

Figure 4-1: Modulus Mastercurves of the Study Materials in log-log Space.

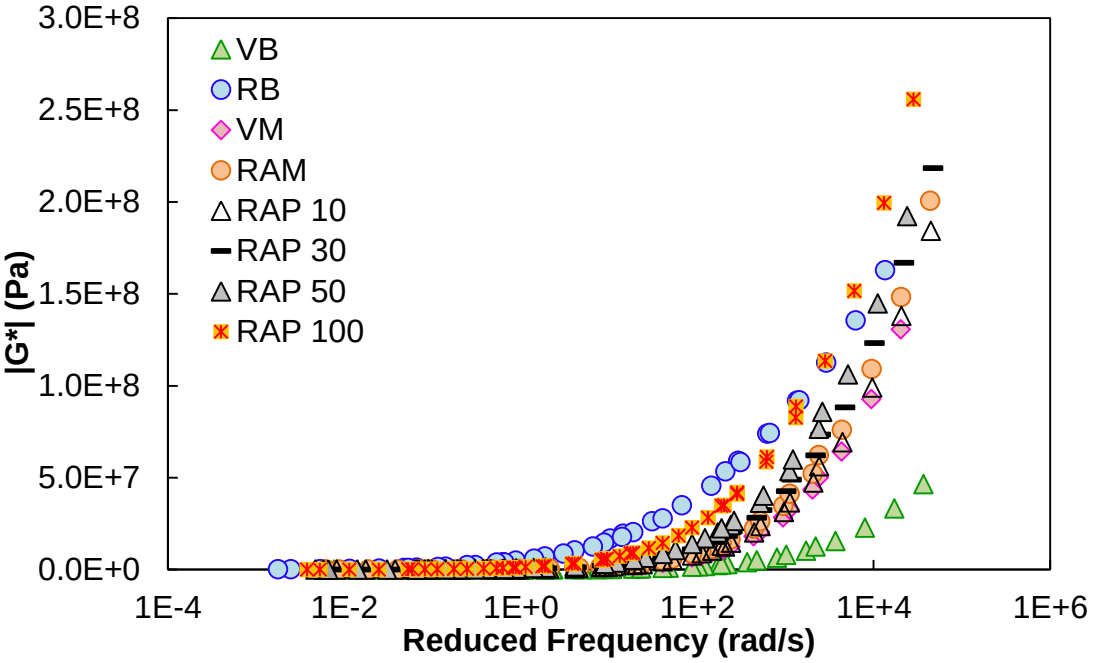

Figure 4-2: Modulus Mastercurves of the Study Materials in semi-log space.

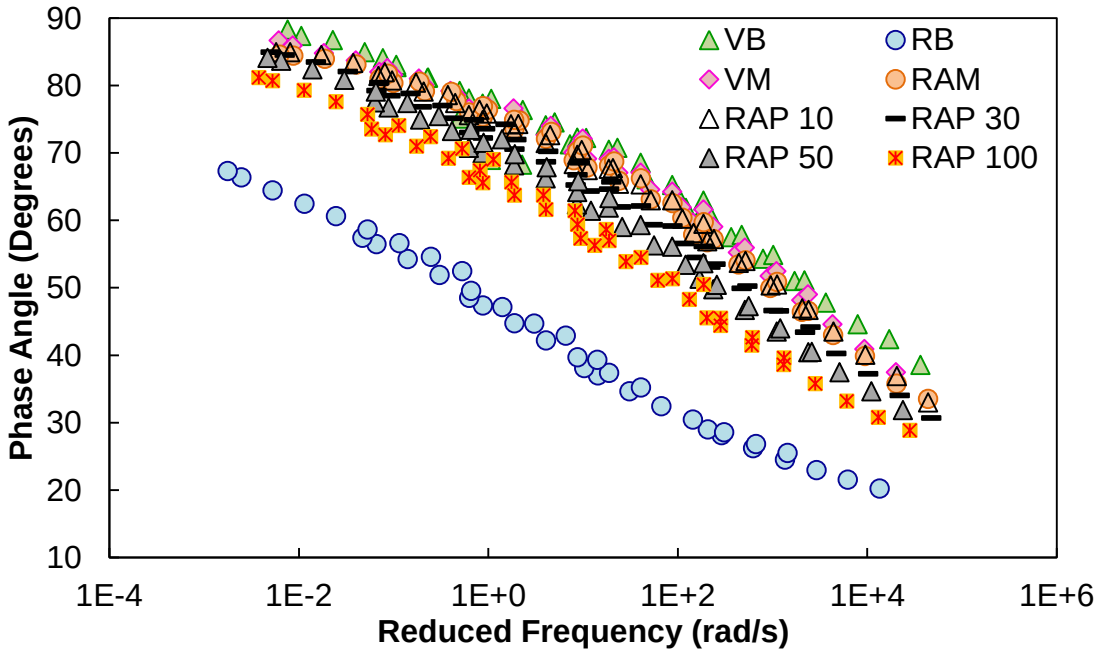

Figure 4-3: Phase Angle Data for the Study Materials

It can be seen from Figure 4-1 that the RB and VB are the stiffest and softest materials respectively. Owing to high stiffness of RAP binder, appreciable data quality

could not be achieved for RB at low temperatures and high frequencies due the torque nearing machine limits. Due to this the ranking of the stiffest material as in Figure 4-2, at low temperatures and high frequencies is not clear. However, the mastics rank clearly according to the percentage of RAP with VM being the softest and RAP 100 being the stiffest. This is an expected trend and is in agreement with the mix modulus trends observed from the studies presented in the literature review [5]. One interesting observation from the modulus data is the proximity of VM and RAP10. This observation is consistent with the literature, where authors did not find a significant difference between virgin mixtures and RAP mixtures at low RAP contents [12]. Also, it is seen that RAM had a slightly higher stiffness than VM and RAP 10. This was unexpected considering that RAM doesn't have any RAP filler in it. But, the differences between the materials are so small that they are unlikely to be significant. The most notably different mastercurve is that of RAP binder which is reflected in the phase angle data, where a clear distinction can be observed between the phase angles of RB and other materials as seen in Figure 4-3. This high stiffness of the extracted RAP binder essentially confirms the effect of field aging on the properties of the binder.

4.2.2 Controlled Strain Fatigue Tests

Strain controlled time sweep experiments were performed on the study materials to assess the fatigue properties and to characterize the continuum damage model. It should be recalled that the tests were carried out at single temperature, 20°C and at three zero to peak strain levels, 1.25%, 2.5% and 5%. The fatigue failure criteria adopted for the present study is that of a phase angle drop observed during the course of the

experiment. The corresponding cycle number at the phase angle drop is the number of cycles to failure for the material at that particular strain level. An example of the phase angle drop for RAP 30 at 5% strain level is shown in Figure 4-4. The number of cycles to failure is taken as the average value obtained from two replicates. In this case both replicates gave similar number of cycles.

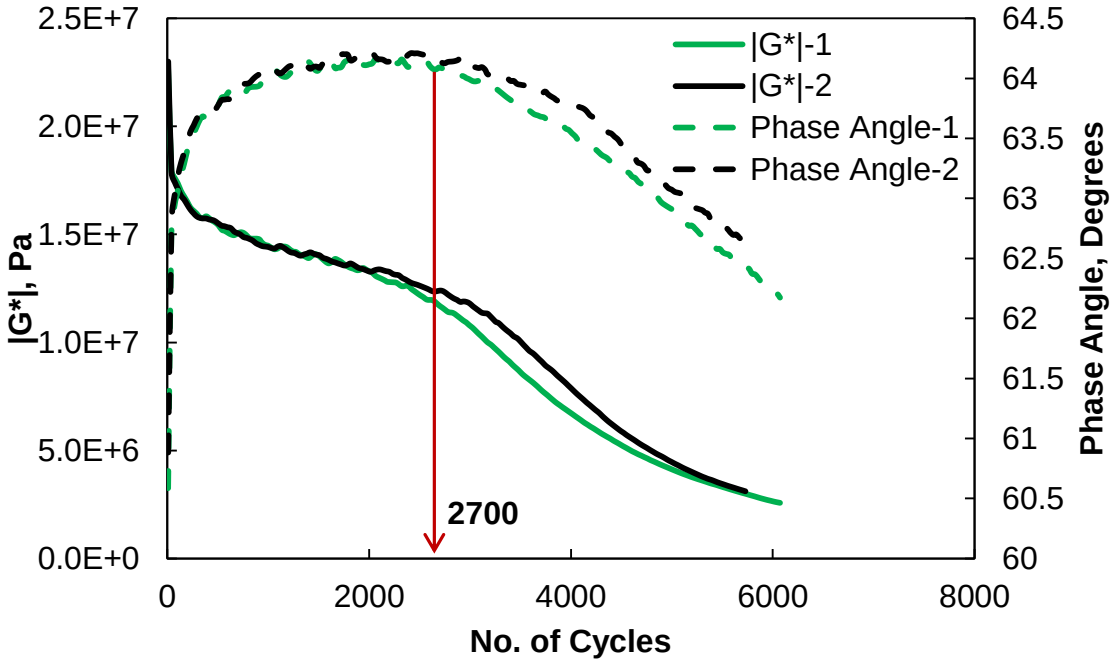

Figure 4-4: An Example of Phase Angle Drop: RAP 30 at 5% Strain Level.

The number of cycles to failure of the test materials at 1.25%, 2.5% and 5% strain level are presented in

Table 4-1, Table 4-2, Table 4-3 respectively and graphically represented in Figure 4-5, Figure 4-6, Figure 4-7 respectively.

Table 4-1: Number of Cycles to Failure, for Test Materials at 1.25% Strain Level

1.25%	N_f
VB	145500
RB	125000
VM	70000
RAM	80000
RAP 10	74500
RAP 30	70000
RAP 50	77500
RAP 100	68000

Table 4-2: Number of Cycles to Failure, for Test Materials at 2.5% Strain Level

2.5%	N_f
VB	24000
RB	1950
VM	11500
RAM	12250
RAP 10	11250
RAP 30	12500
RAP 50	14000
RAP 100	16000

Table 4-3: Number of Cycles to Failure, for Test Materials at 5% Strain Level

5%	N_f
VB	5250
RB	-
VM	2225
RAM	2325
RAP 10	2700
RAP 30	2700
RAP 50	2300
RAP 100	2100

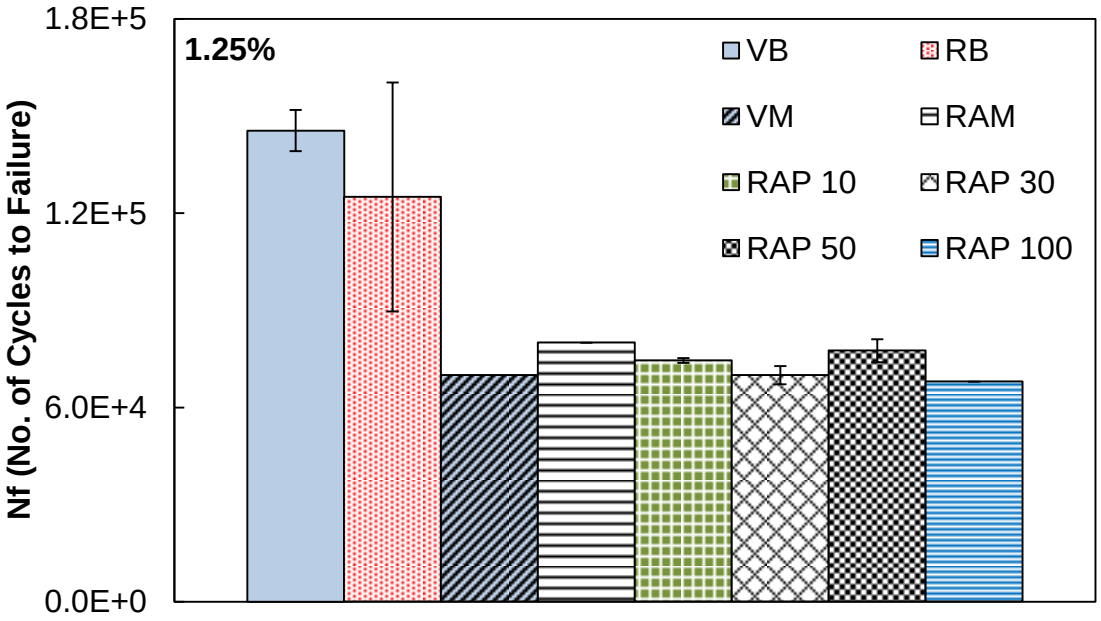

Figure 4-5: Number of Cycles to Failure at 1.25% Strain Level.

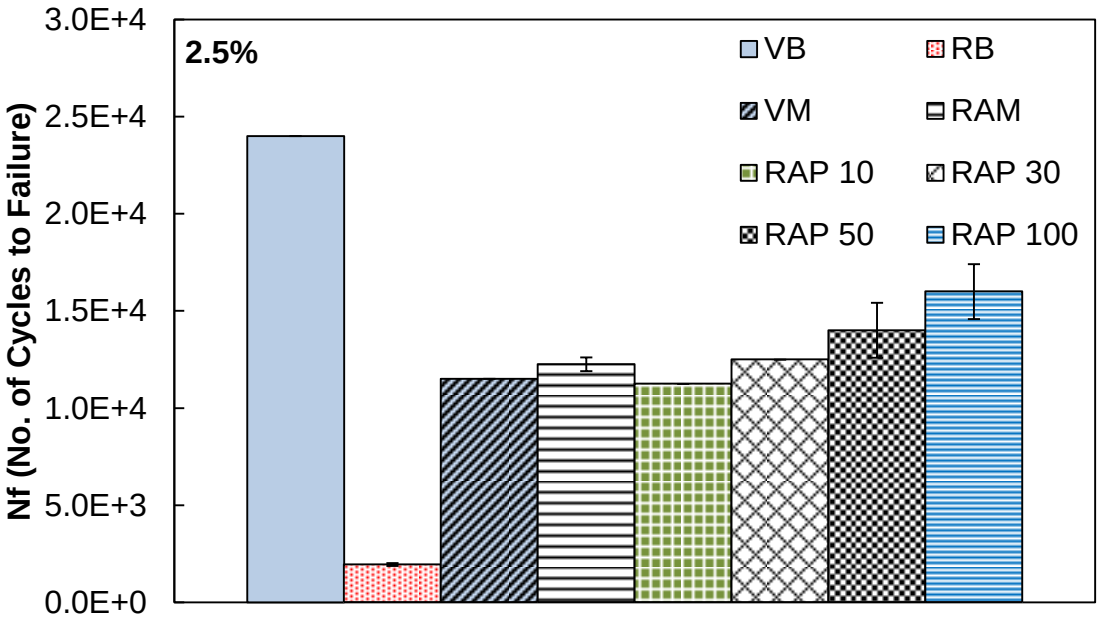

Figure 4-6: Number of Cycles to Failure at 2.5% Strain Level.

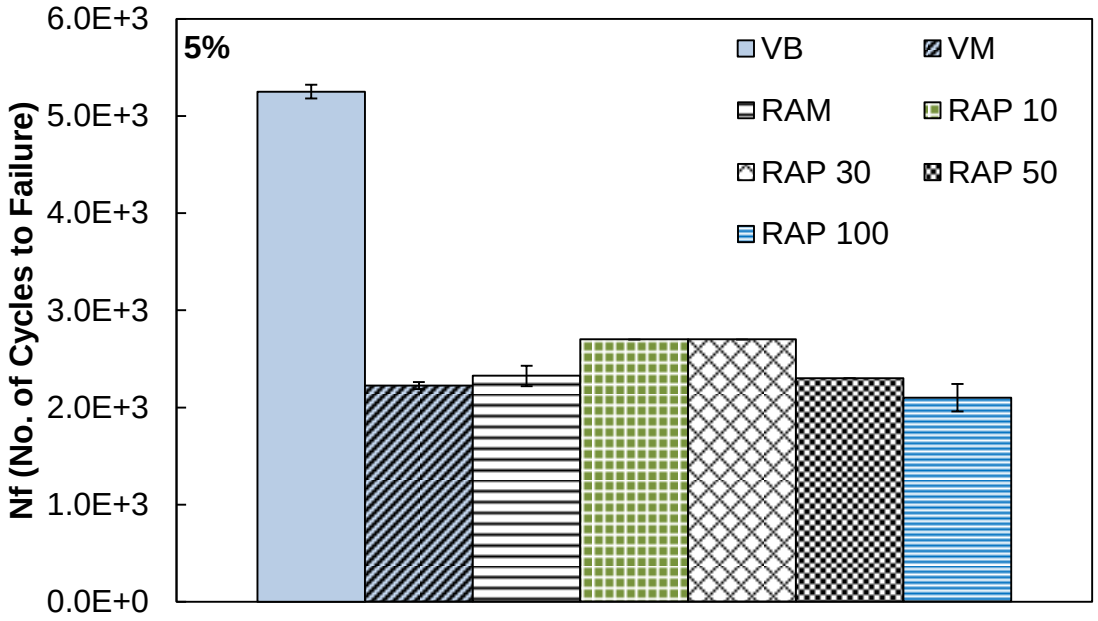

Figure 4-7: Number of Cycles to Failure at 5% Strain Level.

The common observation from all three strain levels is that the virgin binder has the highest number of cycles to failure, which is on expected lines since the stiffness of virgin binder is lowest among all the materials.

At 1.25% strain level we observe that RAP 100 had the lowest number of cycles to to failure. It is interesting to see RB having such high number of cycles to failure, knowing that RAP binder is the stiffest among all materials we would expect it to fail early. It was observed, as shown in Figure 4-8 that during the course of the test no appreciable change in modulus was seen until a long period of time after which a sudden high drop was observed. Also, it was observed that consistency in N_f could not be achieved with RB. With regard to the mastics, at this strain level in general it was observed that increase in RAP percentage in the mastics lowers the number of cycles to

failure. However, the exceptions to this trend were VM and RAP 50. It is to be noted that, as shown in

Table 4-1, the basis for N_f for RAM and RAP 100 was one replicate.

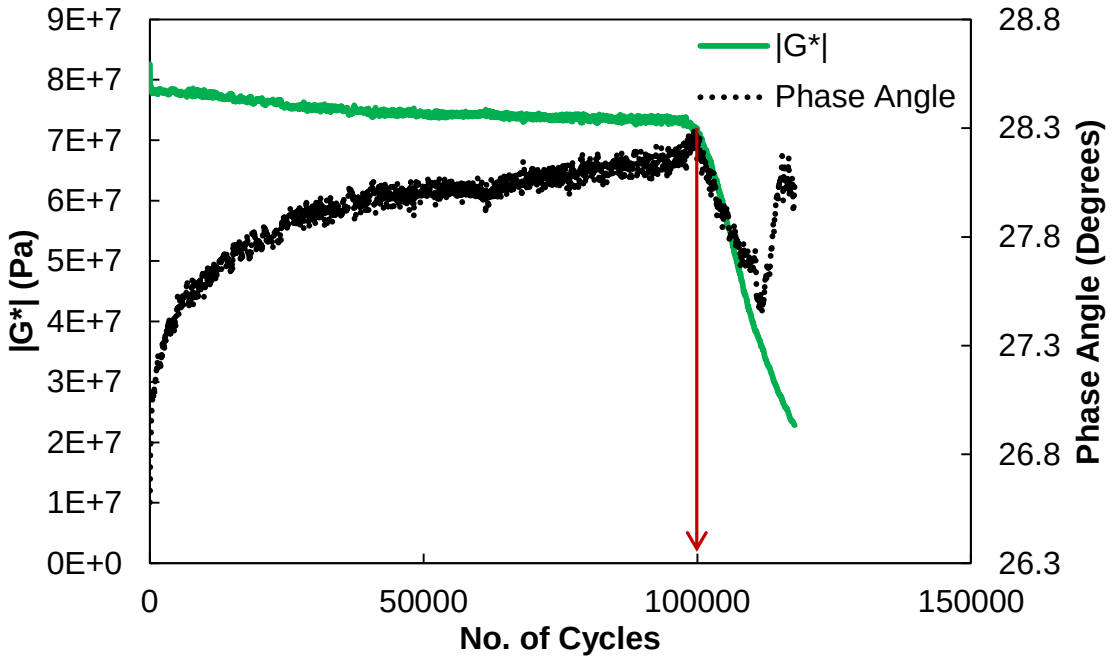

Figure 4-8: Variation of |G*| and Phase Angle for RB at 1.25% Strain Level.

At 2.5% strain level, VB is still seen to have the highest number of cycles to failure, but now RB which is the stiffest material is seen to have the lowest number of cycles to failure. Also, the magnitude of difference in N_f is high when compared to other materials. It could be said that the behavior of RB is on expected lines, but since RB had high N_f in the previous case this observed result was surprising as it was not in line with 1.25% strain level. With regard to the mastics, the results are in contrast to what was observed in 1.25%. It is seen in general that addition of RAP increases the number of cycles to failure in the mastic. However, the differences between the materials are so small that any variability within the replicates can cause the observed trend to change.

At 5%, due to the machine limits the test could not be performed for RB. The trends for the mastics at 5% strain level are similar to that observed at 1.25% strain level. Although, VM has lower number of cycles to failure than other mastics the general observation is that addition of RAP lowers the N_f.

From the time sweep results it is clearly observed that binder and mastics have different fatigue behaviors. However, among the mastics it is hard to distinguish as the differences in N_f are very small.

4.2.2.1 Damage Analysis

The simplified viscoelastic continuum damage (S-VECD) model is derived by Underwood [32] specifically for the asphalt binders and mastics to be applied in the case of parallel plate torsional testing. The author theorized that the S-VECD model applied to the mixture is not sufficient for the binders and mastics. In binders and mastics the concepts of tension and compression do not apply since the material is under torsional loading. In torsional loading, one refers to loading as either positive displacement (clockwise rotation) or negative displacement (counter-clockwise rotation). The damage in torsional loading is likely to occur from anti-plane shearing. The rigorous derivation of the model and its applicability can be found in [32]. Underwood [32] reports that in a simplest sense continuum damage mechanics consider a damaged body with some stiffness as an undamaged body with reduced stiffness. The theory ignores specific microstructural behaviors, but instead characterizes a material using macro scale applications. The linear S-VECD formulation is shown in Equation (4.3) to (4.8). C here

represents the pseudo stiffness, in simple terms it represents te material integrity, whereas S represents the damage parameter as indicated by Schapery [49].

$$C = \frac{\tau}{\gamma^R * DMR},\ for \xi \le \xi_p \tag{4.3}$$

$$C = C^* = \frac{\tau_{0,pp}}{\gamma^R * DMR},\ for \xi \ge \xi_p \tag{4.4}$$

$$dS = (dS_{Transient})_{timestepj} = \left(-\frac{DMR}{2} (\gamma^R)_j^{\ 2} \Delta C_j \right)^{\frac{\alpha}{1+\alpha}} * (\Delta\xi)_j^{1/\alpha},\ for \xi \le \xi_p \tag{4.5}$$

$$dS = (dS_{Cyclic})_{cyclei} = \left(-\frac{DMR}{2} (\gamma_{0,pp}{}^R)^2 \Delta C_i \right)^{\frac{\alpha}{1+\alpha}} * (\Delta\xi_p * \mathrm{B}_1)_j^{1/1+\alpha},\ for \xi > \xi_p \tag{4.6}$$

$$B_1 = f_R \int_{\xi_i}^{\xi_f} (f(\xi))^{2\alpha} * d\xi \tag{4.7}$$

$$f(\xi) = -\frac{1}{2}\cos(\omega\xi) + \frac{(\tau_{peak})_i + (\tau_{valley})_i}{2\left[(\tau_{peak})_i - (\tau_{valley})_i\right]} \tag{4.8}$$

where,

ξ_p = reduced pulse time

$dS_{Transient}$ = early portion of damage calculation

DMR = $\frac{G^*_{fingerprint}}{G^*_{LVE}}$

C = pseudo stiffness in first half of first loading cycle

C^* = pseudo stiffness during the remainder of the test.

Underwood [32] developed S-VECD model formulations to characterize both linear and non-linear behaviors of asphalt binders and mastics. The inputs for the development of the linear model can be had from the temperature-frequency sweep test and the time-sweep (strain controlled fatigue test) conducted on the material. The torque and displacement inputs from the time sweep tests, were obtained using a standalone data acquisition system created in LabVIEW which could acquire a data point approximately every 0.001 seconds. The prony coefficients (relaxation modulus and creep compliance) to be used for the model were obtained from the temperature-frequency test through the process of collocation. The method of collocation was originally proposed by Schapery [49] and the same was applied by Underwood in his model development [32]. The model development was carried out in LabVIEW software, the outputs of which were then used to develop the damage characteristic curve (C vs S). The parameter C represents the loss in modulus that occurs as the test progresses and S is the damage parameter that represents the amount damage that occurs due to cracking. The results from the linear S-VECD model for the test materials are shown in Figure 4-12 to Figure 4-17. It can be seen from part (a) of Figure 4-12 to Figure 4-17 that the collapse of the curves is not good. A clear strain level ranking is found for all materials, with the curves corresponding to lower strain occupying a higher vertical position. Underwood [32] reported that the main difference between asphalt mix and mastics was the sensitivity of non-linear effects to temperature and strain levels. The author found that both of these effects are found to be more important in the overall response of the mastics, than the

mixtures. The author thus opined that it was necessary to consider these non-linear effects in order to model the damage characteristic curves for mastics within the S-VECD framework. In the present study the fatigue tests were conducted at only one temperature, 20°C but at three strain levels, 1.25%, 2.5% and 5%.

Underwood [32] found that, in mixtures and FAM, the consideration of non-linearity did change the final material damage characteristic relationship but it did not affect the collapsibility of the experimental data. As a result the material behavior can be approximated at the mix and FAM scales using the simpler linear based S-VECD formulation [32]. However, the same could not be said for the mastics, as the strain levels need to be very high in order to fail the sample in a reasonable amount of time. At these strain levels the linear based formulation will be lacking as there is bound to be non-linearity involved [32]. A comprehensive non-linear viscoelastic (NLVE) formulation was developed by Underwood and is presented in [32], [50]. In the non- linear viscoelastic continuum damage model the pseudo strain variable is replaced with non-linear pseudo strain which is calculated via Equation (4.9) and(4.10). Simply stated, this pseudo strain is calculated by recognizing that that dynamic shear modulus is strain level dependent.

$$\gamma^R = \gamma^R = \frac{h_1}{G_R}\int_0^{\xi} G(\xi' - \tau')\frac{dh_2\gamma}{d\tau'}d\tau', \; for \xi \leq \xi_p \tag{4.9}$$

$$\left(\gamma^R_{0,pp}\right)_{cyclei} = \frac{1}{G_R} * \left((\gamma_{0,pp})_i * \left|G^*\right|_{NL}\right) for \xi > \xi_p \tag{4.10}$$

In order to assess this strain level non-linearity in the binders/mastics repeated stress sweeps (RSS) were performed on the test materials at 20°C. The details of the test have been presented in Section 3.4.3 and are mentioned in detail in [50]. In the present study, two loading groups are considered. Loading group 1 consists of two blocks and loading group 2 consists of five blocks. The stress levels in the two groups have been presented in Table 3-4. An example of the modulus response pattern for the loading groups is shown in Figure 4-9. The different series shown in the figure corresponding to a particular loading group (G) and block (B).

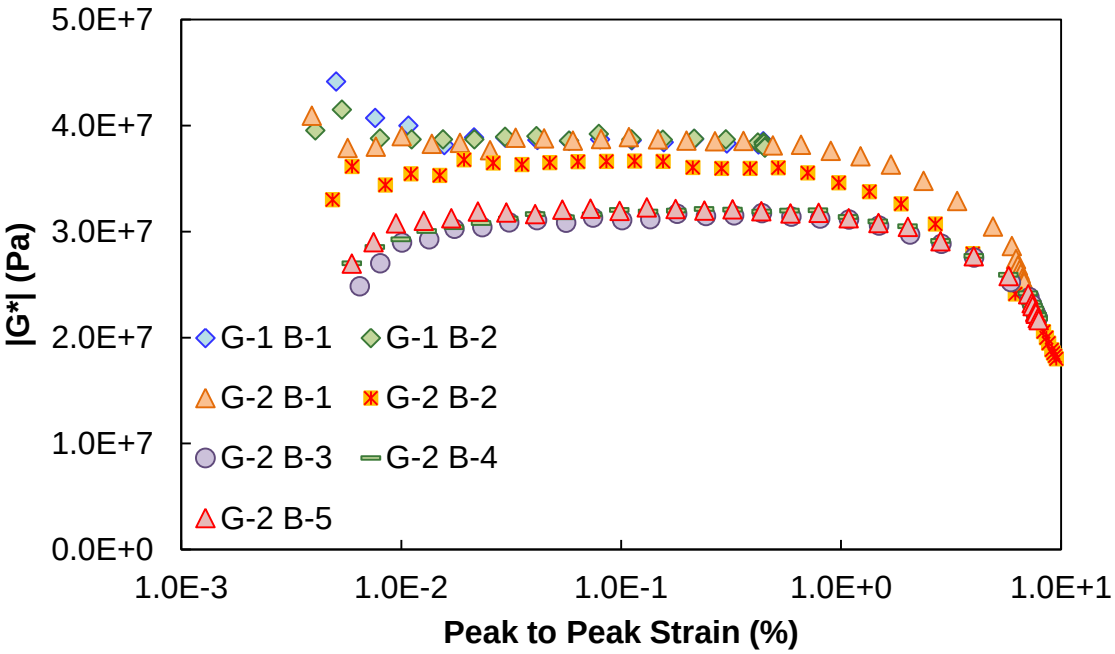

Figure 4-9: Typical Modulus Response of RSS Loading Group.

Summarized below are important observations from Figure 4-9. The observations are in agreement with those presented by Underwood and Kim in [50].

- In both loading groups, the modulus decreases with increase in strain level.

- No permanent change in material is observed during group 1 loading as material response is same for G-1 B-1 and G-1 B-2.
- In group two, the modulus reduction is not fully permanent as the modulus at the beginning of the next block is higher than the modulus at the end of the previous block. For example, modulus at the beginning of block G-2 B-4 is higher than the modulus at the end of G-2 B-3
- The reduction in modulus is not fully recoverable, since the modulus at the smallest strain levels decreases from block to block. For example, compare modulus at the beginning of block G-2 B-2 to beginning of block G-2 B-3.
- After a certain number of block repetitions, the balance between modulus recovery and permanent modulus becomes stable. For example, compare the vertical distance between G-2 B-1 and G-2 B-3 to vertical distance between G-2 B-3, G-2 B-4, and G-2 B-5.

Underwood and Kim [50] postulated that the reduction in modulus can be partly attributed to the NLVE response of the material, while the pattern of apparent partial recovery can be attributed to microstructural damage. This damage will cause a proportional change in the modulus such that $|G^*|_{NL}$, non-linear viscoelastic modulus and $|G^*|_{RSS}$, the modulus values as obtained from the RSS test are related as shown in Equation (4.11) . The proportionality constant C, is expected to evolve slowly and its value will change only from one block to another. But within a block its value for different strains is assumed to be same as long as the $\left|G^*\right|_{RSS}$ data collapse into a single function for subsequent blocks.

$$\left|G^*\right|_{NL} = \frac{\left|G^*\right|_{RSS}}{C} \tag{4.11}$$

From Figure 4-9 it can be seen that group tests (G-1 B-1 and G-1 B-2) are unaffected by damage. In this case C would be equal to one. Group one tests are however insufficient to characterize $|G^*|_{NL}$ as they only extend up to small strain levels of about 0.4%. But group two loading go to higher strain levels and the vertical separation of the modulus response between the blocks, suggests that C is not equal to one for all loading blocks. The overlap of G-2 B-3, G-2 B-4 and G-2 B-5 provides an opportunity to separate non-linearity from damage [50]. Underwood and Kim [50] opined that this type of overlap indicated that minimum amount of damage occurs during G-2 B-3 and the authors assumed that the damage is now constant for all strain levels in blocks four and five. The value of C for G-2 B-5 was determined by calculating the ratio of $|G^*|_{RSS}$ for this block below 0.2% and from G-1 B-1 below 0.2%. This ratio gives the amount of damage that existed in G-2 B-5 cycles. Upon calculating C, Equation (4.11) was used to calculate $|G^*|_{NL}$. The values of C for the study materials for block G-2 B-5 are presented in Table 4-4.

Table 4-4: The Values of C for block G-2 B-5 for the Study Materials.

Material	C @ G-2 B-5
VM	0.85
RAM	0.91
RAP 10	0.86
RAP 30	0.81
RAP 50	0.85
RAP 100	0.70
RB	1.00

The RAP binder did not have any modulus reduction from one block to another and is seen to have a C value of one, which means that there is no damage that had occurred. However non-linearity was observed.

For all the materials the values of $|G^*|_{NL}$ at block G-2 B-5 were then normalized using $|G^*|_{RSS}$ for G-1 B-1 below 0.2%. The normalized values are termed as D. These set of values are then fit to model presented in Equation (4.12).

$$D = a + \frac{b}{\left(1 + c * d^{\varepsilon}\right)} \tag{4.12}$$

Where a, b, c, d are fit coefficients and ε is the zero to peak strain level in percentage. The NLVE response fit data for study materials are shown in Figure 4-10 and Figure 4-11. It is to be noted that the ordinate in both figures should actually end at 1 but is shown up to 1.2 as some data points especially in the linear region have D value slightly greater 1, where the order of difference is only in 2nd decimal. The reason for this can be attributed to the minor variations in data that are observed from cycle to cycle in the linear region.

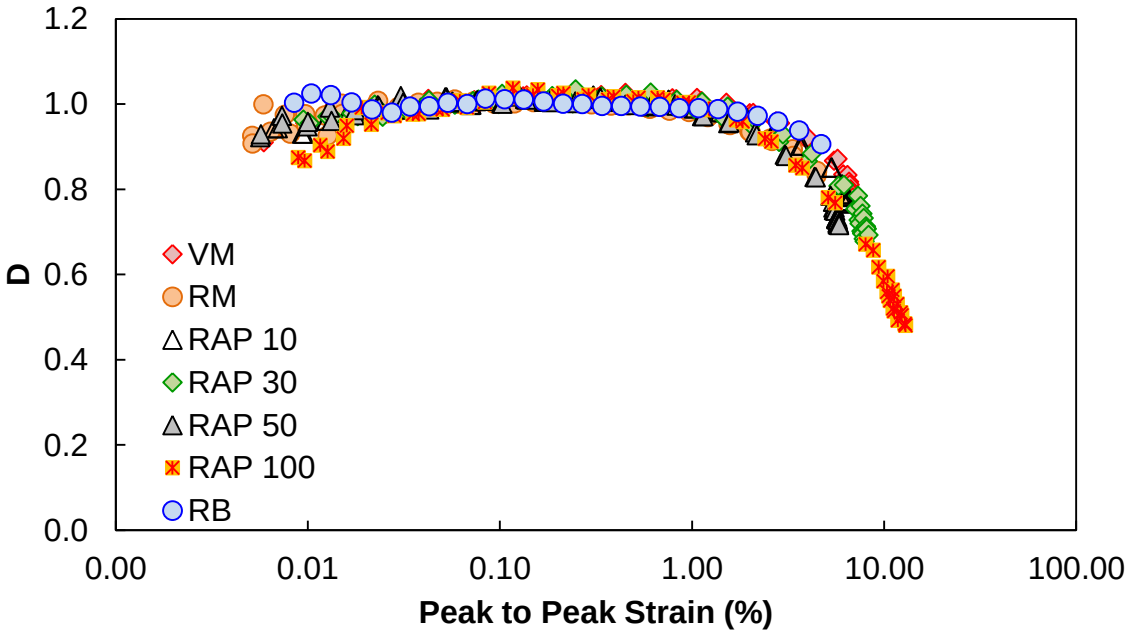

Figure 4-10: NLVE Response of the Study Materials (semi-log).

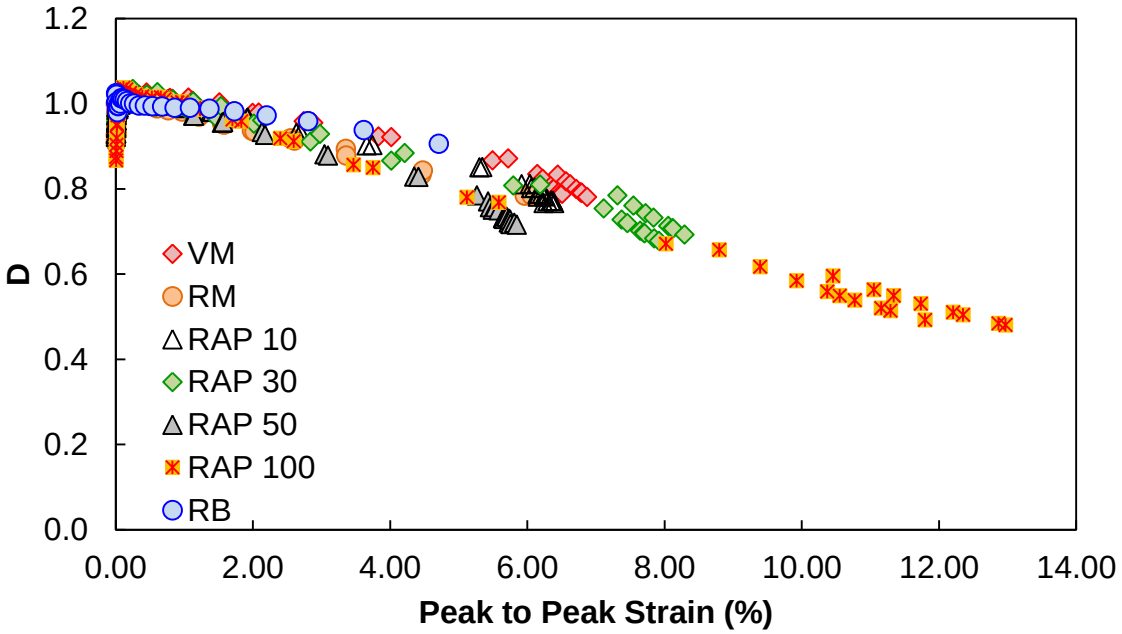

Figure 4-11: NLVE Response of Study Materials.

It should be noted that the virgin binder is absent from the Figure 4-10 and Figure 4-11. The stress levels used for the virgin binder, group 1 (250 Pa to 20,000 Pa) and group 2

(250 Pa to 250,000 Pa), were not sufficient to produce separation between different blocks as shown in Figure 4-9, so it was not possible to characterize non-linearity for the virgin binder based on the obtained data. But it is known from literature [32] that the origin for non-linearity in the mastics is the binder itself. Underwood achieved non-linearity at maximum stress level of about 400,000 Pa which is higher than that used in the present study.

The fit coefficients, a, b, c, d which are indicative of the non-linear behavior of the study materials are now used to refigure the damage characteristic curve. The comprehensive non-linear based S-VECD formulation presented in [32] was adopted to arrive at the damage characteristic curve for the study materials. It can be clearly seen from part (b) of the damage characteristic curves Figure 4-12 to Figure 4-17 that the collapse is better compared to that obtained from linear based S-VECD formulation. However, the same can't said about RB shown in Figure 4-18. The reasons of which can be attributed to the high stiffness of the material and unexpected behavior at 1.25% strain level, where it showed high number of cycles to failure.

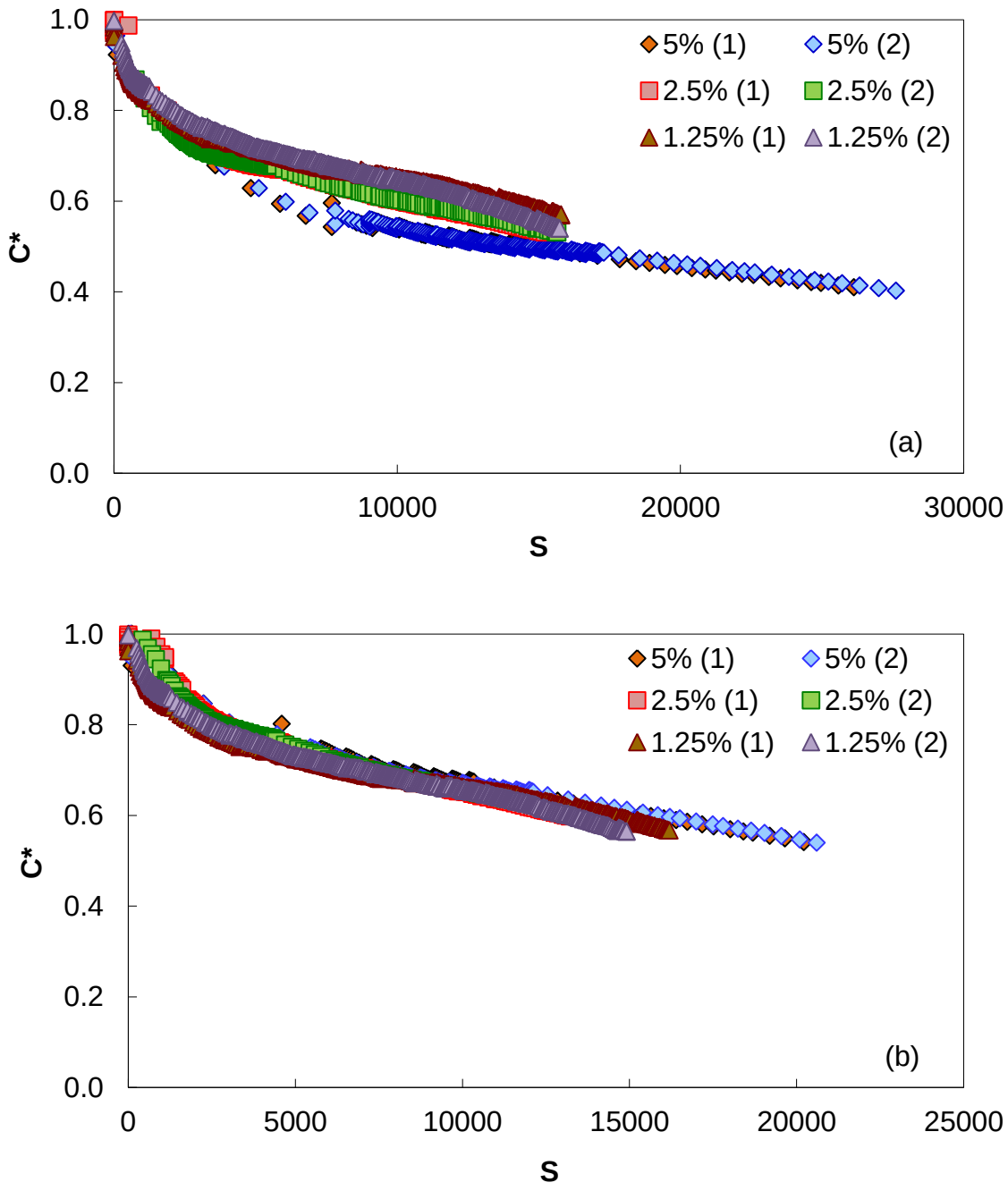

Figure 4-12: Damage Characteristic Curves for VM: (a) Linear Based; (b) Non- Linear Based.

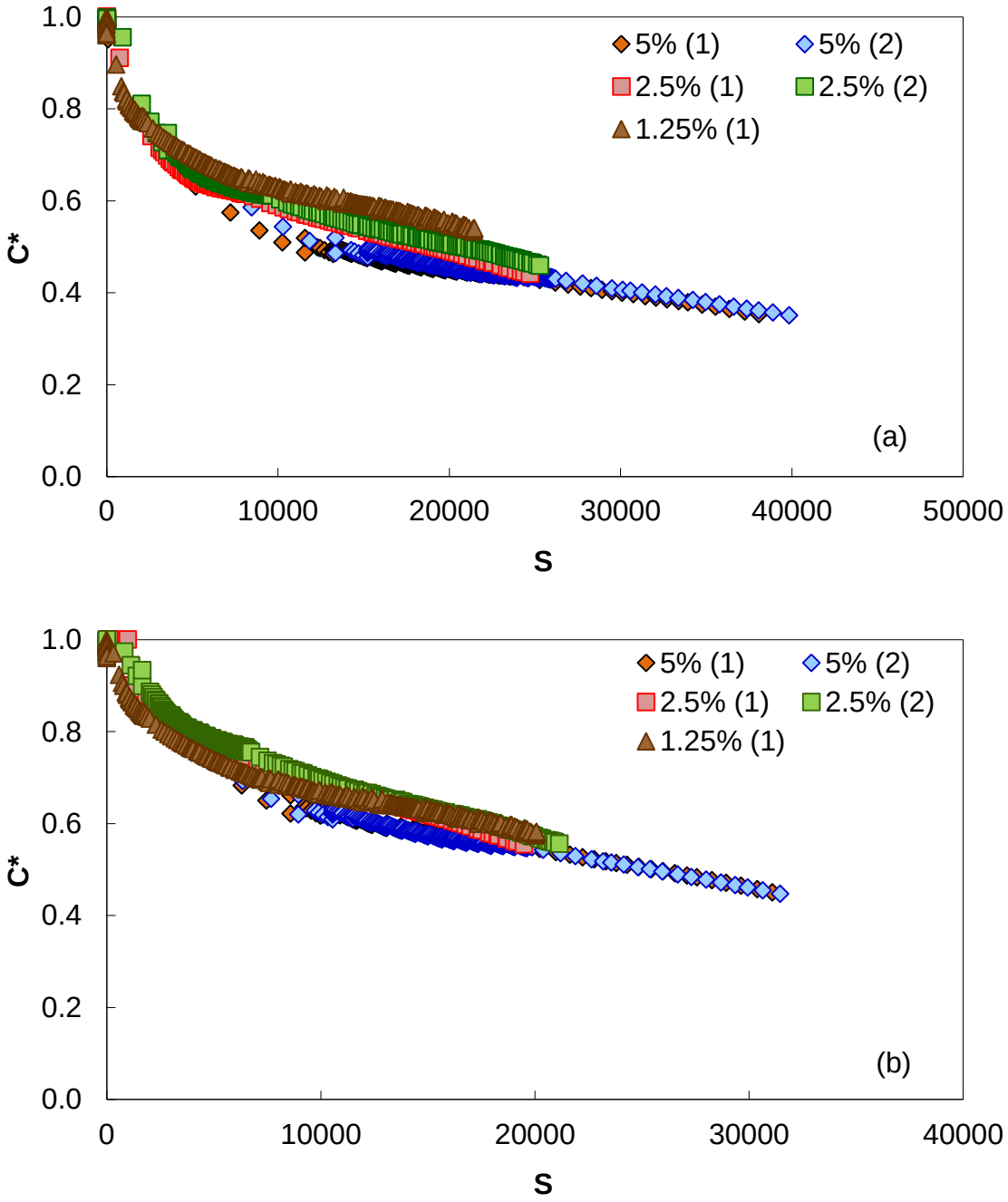

Figure 4-13: Damage Characteristic Curve for RAM: (a) Linear Based; (b) Non-Linear Based.

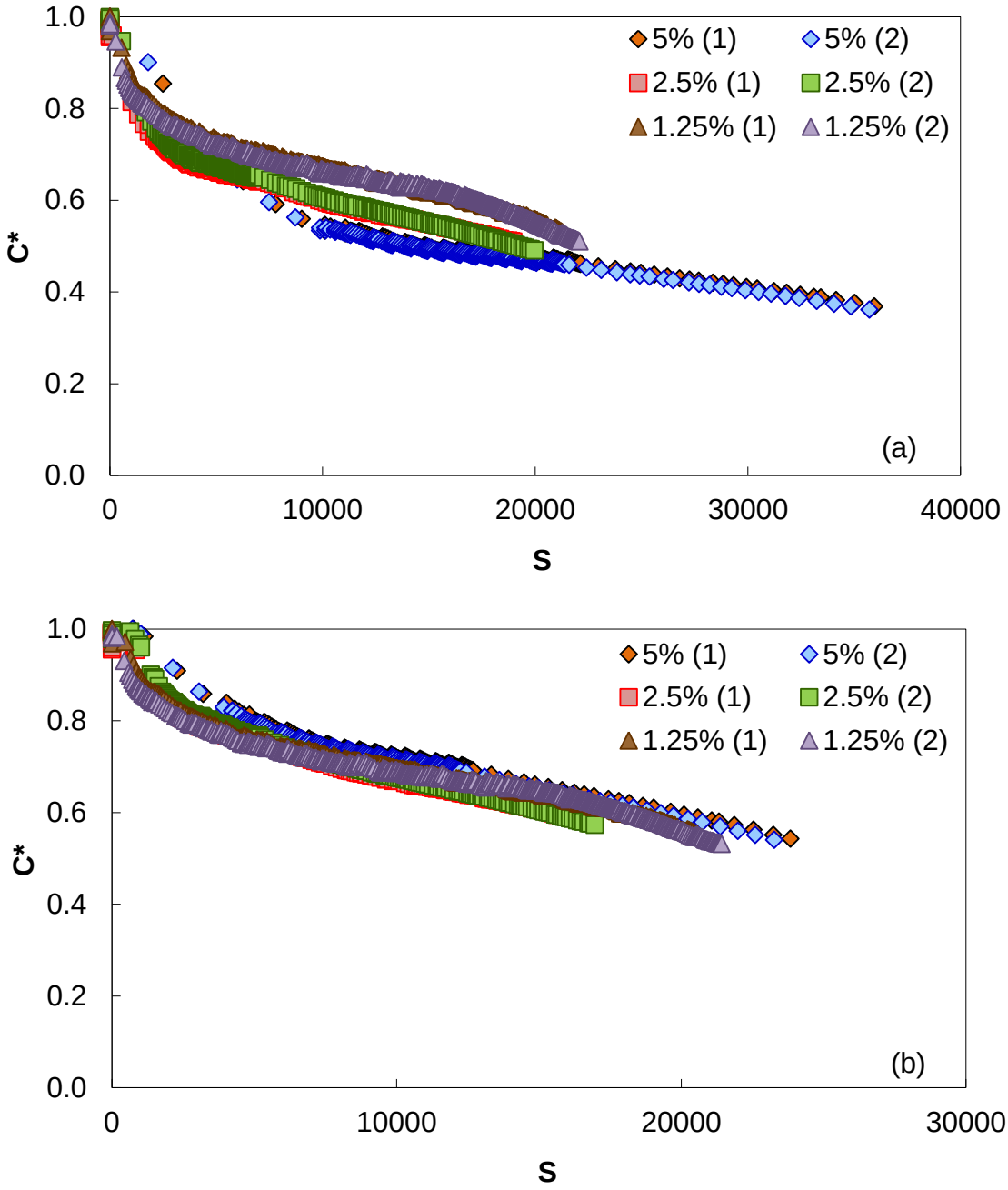

Figure 4-14: Damage Characteristic Curve for RAP 10: (a) Linear Based; (b) Non-Linear Based.

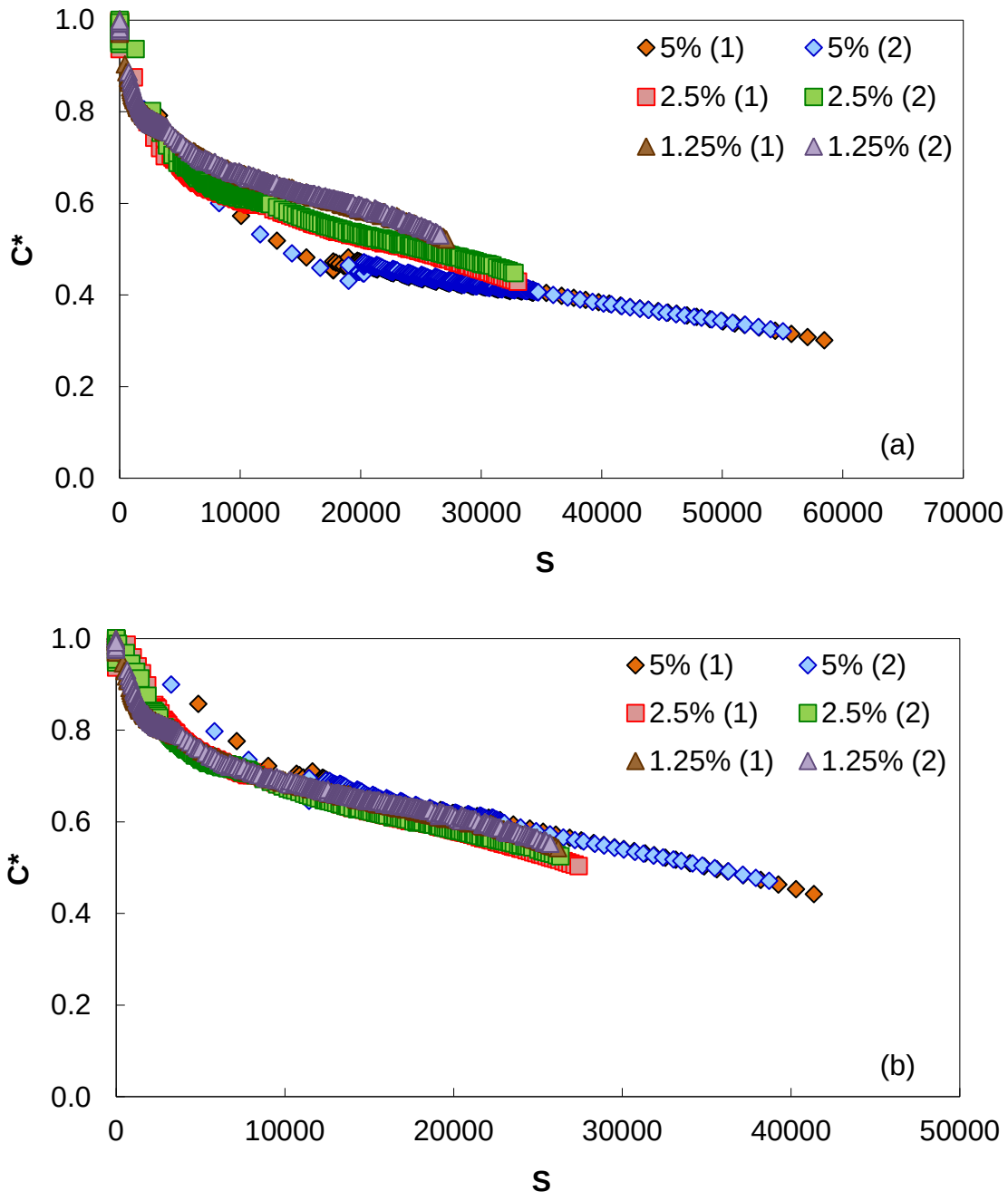

Figure 4-15: Damage Characteristic Curve for RAP 30: (a) Linear Based; (b) Non-Linear Based.

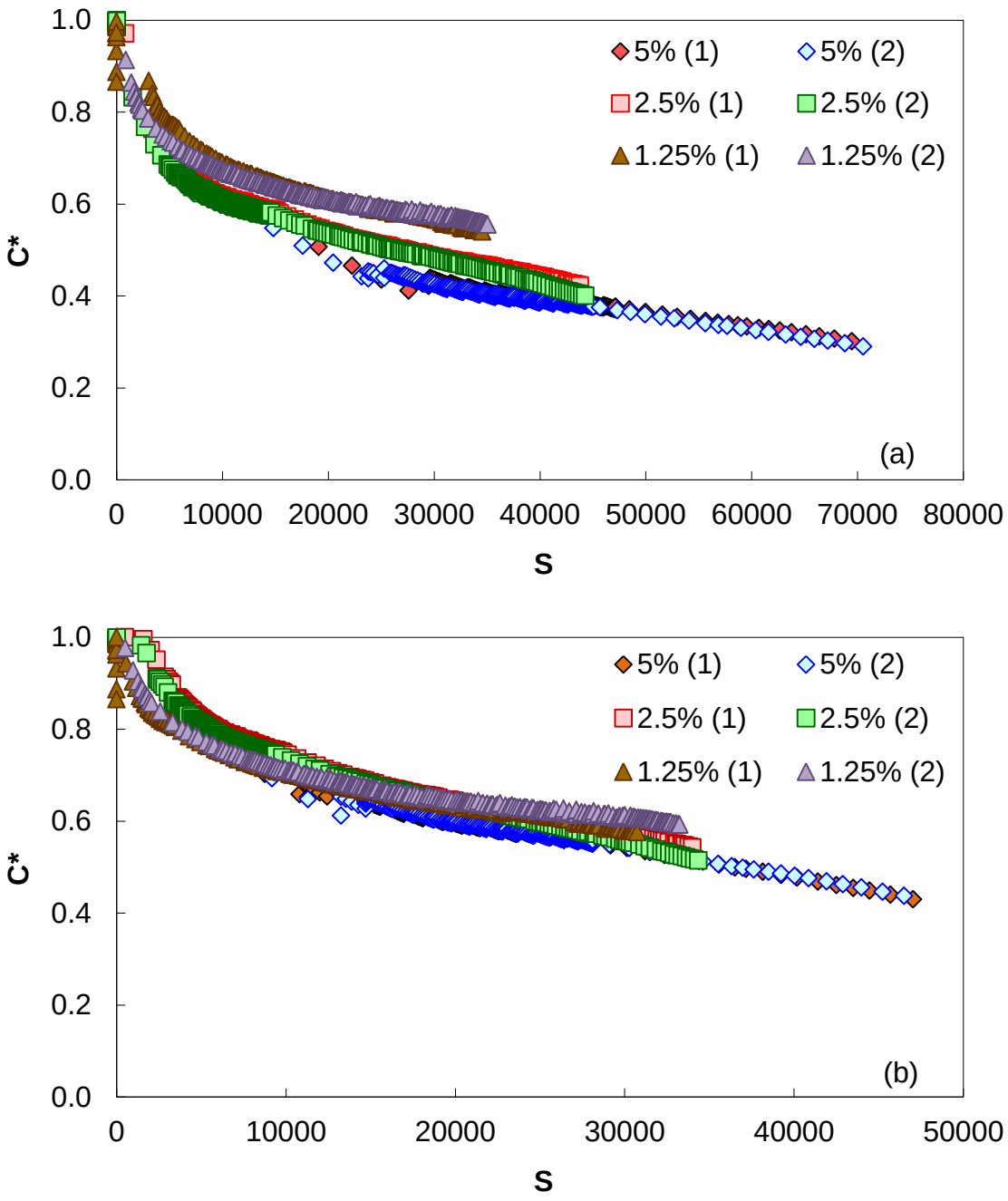

Figure 4-16: Damage Characteristic Curve for RAP 50: (a) Linear Based; (b) Non-Linear Based.

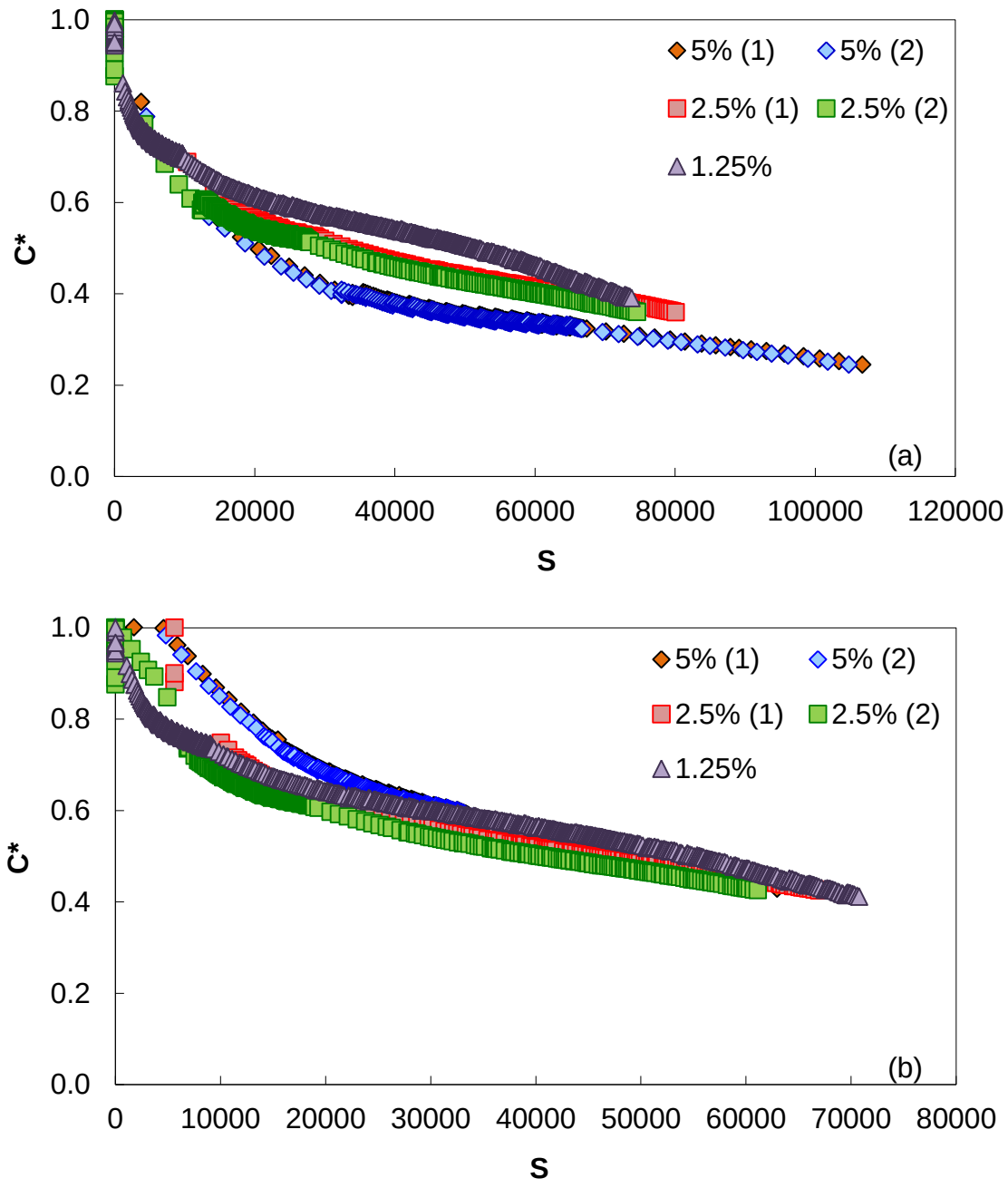

Figure 4-17: Damage Characteristic Curve for RAP 100: (a) Linear Based; (b) Non-Linear Based.

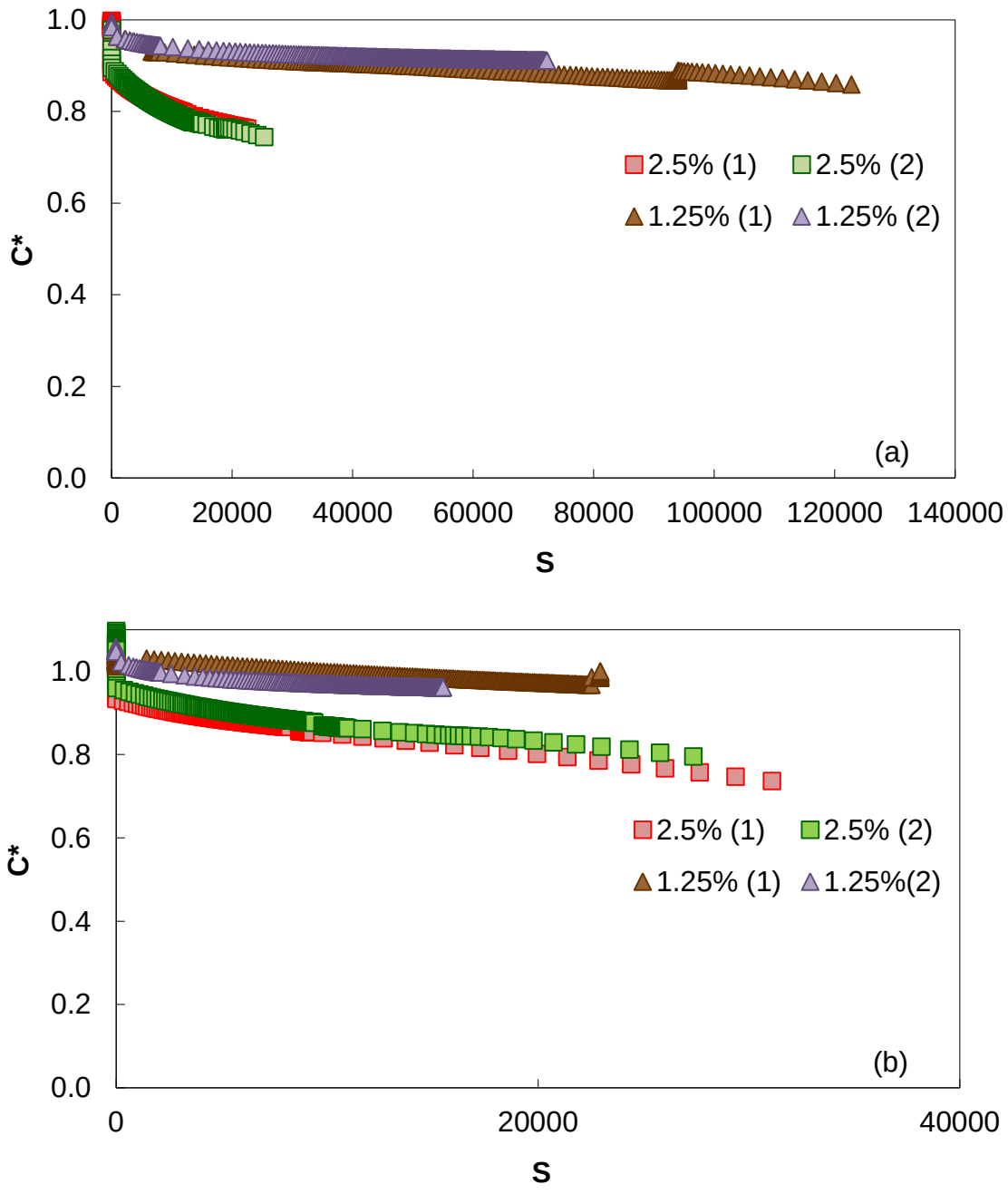

Figure 4-18: Damage Characteristic Curve for RB: (a) Linear Based; (b) Non-Linear Based.

4.3 Micromechanical Modeling of Non-Modified and RAP Modified Mastics

Micromechanical models have been used extensively to predict the properties of the composite when the properties and proportions of individual components are known. Micromechanical models and their applications have continuously evolved over the years. Micromechanical models consider any composite material to of two basic phases, (i) matrix and (ii) rigid inclusions. However, before the use of micromechanical models became common, dilute and empirical formulations which consider the inclusions as isodisperse globules have been formulated [39]. In this section, the empirical formulations are first discussed, followed by the micromechanical models. A comprehensive list of empirical formulations was presented by Underwood [32], few of which are discussed below.

4.3.1 Dilute and Empirical Models

The formulations for these models seek to predict the response of the composite by assuming it as a two material blend consisting of isodisperse globules and a matrix. Einstein [39] derived a formulation, as shown in Equation (4.13), based on the principles of thermodynamics and energy balance.

$$\frac{\eta_c}{\eta} = 1 + 2.5C_v \tag{4.13}$$

In Equation (4.13), C_v is the volumetric concentration of the isodisperse globules, η is the viscosity of the matrix and η_c is the viscosity of the composite. Einstein in his derivation neglected higher order terms, which were determined by De Bruijn [51] and the new formulation is presented in Equation (4.14)

$$\frac{\eta_c}{\eta} = 1 + 2.5C_v + 1.55C_v^{\,2} \tag{4.14}$$

Ward and Whitmore [52] applied DeBruijn's equation to particles having particular size distributions and concluded that for such material the constant factor in front of the particle concentration could range from 2.1 to 3.6. Roscoe [53] used Ward and Whitmore's formulation and developed a solution as shown in Equation (4.15) for particles of graded sizes.

$$\frac{\eta_c}{\eta} = \left(1 - C_v\right)^{-2.5} \tag{4.15}$$

It can be seen that Roscoe's equation is a little similar to Einstein's formulation. In fact Underwood [32] reported that the equation can be reduced to Einstein's equation at low concentrations. Equation (4.15) tends to infinity at volumetric concentration of 100%, so a new formulation shown in Equation (4.16) which limits the volumetric concentration at 74% was developed by Roscoe. The significance of the number 74% stems from the fact that the maximum packing fraction for same sized spherical particles is 74%.

$$\frac{\eta_c}{\eta} = \left(1 - \frac{1}{0.74} C_v\right)^{-2.5} \tag{4.16}$$

There have been other empirical formulations which have been developed by authors over the years, and are presented by Underwood in [32]. The relevance of these models to asphalt mastics is associated with its applicability to $|G^*|$ which has been studied by Underwood [32], Kim [46], and Faheem and Bahia [48].

4.3.2 Micromechanical Models

The very essence of micromechanical models as mentioned in Section 4.1 was to predict the fundamental properties of the composite based upon the principle of micromechanics. Many micromechanical models have been developed by various authors over the years, the most notable contributions being Paul [54], Eshelby [55], Hashin [40], Hashin and Shtrikman [56], Christensen and Lo [38], and Herve and Zaoui [42].

Paul's model formulation [54] is a simple micromechanical solution based on the weighted volumetric concentrations of the different phases in the composite. The model is often referred to as rule of mixtures in literature. Paul proposed a lower and upper bound to the model, as shown in Equations (4.17) and(4.18). G_l^* and G_u^* are the lower and upper bounds for the shear modulus. G_n and V_n are the shear moduli and the volumetric concentration of the n^{th} phase (the total number of phases are denoted by N).

The equations for the lower and upper bounds proposed by Paul are basically solutions to a series and a parallel spring analog respectively as shown in Figure 4-19 and Figure 4-20. The lengths in the series analog and the areas in the parallel analog denote the volumetric concentrations and the stiffness of the springs denote the modulus. The analogs shown below are for N=2 in Paul's model.

$$G_l^* = \left[\sum_{N=1}^{n} \frac{V_n}{G_n} \right]^{-1} \tag{4.17}$$

$$G_u^* = \sum_{N=1}^{n} G_n V_n \tag{4.18}$$

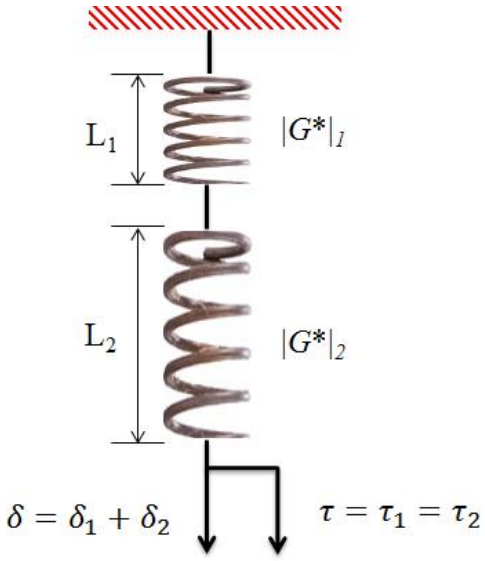

Figure 4-19: Series Spring Analog.

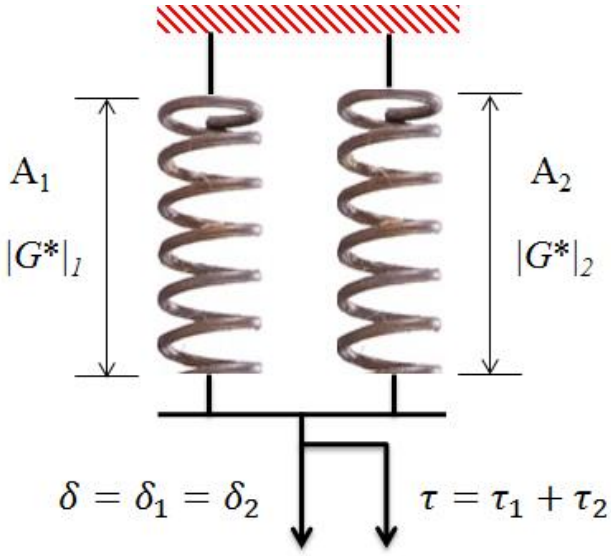

Figure 4-20: Parallel Spring Analog.

Eshelby [55] developed a model for small scale elastic deformations when rigid inclusions are introduced into a medium. The ratio of modulus of composite to the modulus of the matrix modulus of matrix was given by Equation (4.19). G_c, G_m, and G_p

are the modulus of the composite, matrix and the particles respectively. The term v_m represents the Poisson's ratio of the matrix and C_v is the volumetric concentration of the particulates. Underwood [32] reported that this equation is reduced to Einstein's equation as shown in Equation (4.13) when the Poisson's ratio of the matrix is equal to 0.5 and G_p is equal to ∞, i.e. when the particles are rigid.

$$\frac{G_c}{G_m} = 1 - \frac{15(1-\nu_m)\left(1-\frac{G_p}{G_m}\right)}{7-5\nu_m+2(4-5\nu_m)\frac{G_p}{G_m}C_v} \tag{4.19}$$

Hashin [40] derived the bounds for shear moduli by considering the change in strain energy in a homogenous body due to the inclusion of non-homogenities. The author assumed the particles to be spherical and that the action of the surrounding heterogeneous medium on any one inclusion is transmitted via a spherical shell, which is wholly contained in the matrix. Hashin also assumed the ratio of this spherical shell to the size of the particle to be constant. The volume of the material not occupied by the sphere or this surrounding sphere is considered to be in a constant state of deviatoric stress or strain. Hashin idealized that this volume can be reduced to an infinitesimally small fraction by filling in particulates. As a result, at the limit the strain energy of the composite body will approach the summation of the strain energy of the spheres with its spherical shell. Although Hashin developed a lower and upper bound based formulation for the prediction of composite modulus, he derived a closed form solution with an approximation of the bounds being close together and that the resultant modulus always lies between these bounds. The equation for the ratio between shear modulus of the

composite to the matrix is presented in Equation (4.20). The definitions of G_c, G_m, G_p, ν_m, and C_v are the same as mentioned earlier.

$$\frac{G_c^*}{G_m^*} = 1 + \frac{15(1-\nu_m)\left(\frac{G_p}{G_m} - 1\right)C_v}{7 - 5\nu_m + 2(4-5\nu_m)\left[\frac{G_p}{G_m} - \left(\frac{G_p}{G_m} - 1\right)C_v\right]} \tag{4.20}$$

The model developed by Hashin Equation (4.20) is applicable to only two phase materials. Hashin and Shtrikman [56] derived bounds for shear modulus of multiphase materials. The Equations (4.21) and (4.22) show the bounds for a two phase material. The authors considered the constituent materials as mechanical mixtures of a number of different isotropic and homogenous elastic phases. As a result, the resultant composite can be assumed as a quasi-isotropic and quasi-homogeneous material with materials of multiple phases. The authors reported that arriving at the modulus bounds for a quasi-isotropic and quasi-homogeneous material based on the principles of strain energy is an herculean task. However, the authors used variational principles of elasticity in order to bound the strain energy and thus the modulus predictions. The consideration of arbitrary phase geometry was taken up by Paul [54] but the bounds obtained were not close enough. The present model developed by Hashin and Shtrikman is also based on the consideration of arbitrary phase geometry and the objective is to improve the bounds developed by Paul. The authors have found that the bounds developed for shear modulus were farther than what Hashin derived previously. The authors reported that since the definition of the materials is more general and that none of the materials is classified as

either matrix or inclusion, the results are not surprising. The equations presented below are valid when $G_1 < G_2$.

$$G_l^* = G_1 + \frac{V_2}{\frac{1}{(G_2 - G_1)} + \frac{6V_1(K_1 + 2G_1)}{5G_1(3K_1 + 4G_1)}} \tag{4.21}$$

$$G_u^* = G_2 + \frac{V_1}{\frac{1}{(G_1 - G_2)} + \frac{6V_2(K_2 + 2G_2)}{5G_2(3K_2 + 4G_2)}} \tag{4.22}$$

where

G_1, G_2 = shear modulus of phase 1 and phase 2 materials respectively and

K_1, K_2 = bulk modulus of phase 1 and phase 2 materials respectively.

For the present study since the bulk modulus of the materials is not known, they have been converted to shear modulus using Equation (4.23).

$$K = \frac{2G(1+\nu)}{3(1-2\nu)} \tag{4.23}$$

Christensen and Lo [41] developed a model called the generalized self-consistent scheme model which considers the particle to be coated by a matrix shell of known properties. The particle along with the matrix shell is surrounded by a material whose properties are equivalent to that of the coated particle. The schematic of the model is shown in Figure 4-21.

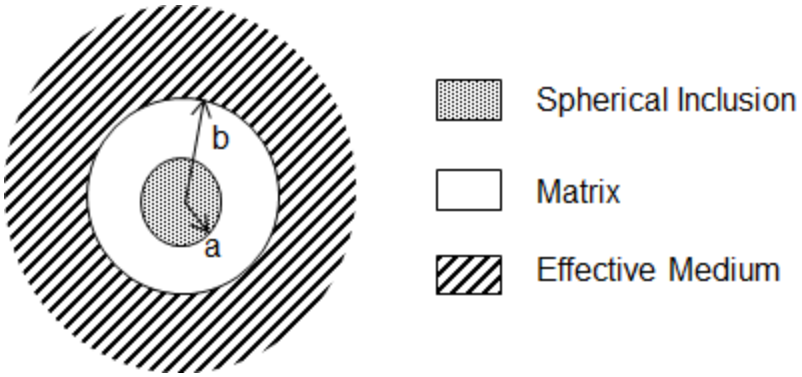

Figure 4-21: Generalized Self Consistent Scheme Model Schematic.

The model solution can be expressed in terms of a simple quadratic equation as shown in Equation (4.24).

$$A\left(\frac{G_c}{G_m}\right)^2 + B\left(\frac{G_c}{G_m}\right) + C = 0 \tag{4.24}$$

where

$$A = 8\left(\frac{G_p}{G_m} - 1\right)\left(4 - 5\nu_m\right)k_1 C_v^{10/3} - 2\left[63\left(\frac{G_p}{G_m} - 1\right)k_2 + 2k_1 k_3\right]C_v^{7/3} + 252\left(\frac{G_p}{G_m} - 1\right)k_2 C_v^{5/3} - 50\left(\frac{G_p}{G_m} - 1\right)\left(7 - 12\nu_m + 8\nu_m^2\right)k_2 C_v + 4\left(7 - 10\nu_m\right)k_2 k_3 \tag{4.25}$$

$$B = -4\left(\frac{G_p}{G_m} - 1\right)\left(1 - 5\nu_m\right)k_1 C_v^{10/3} + 4\left[63\left(\frac{G_p}{G_m} - 1\right)k_2 + 2k_1 k_3\right]C_v^{7/3} - 504\left(\frac{G_p}{G_m} - 1\right)k_2 C_v^{5/3} + 150\left(\frac{G_p}{G_m} - 1\right)\left(3 - \nu_m\right)\nu_m k_2 C_v + 3\left(15\nu_m - 7\right)k_2 k_3 \tag{4.26}$$

$$C = 4\left(\frac{G_p}{G_m}-1\right)\left(5\nu_m-7\right)k_1C_v^{10/3} - 2\left[63\left(\frac{G_p}{G_m}-1\right)k_2 + 2k_1k_3\right]C_v^{7/3} + 252\left(\frac{G_p}{G_m}-1\right)k_2C_v^{5/3} + 25\left(\frac{G_p}{G_m}-1\right)\left(\nu_m^2-7\right)k_2C_v - \left(7+5\nu_m\right)k_2k_3 \quad (4.27)$$

$$k_1 = \left(\frac{G_p}{G_m}-1\right)\left(49-50\nu_p\nu_m\right) + 35\left(\frac{G_p}{G_m}\right)\left(\nu_p-2\nu_m\right) + 35\left(2\nu_p-\nu_m\right), \quad (4.28)$$

$$k_2 = 5\nu_p\left(\frac{G_p}{G_m}-8\right) + 7\left(\frac{G_p}{G_m}+4\right), \quad (4.29)$$

$$k_3 = \left(\frac{G_p}{G_m}\right)\left(8-10\nu_m\right) + \left(7-5\nu_m\right), \quad (4.30)$$

G_p = modulus of the filler

G_m = modulus of the matrix

v_p = Poisson's ratio of the filler

v_m = Poisson's ratio of the matrix, and

C_v = Volumetric concentration of the filler

Herve and Zaoui [42] proposed an *n*-layered inclusion based micromechanical model which is a generalized form of the model proposed by Christensen and Lo [41]. The model accounts for inclusions coated with *n* number layers which are distinct. Along with the inclusion the model can be treated as a *n+1* phase model. Due to the generalization of the model, its complexity has also increased. The conventions used by Underwood in [32] have been replicated and presented below. Underwood [32] reports that under simple shear, the model reduces to the form shown in Equation (4.24). However the coefficients *A*, *B*, and *C* are defined differently as shown in Equations (4.31)

, (4.32), (4.33). The conventions followed in the equations are consistent with that of Herve and Zaoui where *n* denotes the matrix and *n-1* denotes the layer immediately adjacent to the matrix. For example, consider a spherical inclusion coated uniformly with material *A* and present in a matrix of material *B*, then *A* would be the *n-1* layer and *B* would be the n^{th} layer. R_k is the radius at the interface and the index used is such that $R_1 < R_2 < R_3 < R_n$. In all of the conventions the lowest number is assigned to the innermost material. The radius of the outer shell R_n is assumed to be unity and from that the radius of other phases can be calculated based on their respective volume concentrations. For the inclusion, the radius is given by Equation (4.38) and in general by Equation (4.39).

$$A = 4(1-2\nu_n)(7-10\nu_n)\,Z_{12} + 20(7-12\nu_n+8\nu_n^{\,2})\,Z_{42} + 12(1-2\nu_n)(Z_{14}-7Z_{23}) + 20\left(1-2\nu_n\right)^2 Z_{13} + 16(4-5\nu_n)(1-2\nu_n)\,Z_{43} \tag{4.31}$$

$$B = 3(1-2\nu_n)(15\nu_n-7)\,Z_{12} + 60(\nu_n-3)\nu_n\,Z_{42} - 24(1-2\nu_n)(Z_{14}-7Z_{23}) - 40\left(1-2\nu_n\right)^2 Z_{13} - 8(1-5\nu_n)(1-2\nu_n)\,Z_{43} \tag{4.32}$$

$$C = -(1-2\nu_n)(7+5\nu_n)\,Z_{12} + 10(7-\nu_n^{\,2})\,Z_{42} + 12(1-2\nu_n)(Z_{14}-7Z_{23}) + 20\left(1-2\nu_n\right)^2 Z_{13} - 8(7-5\nu_n)(1-2\nu_n)\,Z_{43} \tag{4.33}$$

where

$$Z_{\alpha\beta} = P_{\alpha 1}^{(n-1)} P_{\beta 2}^{(n-1)} - P_{\beta 1}^{(n-1)} P_{\alpha 2}^{(n-1)} \tag{4.34}$$

$$\mathbf{P}^{(n-1)} = \prod_{j=1}^{n-1} \mathbf{M}^{(j)} \tag{4.35}$$

$$\mathbf{M}^{(k)} = \mathbf{L}_{k+1}^{-1}(R_k)\mathbf{L}_k(R_k) \tag{4.36}$$

$$\mathbf{L}_i(r)=\begin{bmatrix} r & -\frac{6\nu_i}{1-2\nu_i}r^3 & \frac{3}{r^4} & \frac{5-4\nu_i}{1-2\nu_i}\frac{1}{r^2} \\ r & -\frac{7-4\nu_i}{1-2\nu_i}r^3 & -\frac{2}{r^4} & \frac{2}{r^2} \\ G_i & \frac{3G_i\nu_i}{1-2\nu_i}r^2 & -\frac{12G_i}{r^5} & \frac{2G_i(\nu_i-5)}{1-2\nu_i}\frac{1}{r^3} \\ G_i & -\frac{G_i(7+2\nu_i)}{1-2\nu_i}r^2 & \frac{8G_i}{r^5} & \frac{2G_i(1+\nu_i)}{1-2\nu_i}\frac{1}{r^3} \end{bmatrix} \tag{4.37}$$

$$R_1=(C_v)^{1/3} \tag{4.38}$$

$$R_k=\left[\frac{V_k}{100}-R_{k-1}^3\right]^{1/3} \tag{4.39}$$

4.3.3 Applications of Micromechanical Models to Non-Modified and RAP Modified Asphalt Mastics

Micromechanical models can be used to predict the modulus of the composite when the properties and concentrations of the constituent phases are known. In the present study, the micromechanical models discussed in Section 4.3.2 are applied to predict the modulus of both RAP modified and non-RAP modified asphalt mastics. However, the application of the models to RAP modified mastics is a bit challenging. All the models discussed in Section 4.3.2, except for Herve and Zaoui model limit the number of phases present in the composite. This limitation in particular makes it challenging to predict the blended RAP mastics, RAP 10, RAP 30, RAP 50 and RAP 100 as these are known to have both virgin and RAP components, thereby corresponding to multiple phases. So, in order to make the predictions a little simpler, the individual material components of the blended RAP mastics have been smeared together i.e. the

RAP mastics (RAP 10, RAP 30 and RAP 50) can now be described as a blend of two components, RAP 100 and VM. Accordingly the volumetric calculations have been worked out and are as shown in APPENDIX C. A summary of the calculations showing the volumetric proportions of RAP 100 and VM in RAP mastics are shown in Table 4-5.

Table 4-5: The Proportions of VM and RAP 100 in RAP 10, RAP 30 and RAP 50

Material	% VM	% RAP 100
RAP 10	84.63	15.37
RAP 30	58.78	41.22
RAP 50	37.86	62.14

Modeling VM and RAM is straight forward as the volumetric concentrations of filler and binder are known to be 27% and 73% respectively. The results for each of the study materials for a particular model are presented at three temperatures, 10°, 30°, and 54°C and at three frequencies 15 Hz, 5 Hz and 0.5 Hz representing high, moderate and low frequencies.

4.3.3.1 Paul's Rule of Mixtures

The predictions were made using Equations (4.17) and (4.18). For the present case, N=2, where G_1 , G_2 are the modulus of RAP 100 and VM , and V_1, V_2 refer to their corresponding volumes as indicated in Table 4-5. The important observations made from predictions of the study materials, as shown in Figure 4-22 to Figure 4-27, using Paul's rule of mixtures are as below:

- All the mastics, both RAP modified and non- RAP modified plot near the lower bound of the model. This finding is consistent with findings of Buttlar et al. [44] who attributed the behavior to minimal particle interactions. If the composite had

more rigid particle interactions, then the predicted values would be closer to upper bounds.

- It is found that as the temperature increases, the area between the bounds increases, which means the error in prediction, will increase with increase in temperature.
- Comparing the predictions for RAP modified and non-RAP modified mastics, it is seen that the area between the bounds is greater for non-RAP modified mastics. This can be attributed to the greater difference in stiffness of constituents in the non-RAP modified mastics.

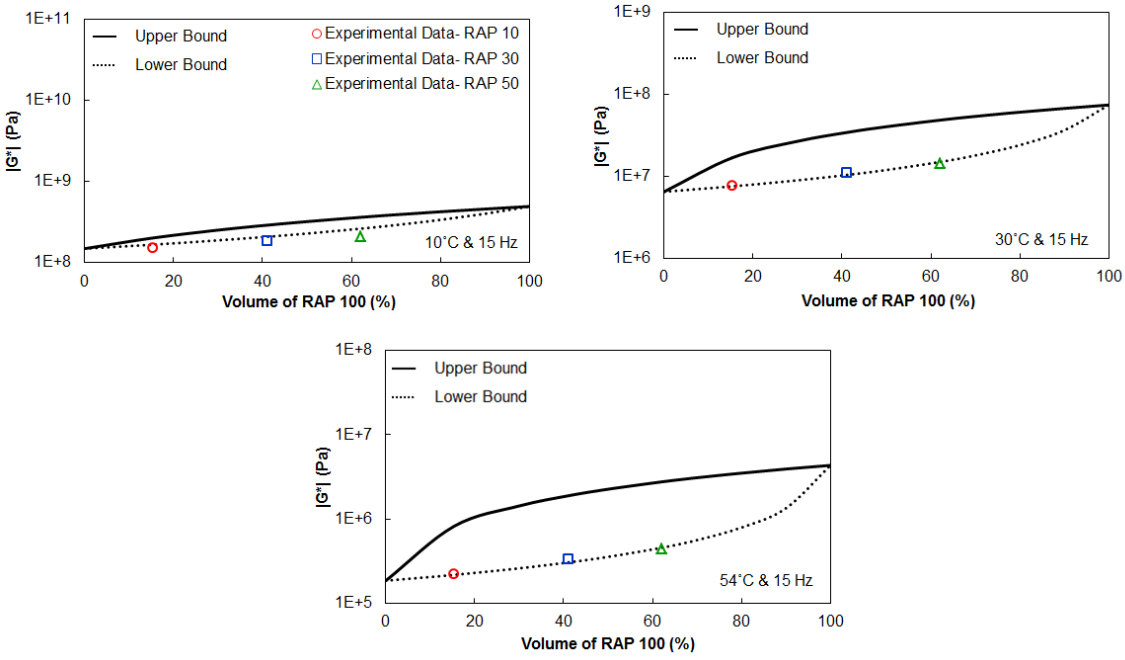

Figure 4-22: Predictions for RAP Modified Mastics at High Frequency Using Paul's Rule of Mixtures.

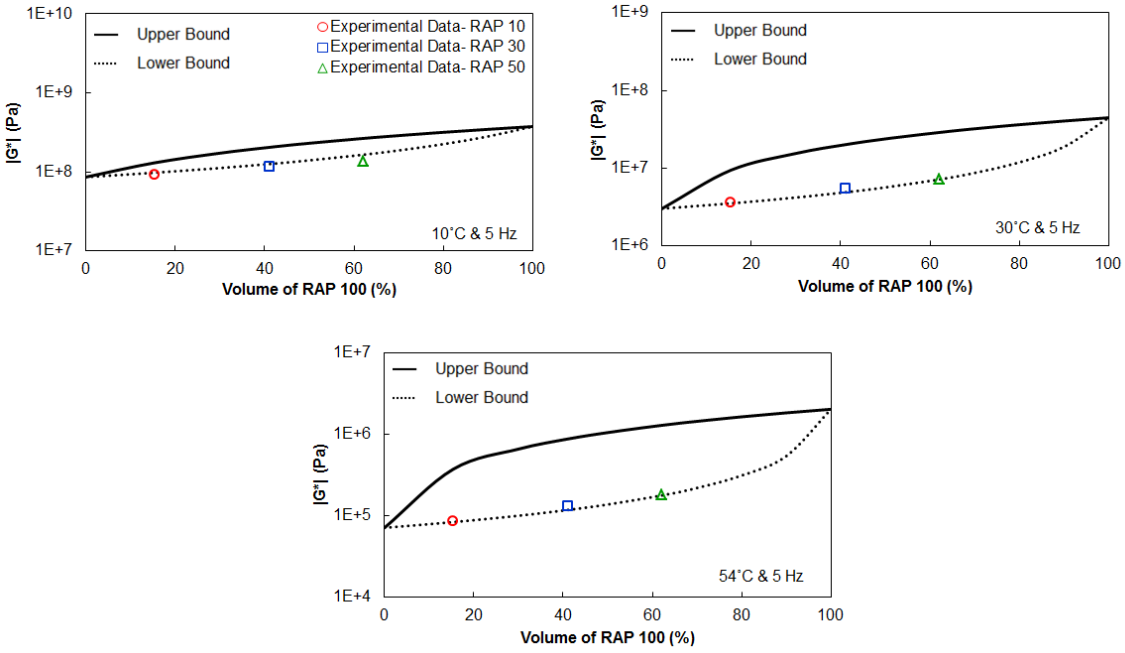

Figure 4-23: Predictions for RAP Modified Mastics at Moderate Frequency Using Paul's Rule of Mixtures.

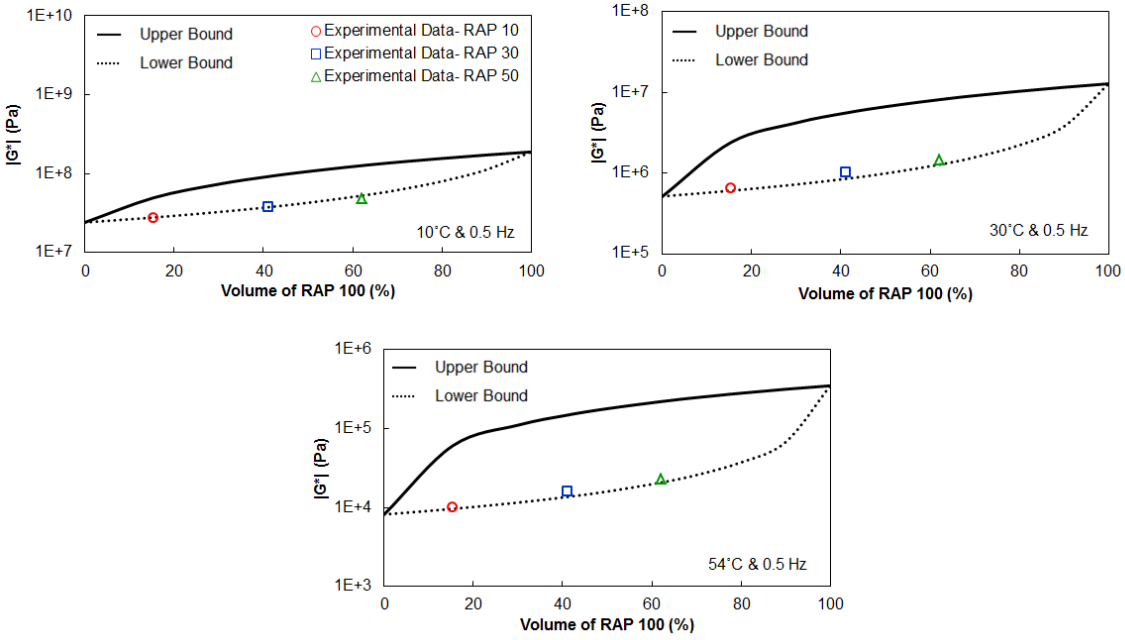

Figure 4-24: Predictions for RAP Modified Mastics at Low Frequency Using Paul's Rule of Mixtures.

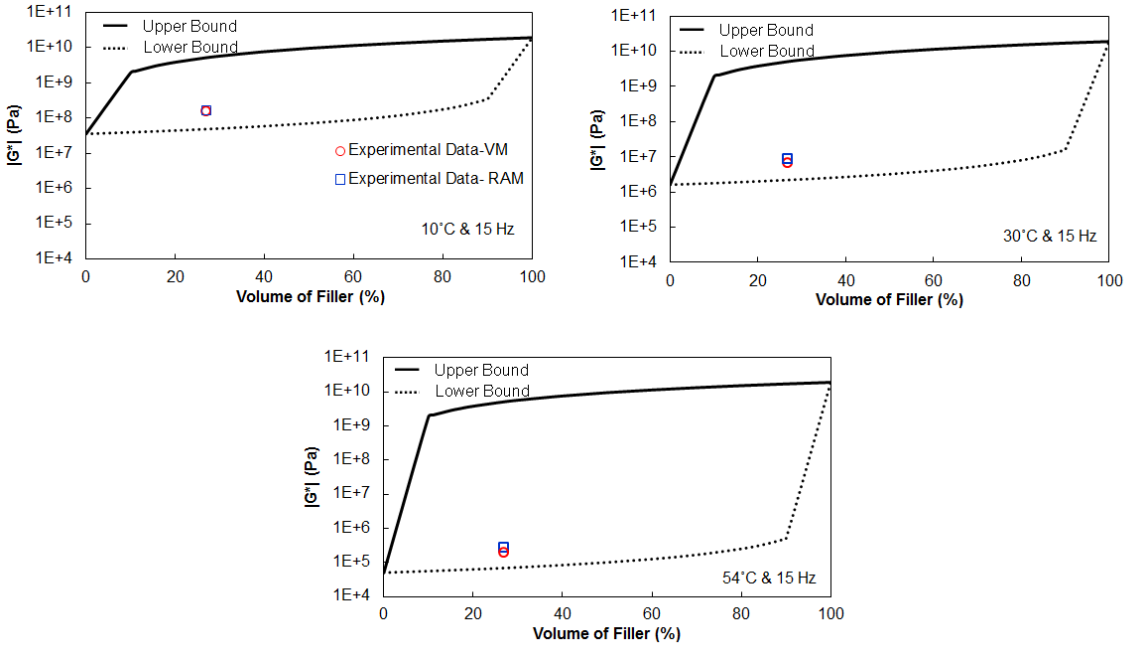

Figure 4-25: Predictions for VM and RAM at High Frequency Using Paul's Rule of Mixtures.

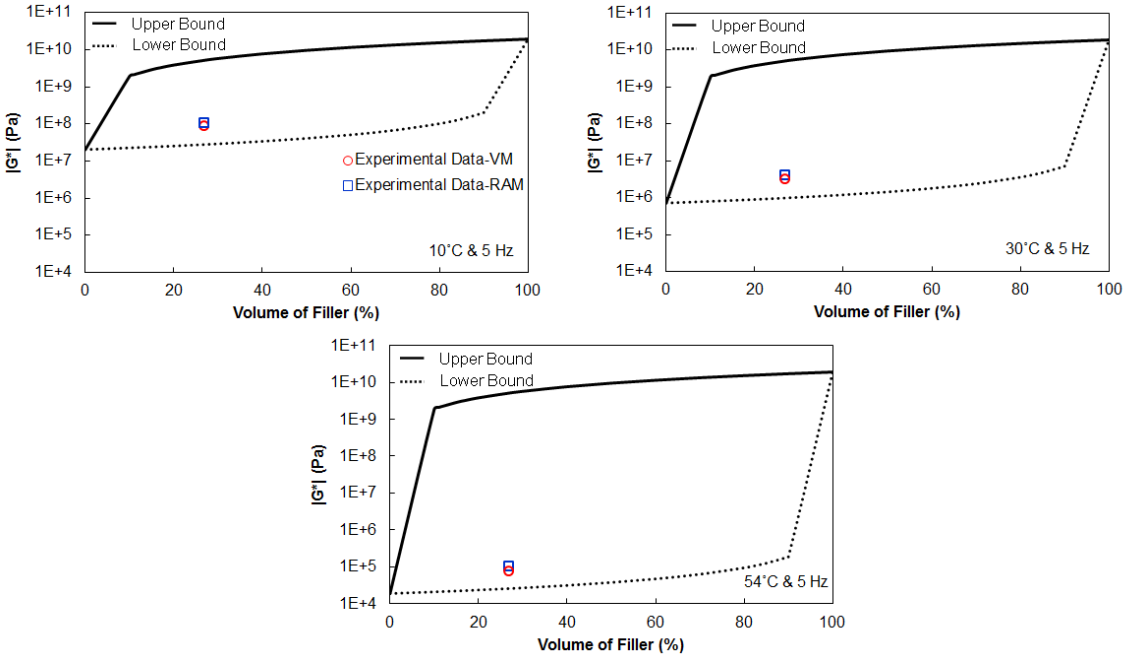

Figure 4-26: Predictions for VM and RAM at Moderate Frequency Using Paul's Rule of Mixtures.

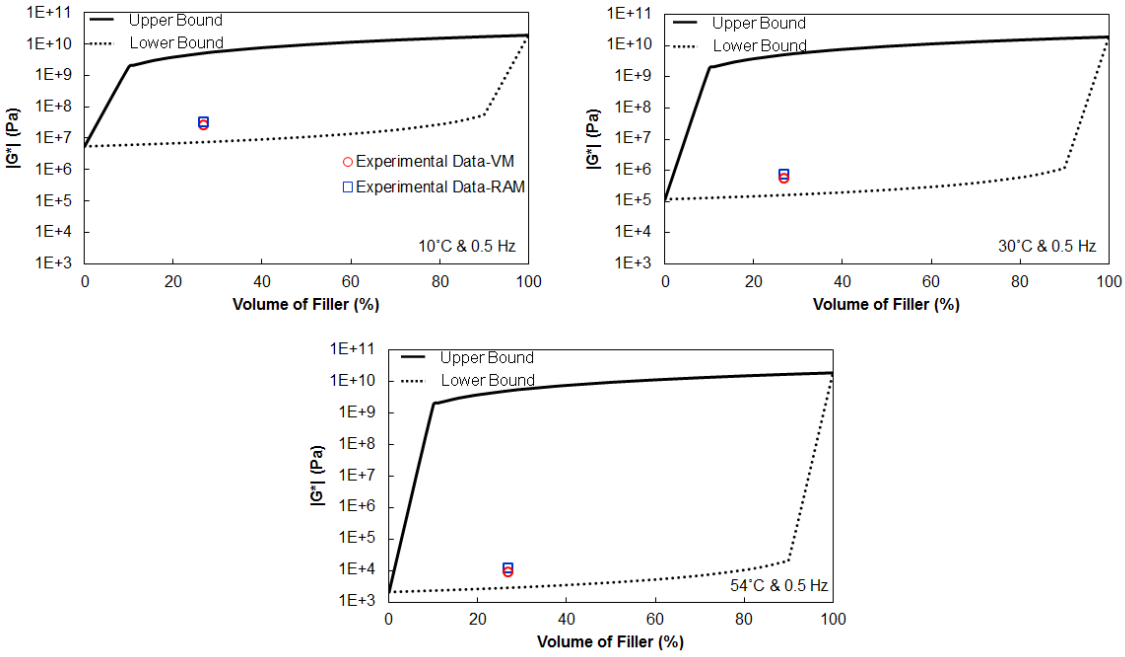

Figure 4-27: Predictions for VM and RAM at Low Frequency Using Paul's Rule of Mixtures.

Although the predictions for the RAP mastics are closer to the lower bound of the model, it cannot be considered acceptable prediction based on the blending assumptions, the poor predictions for VM and RAM, and lack of physical insight.

4.3.3.2 Hashin's Model

The model proposed by Hashin, Equation (4.20), was used to predict the stiffness of the unmodified and RAP modified composites. Since, the equation is a closed form solution, actual predicted values were arrived at instead of bounded solutions. The predictions were carried out at the same conditions as mentioned earlier. For, the RAP modified mastics, RAP 10, RAP 30, and RAP 50 the constituents were assumed to as VM and RAP 100. VM was considered as the matrix and RAP 100 was considered as the particulates. The percentage difference between predicted and experimental data was

used to gauge the quality of prediction. The observations made from the predictions are as follows and the data is presented in Figure 4-28 to Figure 4-35 :

- The model greatly underestimates the modulus of VM and RAM. For VM, the percentage difference for the temperatures and frequencies evaluated are in the range of 93% - 128%. For RAM, the percentage differences range from 130% - 210%.
- The predictions for the RAP modified mastics were better than those for VM or RAM. The model overestimated the stiffness values for RAP 10, RAP 30, and RAP 50.The percentage difference for RAP 10 ranged from 12% to 16%, for RAP 30 from 20% to 30%, and for RAP 50 from 33% to 42%.
- The observation from the predictions of RAP modified mastic seem to support the finding from VM and RAM, that is the error in prediction increases with increase in difference in stiffness between the component materials.
- Also, it is seen that in general the error in predictions increased with temperature. As temperature increases, stiffness difference between the components increases, thus resulting in higher error's.

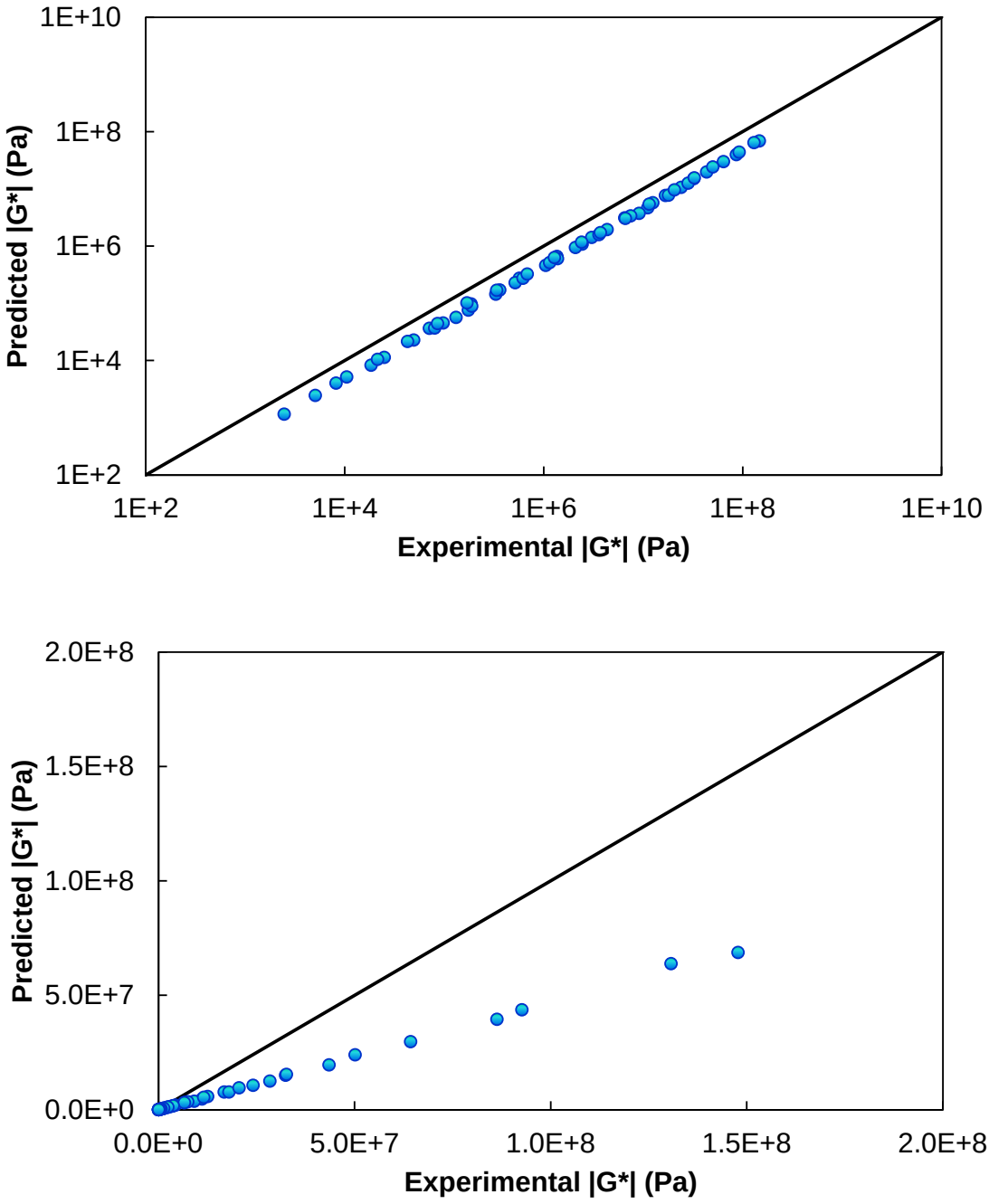

Figure 4-28: Verification of Hashin's Model for VM: (a) log-log space; (b) arithmetic space

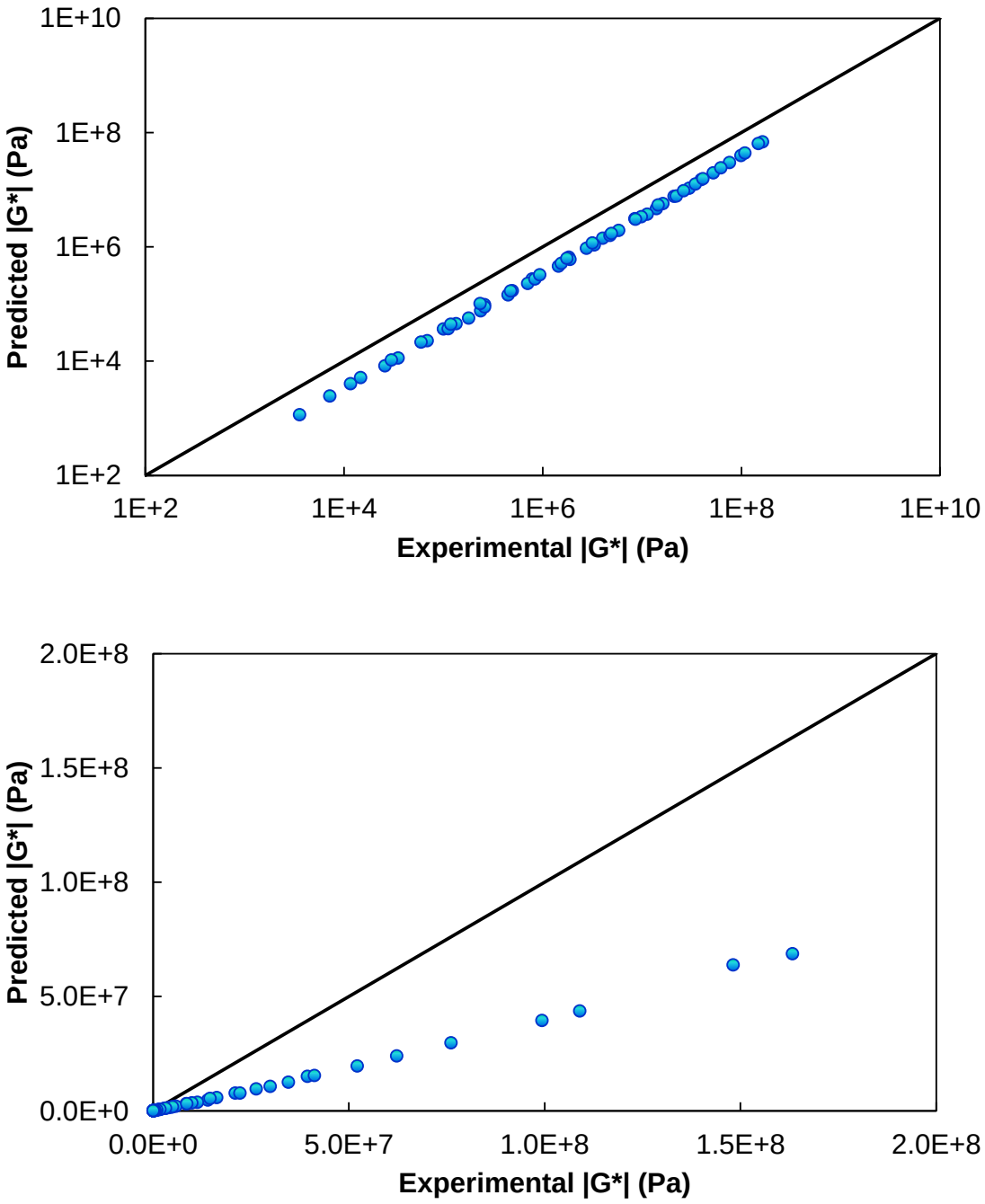

Figure 4-29: Verification of Hashin's Model for RAM: (a) log-log space; (b) arithmetic space.

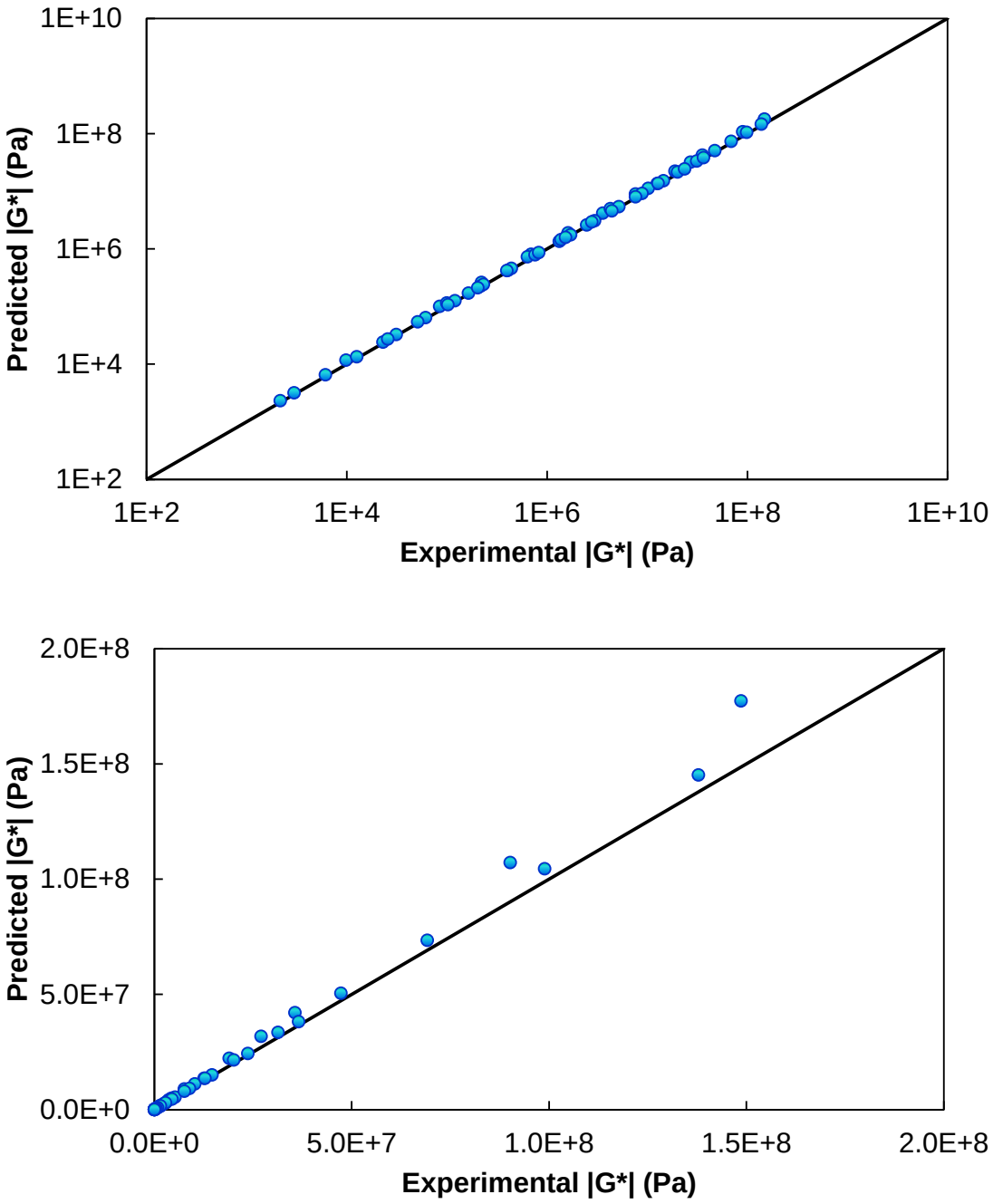

Figure 4-30: Verification of Hashin's Model for RAP 10: (a) log-log space; (b) arithmetic space.

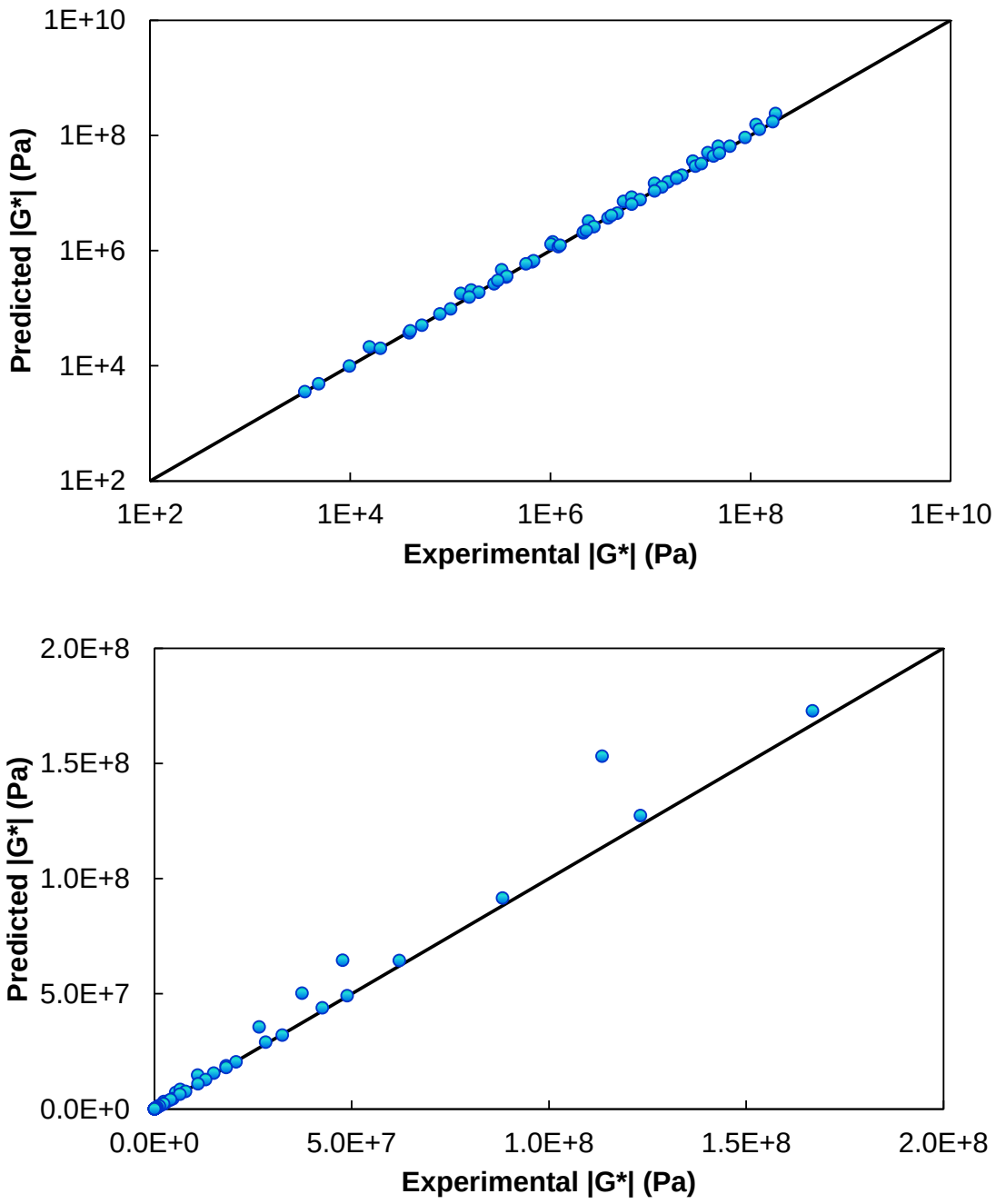

Figure 4-31: Verification of Hashin's Model for RAP 30: (a) log-log space; (b) arithmetic space.

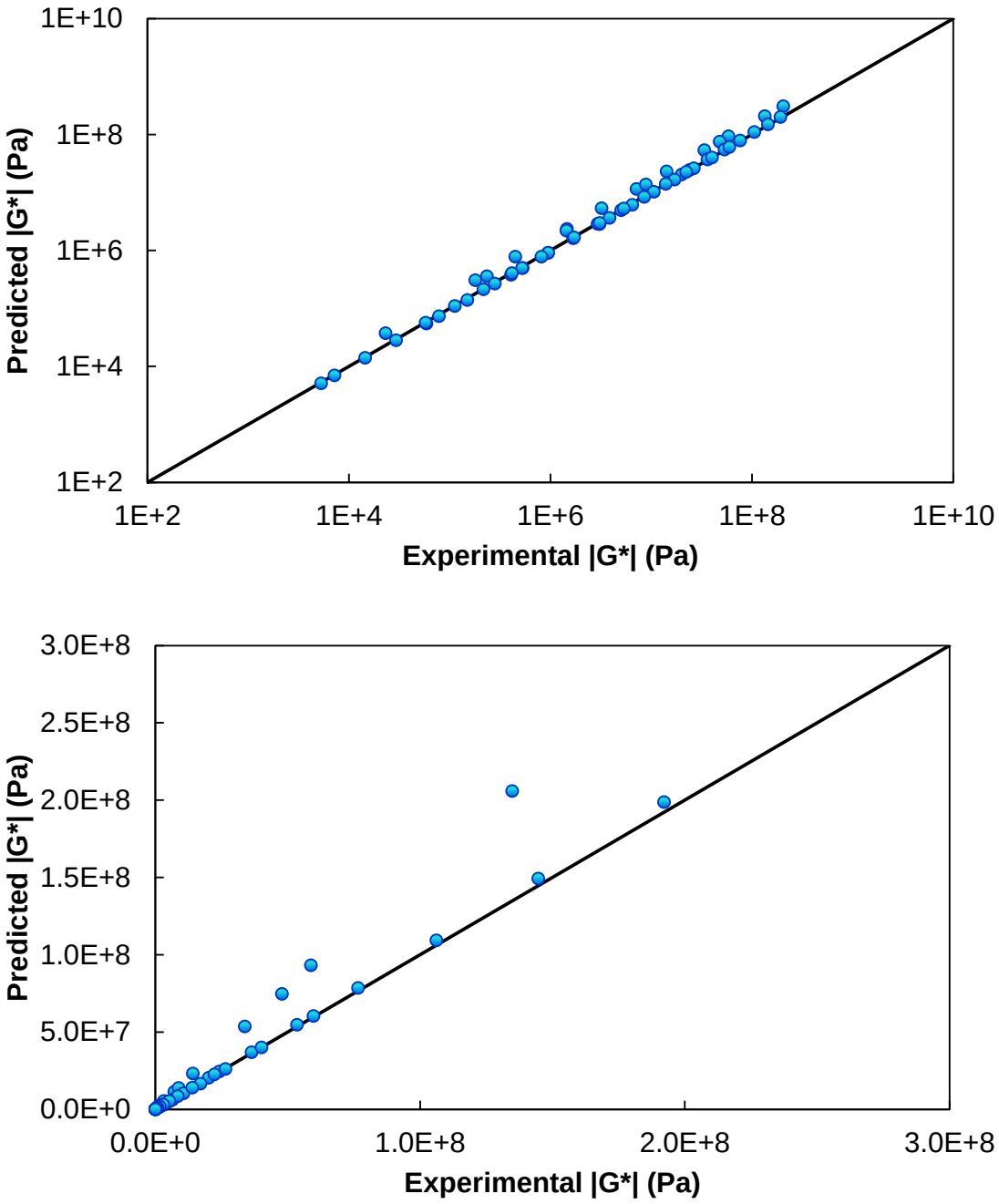

Figure 4-32: Verification of Hashin's Model for RAP 50: (a) log-log space; (b) arithmetic space.

4.3.3.3 Hashin and Shtrikman Arbitrary Phase Geometry (APG) Model

The authors developed the present model to improve the prediction of composite stiffness of materials containing arbitrary phases. Paul's rule of mixtures model is also applicable to arbitrary phases. However, bounds were very far apart. This was also seen in the present study. Hashin and Shtrikman's model seeks to improve the bounds developed by Paul. The present model was only evaluated for RAP modified mastics, as the theory of arbitrary phases fits the assumption of VM and RAP 100 as constituents well. It should be recalled that RAP 10, RAP 30 and RAP 50 are modelled on the assumption that they are made up of RAP 100 and VM. Even though the present model gives us a bounded solution, attempts were made to arrive at a particular solution using Equation (4.40). G_c^* represents the composite modulus, whereas G_l^* , G_u^* are the lower and upper bounds as obtained by Equations (4.21) and (4.22). The parameter *s* is an optimization parameter. Predicted values were arrived at using Equation (4.40), after which the parameter *s* was optimized to minimize the error between predicted and experimental values. The predicted bounds are presented in Figure 4-33 to Figure 4-35. The observations from the predictions are presented below:

$$G_c^* = G_l^* + s(G_u^* - G_l^*) \tag{4.40}$$

- The bounds obtained from this model are closer than the bounds obtained through Paul's model.
- It is seen that the optimization parameter tends to a value of zero, which means G^*_c is equal to G^*_l. This is not entirely unexpected, given the proximity of the experimental data to the lower bound of the model.

- Based on this, the percentage error between G^*_c and the experimental data was calculated. For RAP 10 the error varied from 6% to 14%. For RAP 30 it ranged between 9% and 22% and for RAP 50 it varied from 20% to 32%.
- It was also observed that in general the error in prediction reduced as the frequency went from high to low.

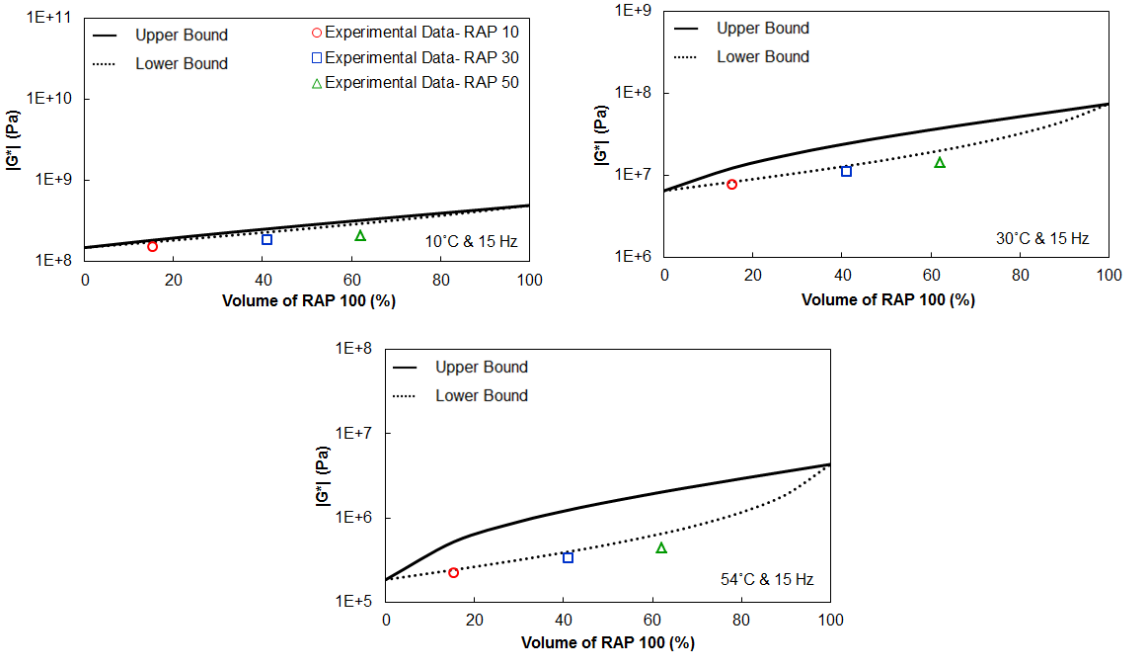

Figure 4-33: Predictions for RAP Modified Mastics at High Frequency Using Hashin and Shtrikman's APG Model.

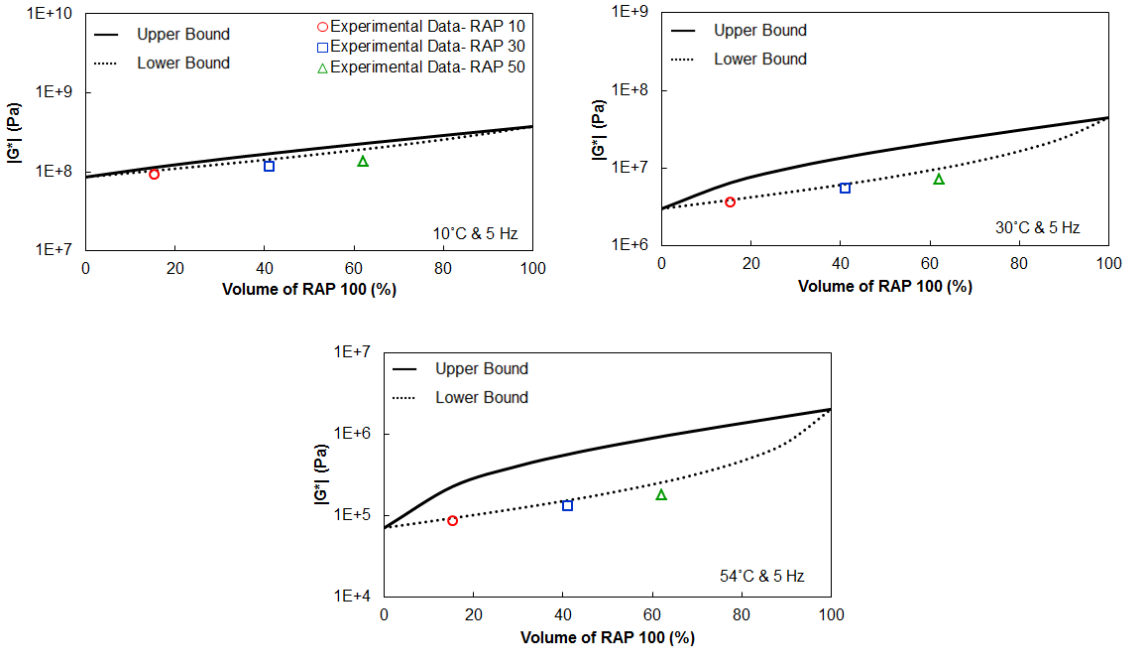

Figure 4-34: Predictions for RAP Modified Mastics at Moderate Frequency Using Hashin and Shtrikman's APG Model.

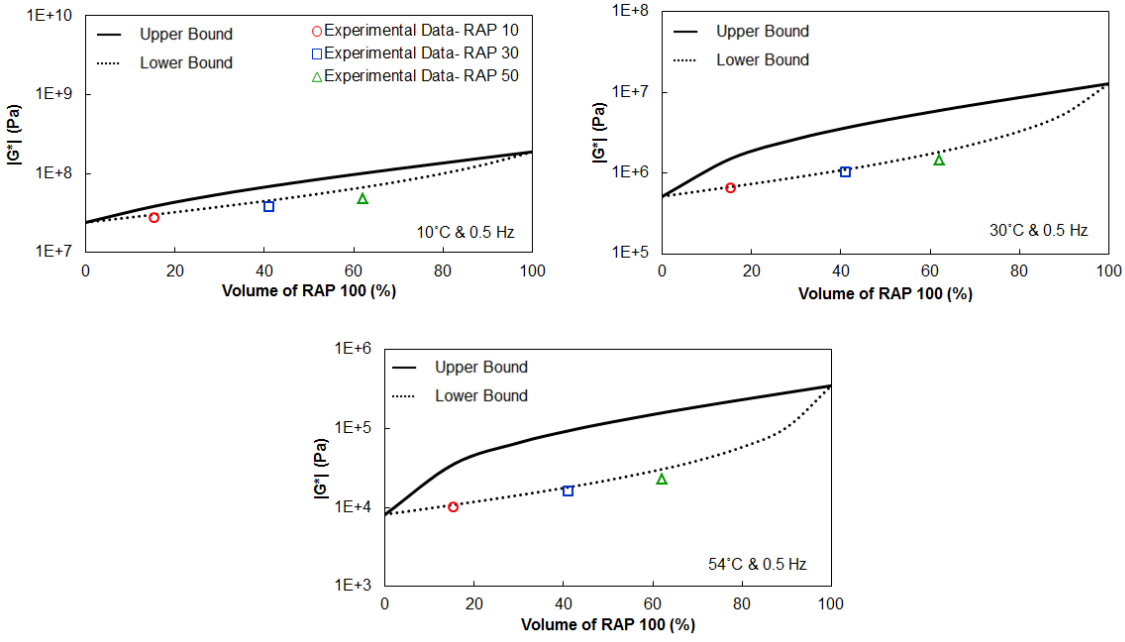

Figure 4-35: Predictions for RAP Modified Mastics at Low Frequency Using Hashin and Shtrikman's APG Model.

4.3.3.4 Christensen and Lo- Generalized Self Consistent Scheme Model

The model proposed by Christensen and Lo, Equation (4.24) through (4.30), was incorporated into a spreadsheet and stiffness predictions for RAP modified and non-RAP modified mastics were carried out. The assumption regarding the smeared constituents of RAP modified mastics was implemented in the present model also, wherein RAP100 was assumed as particulate and VM as the matrix. The Poisson's ratio of the binder, filler and mastic were assumed as 0.5, 0.35, and 0.5 respectively. The error in prediction is expressed as the percentage difference between predicted and experimental data. The data is plotted in figures . Due to the tedious process of calculation, unlike Hashin only few data points are presented. The presented points are at the evaluation conditions selected, i.e. at three temperatures, 10°, 30°, and 54°C and at three frequencies 15 Hz, 5 Hz and 0.5 Hz. The observations from the predictions are as below:

- The model highly underestimates the stiffness values for VM and RAM. The error in prediction for VM are in the range of 70%-100%, where for RAM they vary from 110%-150%.
- It is seen that for the RAP modified mastics, the stiffness is overestimated. The error in prediction varies from 14% to 17% for RAP10, 27% to 43% for RAP 30 and 35% to 48% for RAP 50.
- The observed predictions are close to the predictions of Hashin as presented in Section 4.3.3.2, but Christensen and Lo's predictions over predict for RAP mastics.

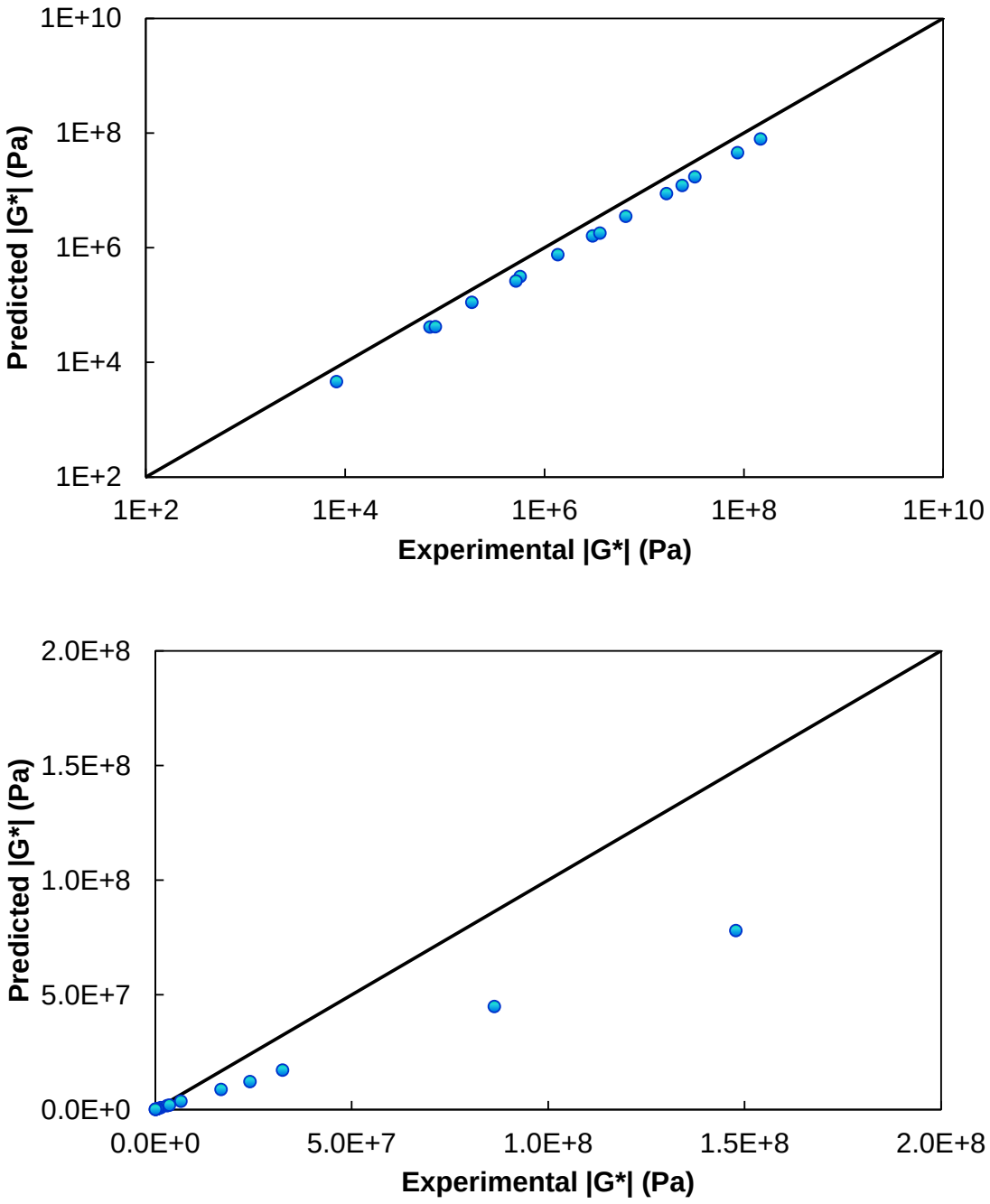

Figure 4-36: Verification of Christensen and Lo GSCS Model for VM: (a) log-log space; (b) arithmetic space.

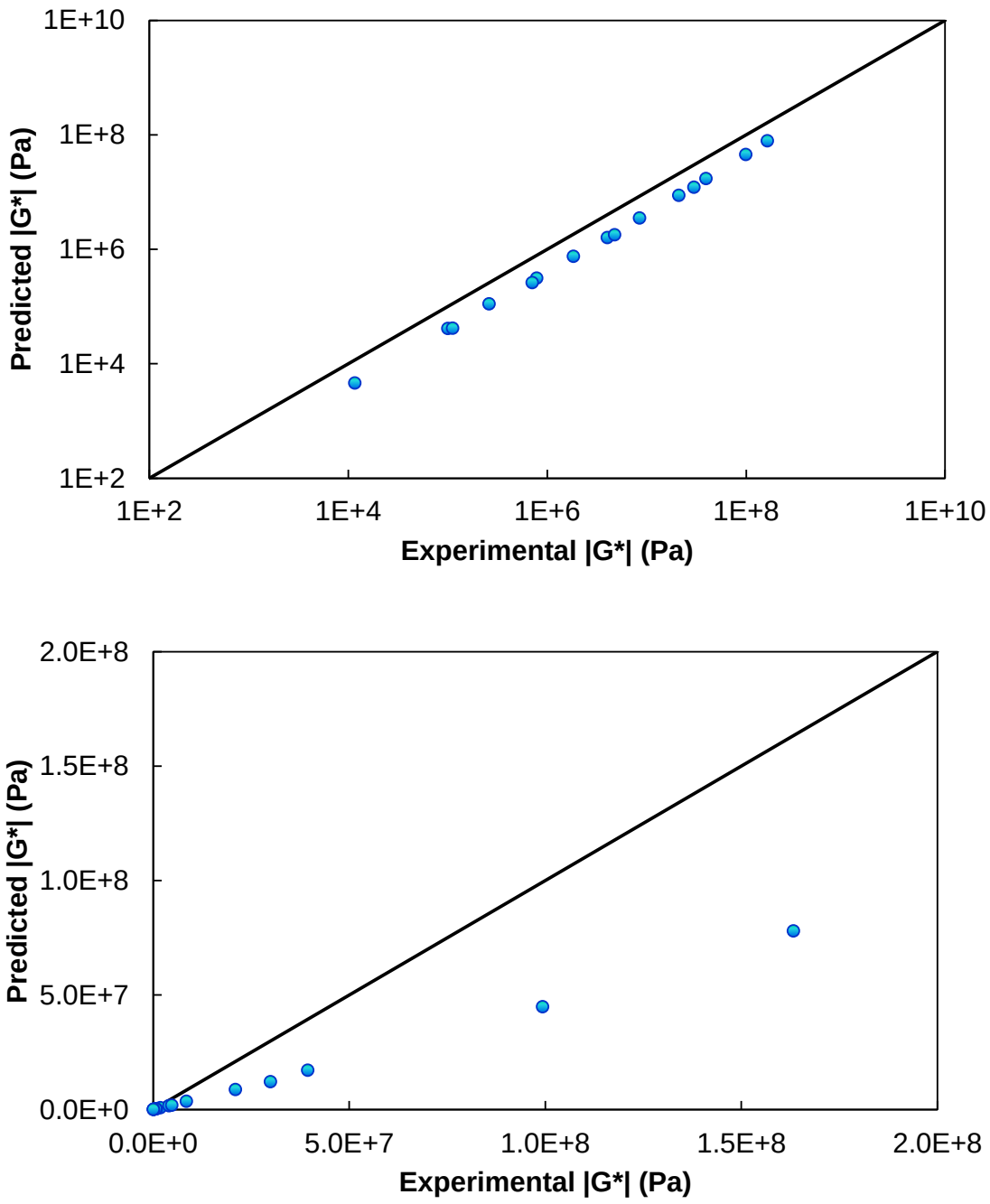

Figure 4-37: Verification of Christensen and Lo GSCS Model for RAM: (a) log-log space; (b) arithmetic space.

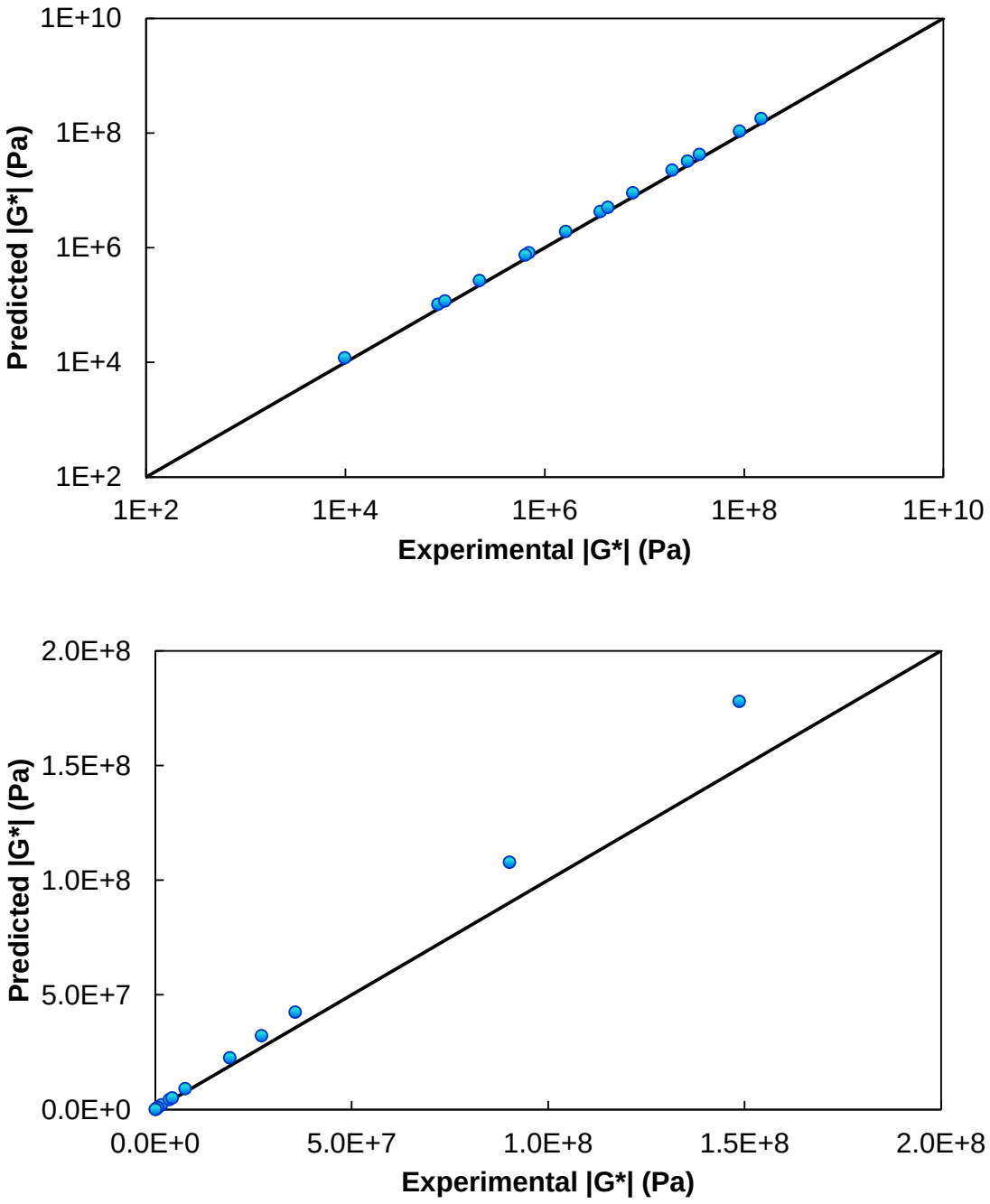

Figure 4-38: Verification of Christensen and Lo GSCS Model for RAP 10: (a) log-log space; (b) arithmetic space.

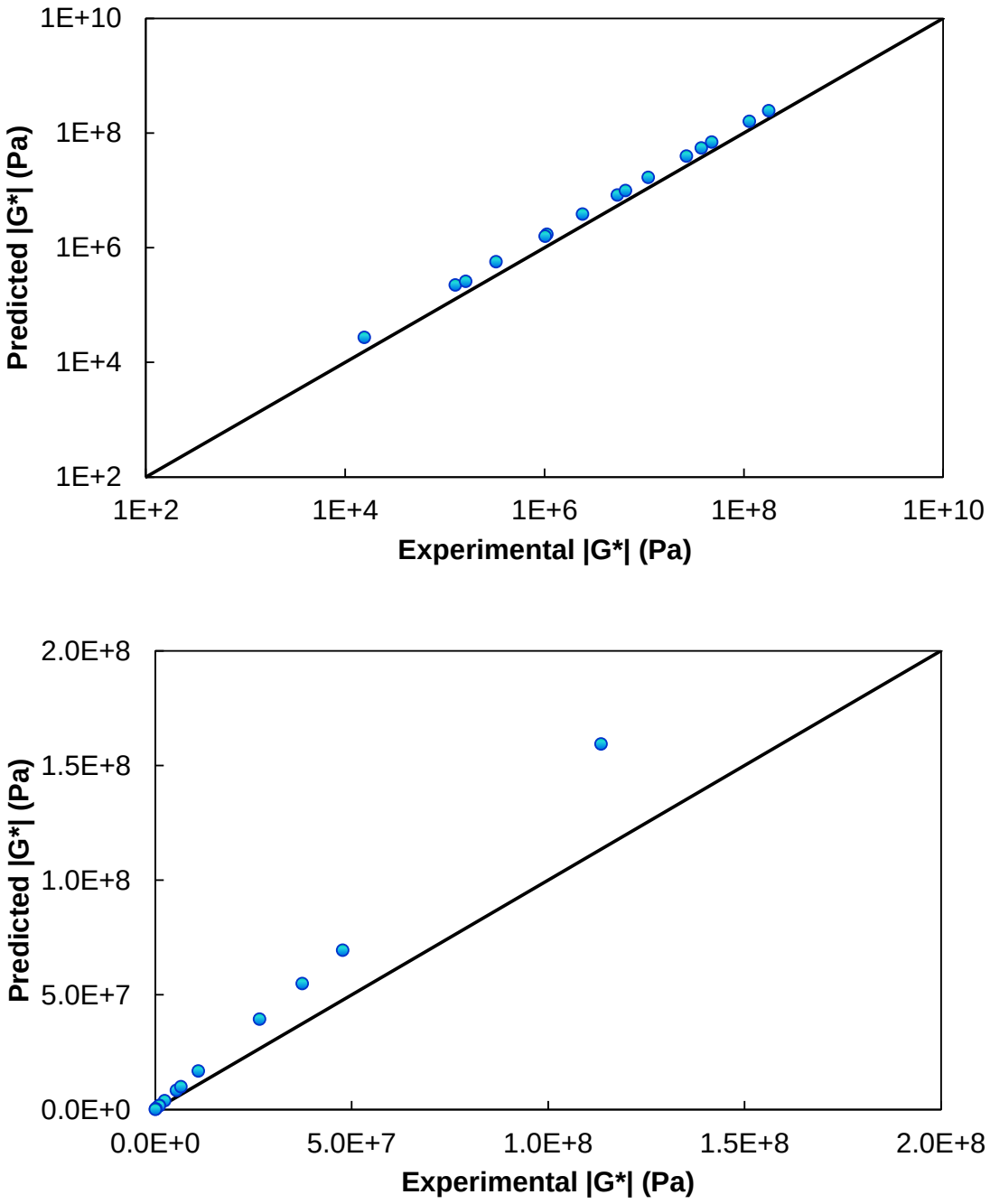

Figure 4-39: Verification of Christensen and Lo GSCS Model for RAP 30: (a) log-log space; (b) arithmetic space.

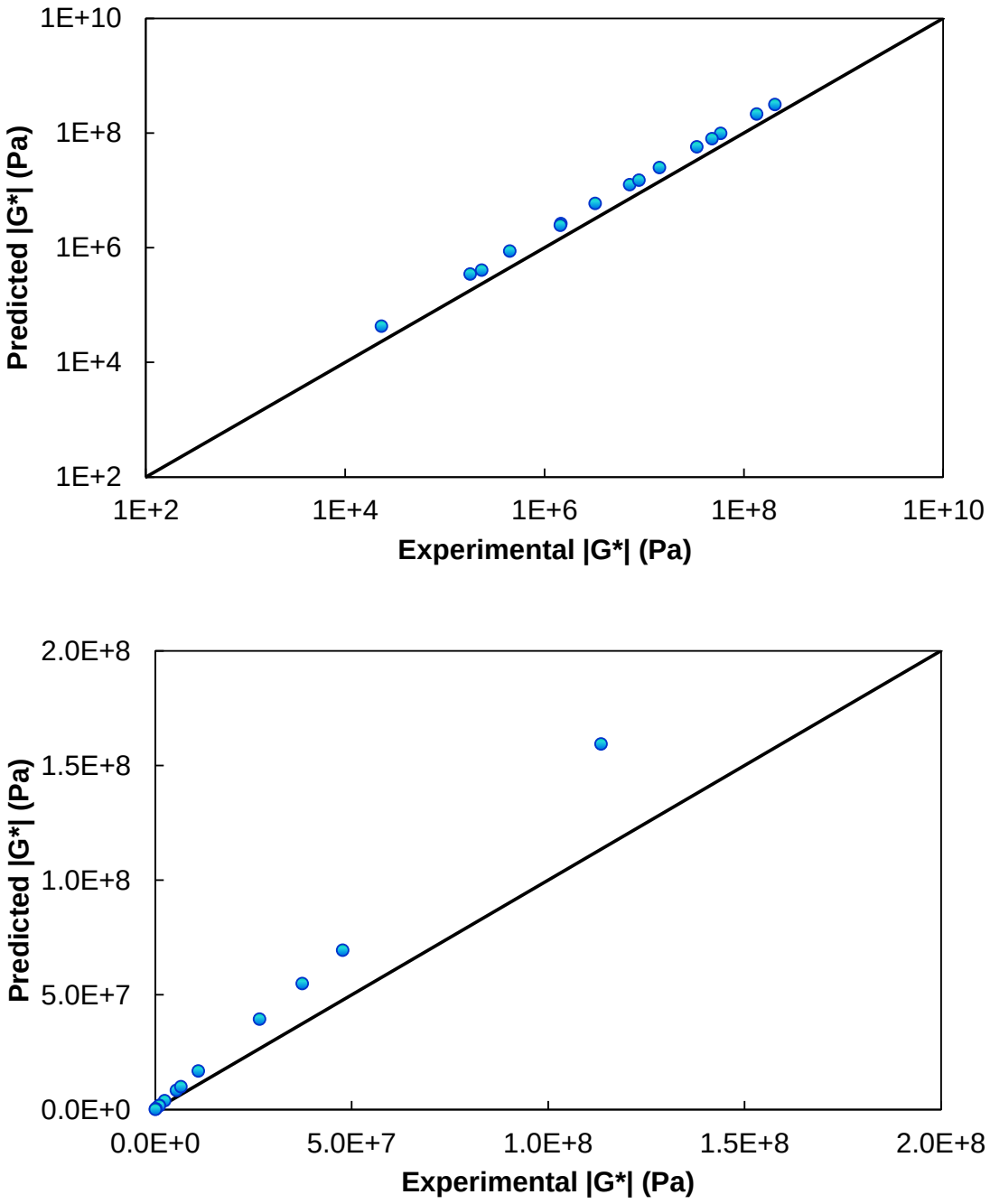

Figure 4-40: Verification of Christensen and Lo GSCS Model for RAP 50: (a) log-log space; (b) arithmetic space.

It is seen from all the above models that the errors in predictions are extremely high for VM and RAM. Although, the errors for RAP modified mastics are much lower

than non-RAP modified cases, it should be remembered that the method used for the stiffness prediction of RAP modified mastics is a surrogate method based on a certain assumption.

The main drawback of the models presented above in its application to the mastics is its failure to account for the physicochemical interactions between aggregate and the binder [32],[44]. Researchers over the years have shown the importance of these physicochemical interactions, in terms of the profound effect they have on the stiffness of the composite [2],[43]. In the following section, these physicochemical aspects will be considered and modeled by using Herve and Zaoui model.

4.4 Modeling of RAP Mastics using Herve and Zaoui Model

The micromechanical models discussed in Section 4.3.3 have a limitation on the number of phases that can exist in the composite. Also, the models do not account for the physicochemical interactions between aggregate and the binder. The micromechanical models discussed in Section 4.3.3 smear the effects of interaction between RAP binder and virgin binder. It should be recalled that in Section 4.3.3, the blended mastics, RAP 10, RAP 30, and RAP 50 were modeled considering that they basically contained two constituents, VM and RAP 100. Herve and Zaoui model [42] as indicated in Section 4.3.2 is n-layered inclusion based micromechanical model, which was proposed to eliminate the phase limitations of the models that various authors proposed earlier [40],[41], [54]-[56]. In asphalt mastics, Underwood and Kim have shown that the model has the capability to explicitly account for the physicochemical interactions between the filler and the binder [32], [43]. However, its application to RAP mastics is novel. Many

authors [3], [5]. [20], [23] have investigated the interaction of virgin and RAP binders on the binder and mixture scale, which underlines the importance of the level of interaction between RAP and virgin binders for the overall performance of the RAP modified asphalt concrete mixtures. Using the Herve and Zaoui model, these interactions can be explicitly accounted for while predicting the modulus of the RAP mastics.

The present section is divided into three parts. The first part discusses the conceptualization of the hypothetical blend structure in the RAP mastics. In the second part, the methodology adopted for implementing the model to match the hypothesized structure is discussed. The third part consists of modulus predictions from the model as well as the predicted percentage blending between RAP binder and virgin binder for RAP 10, 30, 50 and 100.

4.4.1 Hypothesized RAP Mastic Structure

It should be recalled that the RAP mastics consist three main constituents: (a) RAP filler (b) virgin filler (c) virgin binder. However RAP 100 will only consist of two constituents as virgin filler is not present. The RAP filler further consists of two components, coated RAP filler containing the RAP binder coating and uncoated RAP filler whose coating is lost during the RAP separation and handling process. The uncoated filler here is same as the recovered filler as discussed in Chapter 3. It is to be noted that the total filler concentration of all the mastics is the same i.e. 27% by volume. However, the form in which the total filler exists varies from mastic to mastic. For example, RAP 50 will have more filler in the form of RAP filler than RAP 30, consequently RAP 30 will have more virgin filler than RAP 50 but, the total amount of

filler is same in both cases. The generalized RAP mastic structure hypothesized for the present study is presented in Figure 4-41. The entire structure is divided into three groups, A, B, and C as shown in Figure 4-41. The description of the individual groups is as below:

1. Group A: Group A consists of the RAP filler particle with its coating intact. The structural schematic consists of uncoated RAP filler particle along with the adsorbed RAP binder component. Encompassing this adsorbed RAP binder component is the non-adsorbed and non-blended RAP binder. This binder component refers to the RAP binder which is neither adsorbed onto the aggregate surface, nor participating in blending with the virgin binder. The blended RAP and virgin binder forms the last layer. The blended binder is formed from the non-adsorbed RAP binder components of coated RAP particles and non- adsorbed virgin binder components of virgin and uncoated fillers.
2. Group B: This group consists of the mastic that is formed from the uncoated RAP filler particles and the blended binder.
3. Group C: This group consists of the mastic that is formed from the virgin filler and blended binder.

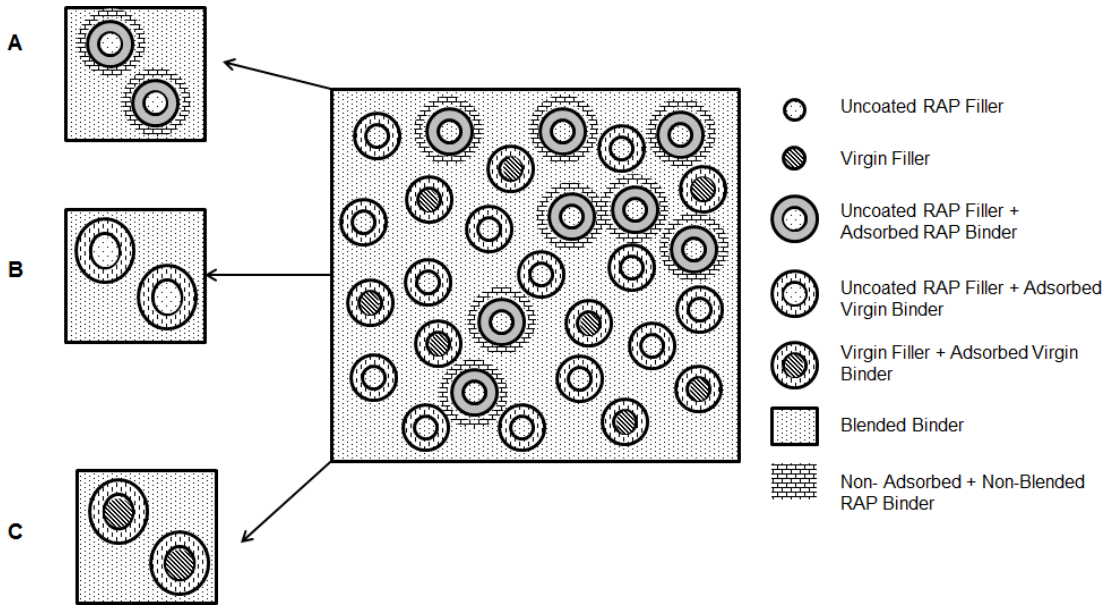

Figure 4-41: Hypothesized Blended Structure of RAP Mastics, Applicable to RAP 10, RAP 30, and RAP 50.

The structural hypothesis for RAP 100 is also very similar. However, in this case there will be no virgin filler in the structure. The schematic of the structure is shown in Figure 4-42. Groups B and C in Figure 4-41 and group B in Figure 4-42 is a four phase composite as each consists of an inclusion, an adsorbed binder phase, blended binder phase and an equivalent medium that consists the above three phases. Group A in both figures is a five phase model, consisting of an inclusion, an adsorbed binder phase, a non-adsorbed binder phase, blended binder phase and an equivalent medium that consists the above four phases.

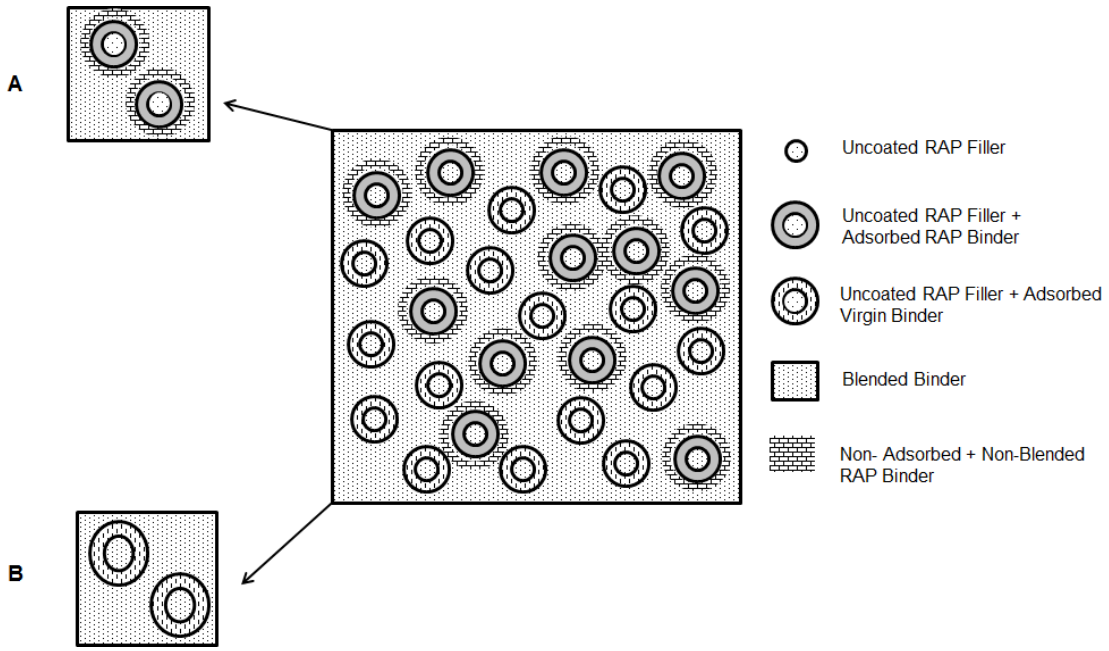

Figure 4-42: Hypothesized Blended Structure of RAP 100.

4.4.2 Methodology for Model Implementation

Although the implementation of the model is not entirely complex, it is little involved. The basic steps for implementation of the model were shown by Underwood and Kim [43]. However, the implementation of the model and its subsequent modulus prediction depends on the interactions between the groups, as shown in Figure 4-41 and Figure 4-42, and their constituents. So an interaction theory for the RAP mastics was developed. A step wise explanation of the hypothesized interaction theory is presented below.

1. The RAP mastic sample preparation was carried out by heating the virgin aggregate at 160°C for a minimum of 6 hours and RAP filler at 110°C for two hours prior to mixing. The two components are quickly blended together and

subsequently asphalt binder which is at 160°C is added and blended together using a mechanical blender.

2. A portion of the virgin binder then adsorbs onto the surface of the uncoated RAP filler and the virgin filler.
3. The aggregate in the coated RAP filler already has an adsorbed binder component. Since the coated and un-coated RAP filler have same aggregate, it is assumed that the nature of adsorption of binder onto the aggregate will also be similar. So, the stiffness of adsorbed binder that is inherently present on coated RAP filler is assumed to be similar to the stiffness of virgin binder that is adsorbed onto the surface of the uncoated RAP filler.
4. A portion of the non- adsorbed RAP binder on the coated RAP filler is assumed to blend with the non-adsorbed virgin binder on the virgin and non-coated fillers.
5. This blended binder is now assumed to coat all the particles in the system.
6. The entire blend can now be divided into three groups A, B, and C as shown in Figure 4-41.
7. Group B and C is now modeled as a four phase composite and group A as a five phase composite. The model is set up in LabVIEW. The result from the model is a ratio between the composite stiffness and the stiffness of the outermost layer. The latter should be known as it is one of the required inputs for the model. So, the stiffness of the composite can now be calculated.
8. After arriving at the stiffness for each of the three groups, they are now integrated together using a parallel model as shown in Equation (4.41) . The volumetric

percentage of each group in the composite was found out using volumetric calculations.

$$G_{composite} = G_A * V_A + G_B * V_B + G_C * V_C \quad (4.41)$$

where,

G_A, G_B, G_C = Modulus of group A, B, and C respectively,

V_A, V_B, V_C = Volumetric percentages of each group,

$V_A + V_B + V_C = 1$

The implementation of the model is divided into two stages. For the purpose of conceptual clarity, both stages are depicted using flowcharts. Stage 1 consists of prediction of adsorbed and non-adsorbed binder components associated with the virgin and the uncoated RAP filler. The process is a trial and error procedure, as mentioned by Underwood and Kim [43]. The step by step implementation of stage 1 is shown in the form of a flowchart as shown in Figure 4-43. In stage 1, the composites modeled were VM and RAM. The adsorbed binder values obtained by the trial and error process were fit to a sigmoidal function and the non-adsorbed modulus was recalculated using Equation (4.42).

$$\left|G^*\right|_{composite} = \frac{\left|G^*\right|_{bulk} * \left|G^*\right|_{adsorbed} * V_{non-adsorbed}}{\left|G^*\right|_{adsorbed} - (\left|G^*\right|_{bulk} * V_{non-adsorbed})} \quad (4.42)$$

where

$\left|G^*\right|_{non-adsorbed}$ = the modulus of non-adsorbed asphalt binder,

$\left|G^*\right|_{adsorbed}$ = the modulus of adsorbed asphalt binder,

$\left|G^*\right|_{bulk}$ = the modulus of asphalt binder measured by DSR equipment,

$V_{non-adsorbed}$ = the proportion of total asphalt binder which is not adsorbed on the aggregate surface.

$V_{adsorbed}$ = the proportion of total asphalt binder which is adsorbed on the aggregate surface.

The fit adsorbed binder modulus and the recalculated non-adsorbed binder modulus are used as inputs for stage 2.

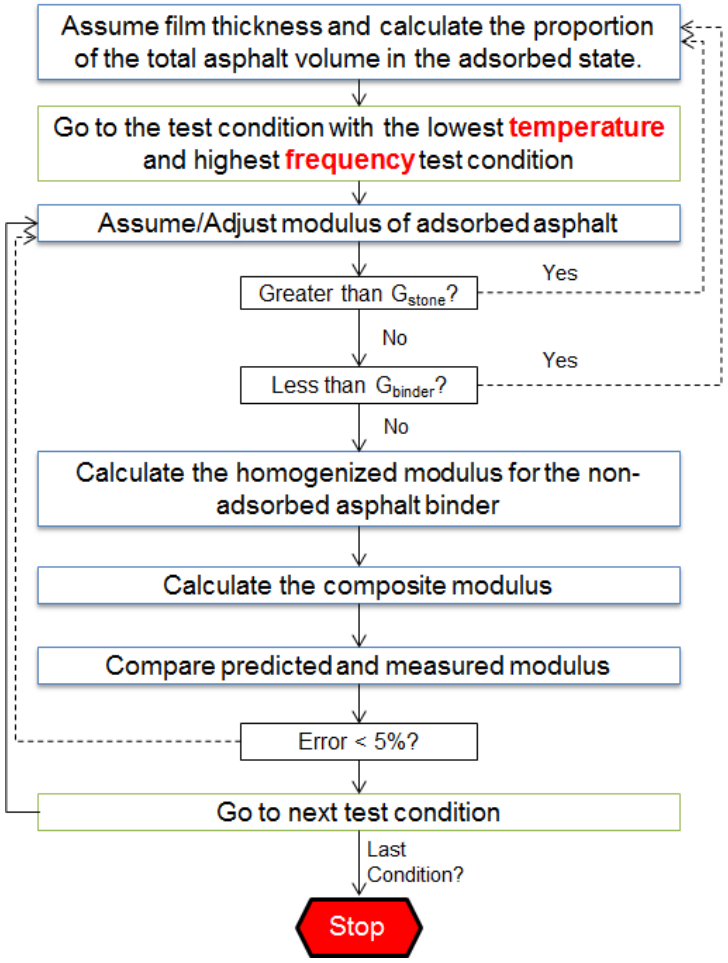

Figure 4-43: Stage 1: Procedure for Calculation of Adsorbed and Non-Adsorbed Binder Stiffness and the Stiffness of Four Phase Asphalt Mastic [43].

Stage 2 consists of series of steps implemented to arrive at the final composite modulus. The steps involved are shown in Figure 4-44.

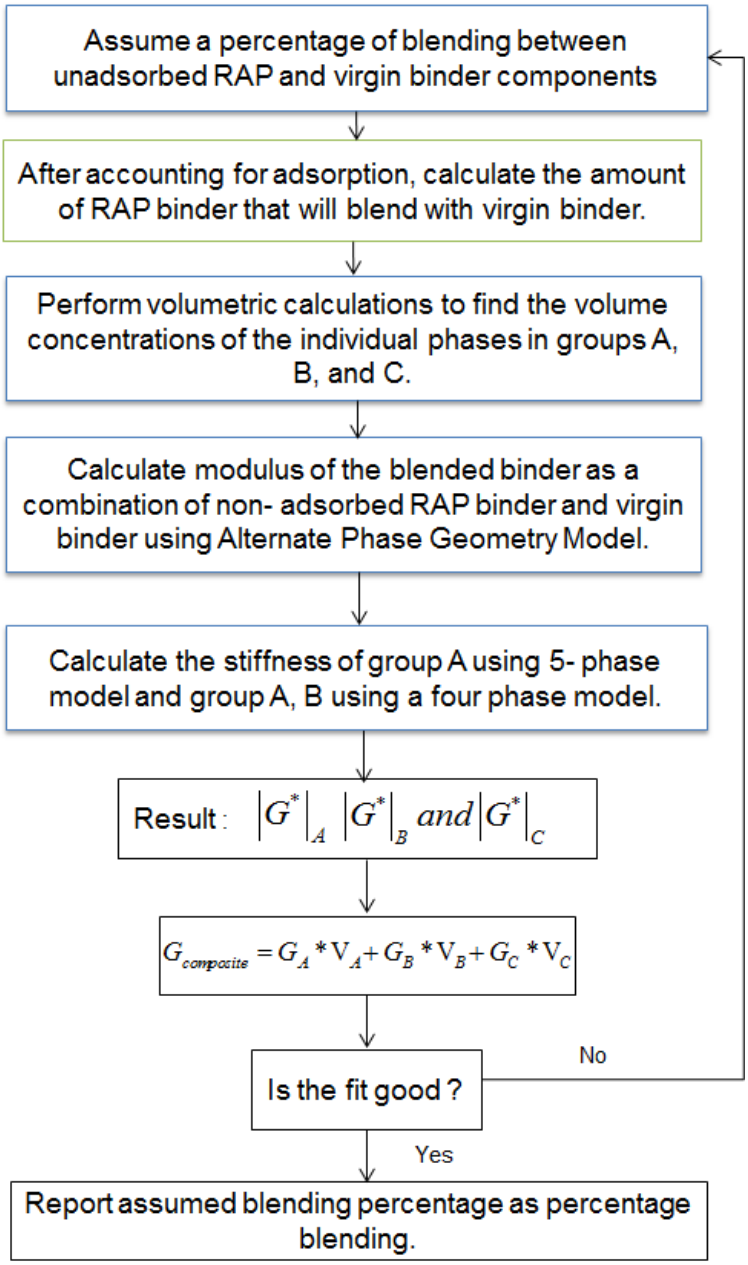

Figure 4-44: Stage 2: Procedure for Calculation of Composite Modulus of RAP Mastics and the Percentage of Blending.

4.4.3 Modulus Predictions from Herve and Zaoui Model

As mentioned in stage 1 and stage 2 of Section 4.4.2. Modulus predictions were carried out on VM, RAM and RAP 10, RAP 30, RAP 50 and RAP 100 using the

methodology presented in stage 1 and stage 2 respectively of Section 4.4.2. For the predictions in stage 2, a blending percentage (P_b) was first assumed and thenn the composite modulus was predicted. The predictions for VM are presented in Figure 4-45 looked good and also the adsorbed modulus fit well to the sigmoidal function. For RAM as shown in Figure 4-46, although the predictions collapsed well with the measured data, a good fit was not achieved for adsorbed modulus. All the input parameters for VM and RAM were very similar and also the final composite modulus, so it was surprising to see that adsorbed binder modulus for RAM being higher by almost a magnitude.

For the RAP mastics, a blending percentage was first adopted, subsequently the steps shown in Figure 4-44 were followed to arrive at the final composite modulus. For RAP 10 it was seen that a Pb of 50% produces a good fit of the data. Similarly for RAP 30, RAP 50 and RAP 100 reasonably good fits at lower temperatures were observed at Pb of 27%, 20%, and 15%. In all the cases it was observed the predicted data did not match well the measured data at moderately high to high temperatures. The error in prediction was another parameter that was looked at before making the judgment on acceptability of the fit. It was seen that at the above mentioned Pb levels that the error for RAP 10 and RAP 100 were lower compared to RAP 30 and RAP 50. Also while performing the iterations it was seen that lowering the Pb reduces the error, however for RAP 30 lowering the Pb by 8% resulted in only 1.5% reduction in average error and also it did not improve the fit by much. Based on this finding it was decided to consider the percentage blending values for RAP 10, RAP 30, RAP 50 and RAP 100 as 50%, 27%, 20% and 15% respectively. The modulus predictions using these values are presented in Figure 4-47 to

Figure 4-50. The general trend as observed in Figure 4-51 is that the percentage blending reduces with increase in RAP dosage.

Also, It is known that percentage blending improves with increase in blending temperature [57]. In the present case during the time of mixing, RAP 100 possed the lowest temperature as the entire aggregate was at 110°C. Similarly for RAP 10, majority of the portion was at 160°C. Similar observations can be made with RAP 30 and RAP 50 as well. It is seen that as the percentage of RAP increases the overall temperature of mix tends to go down thus the blending also reduces.

4.4.3.1 Virgin Mastic

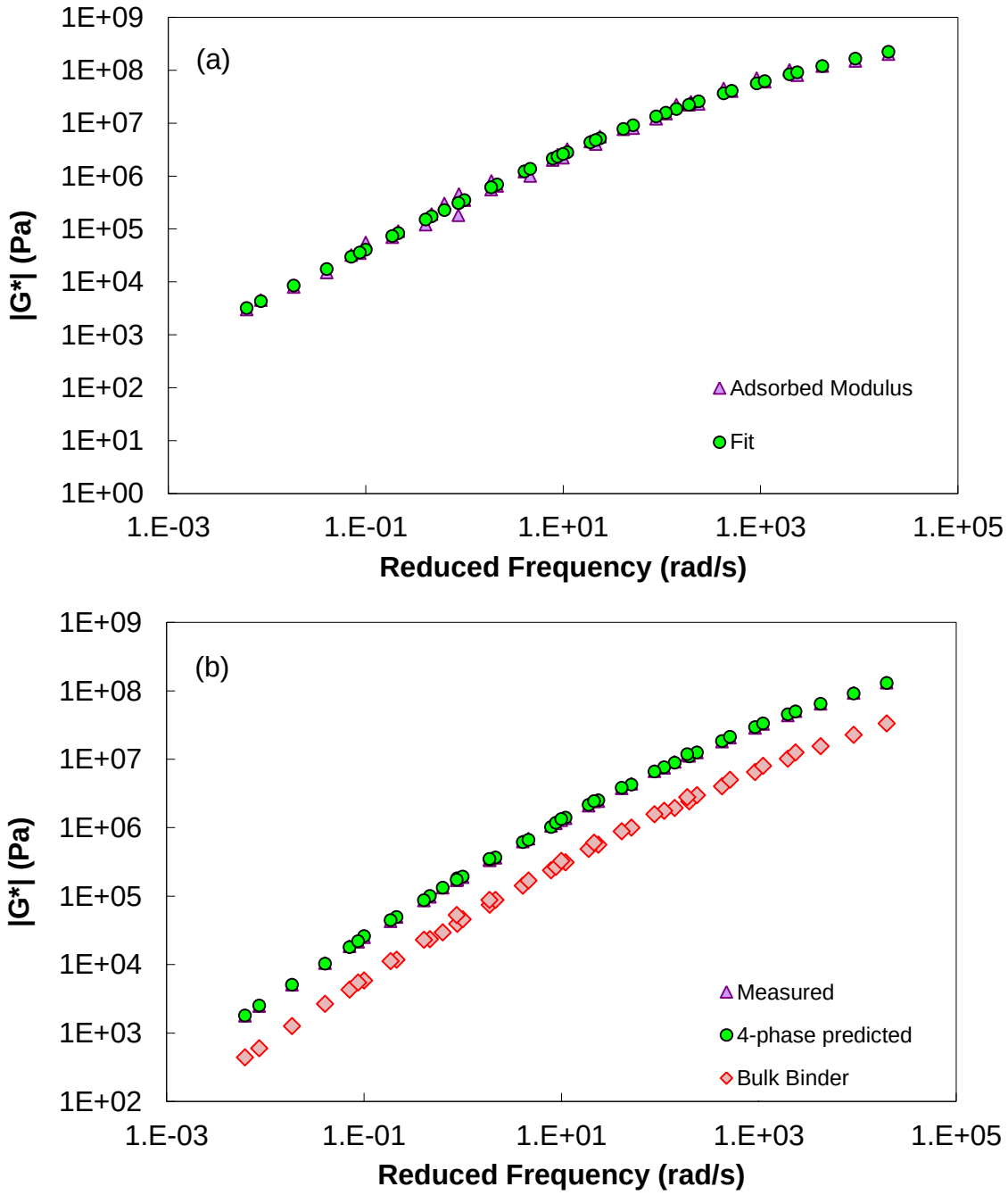

Figure 4-45: Predictions for VM Using Herve and Zaoui model: (a) Adsorbed modulus fit; (b) VM fit

4.4.3.2 RAM

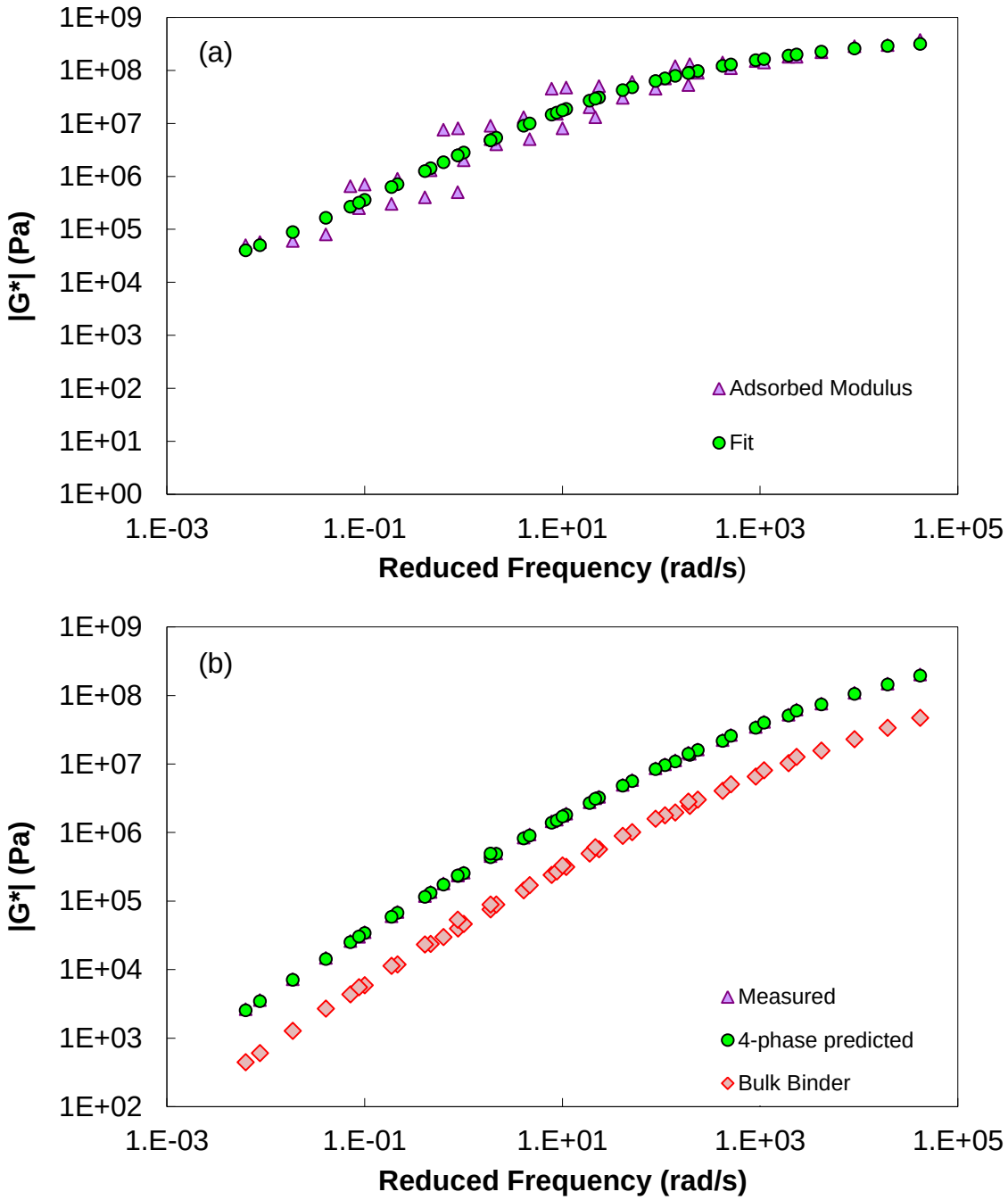

Figure 4-46: Predictions for RAM Using Herve and Zaoui Model: (a) Adsorbed modulus fit; (b) VM fit

4.4.3.3 RAP 10

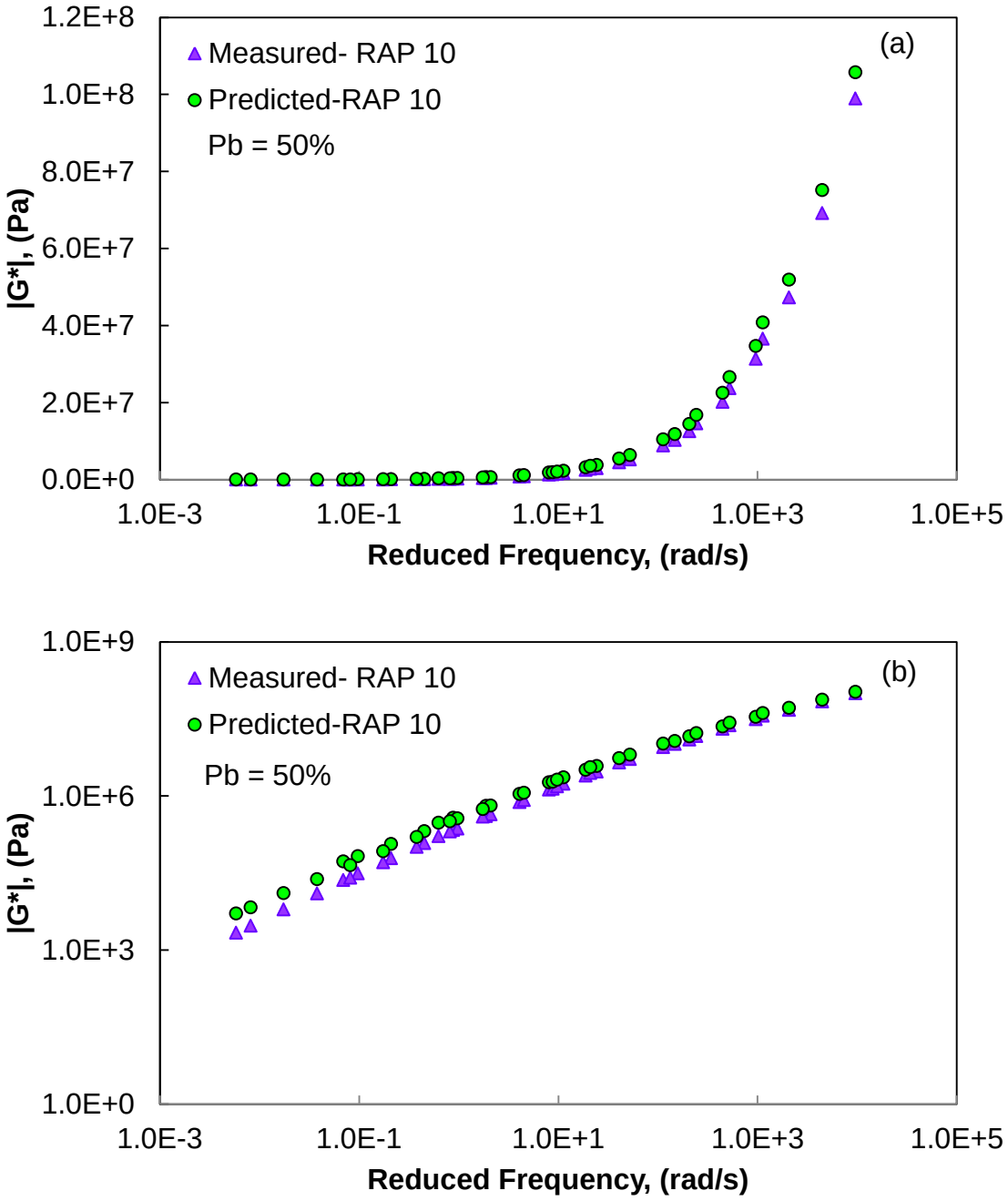

Figure 4-47: Predictions for RAP 10 at Pb = 50% using Herve and Zaoui Model: (a) semi-log scale; (b) log-log scale.

4.4.3.4 RAP 30

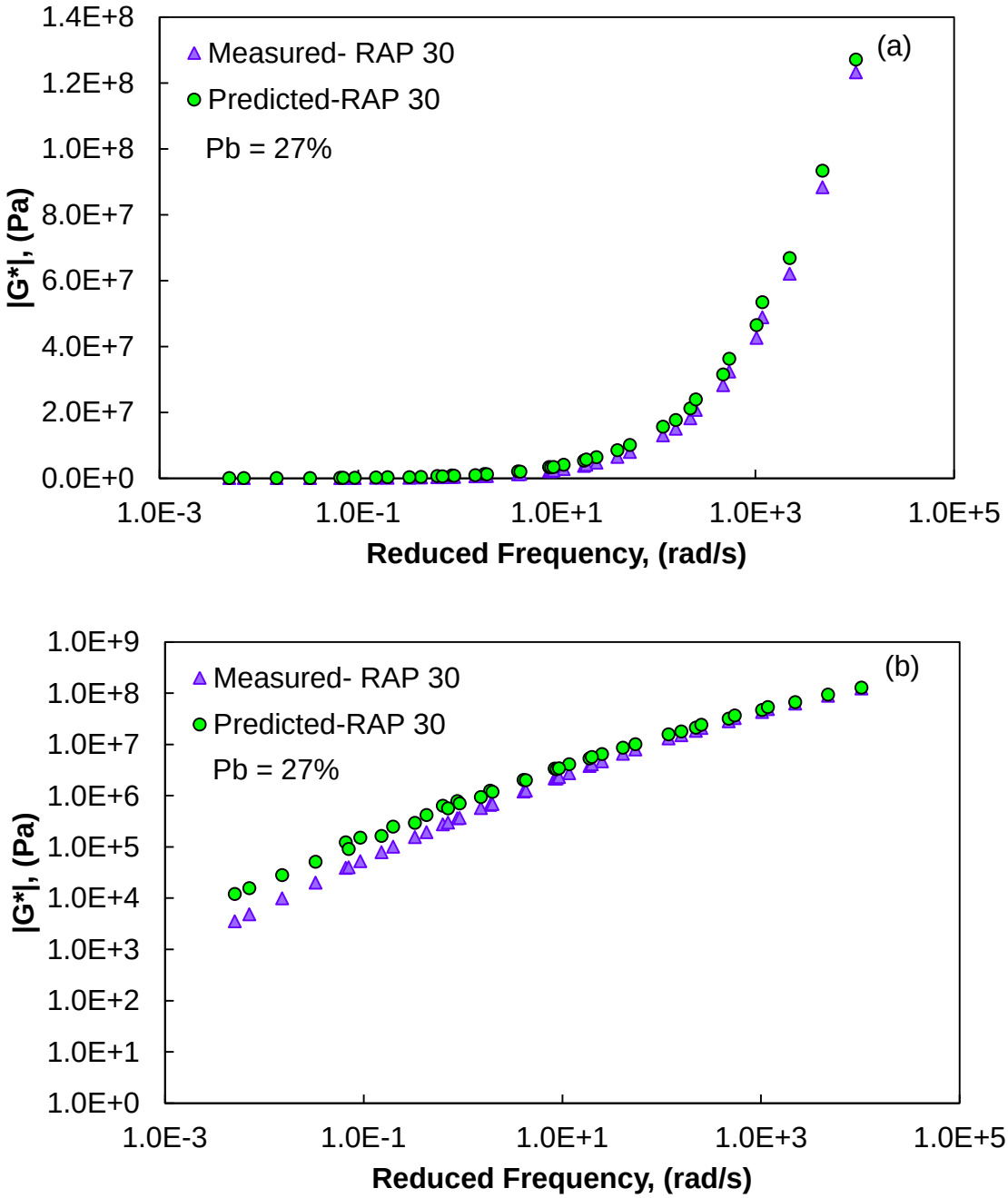

Figure 4-48: Predictions for RAP 30 at Pb = 27% Using Herve and Zaoui model: (a) semi-log scale; (b) log-log scale.

4.4.3.5 RAP 50

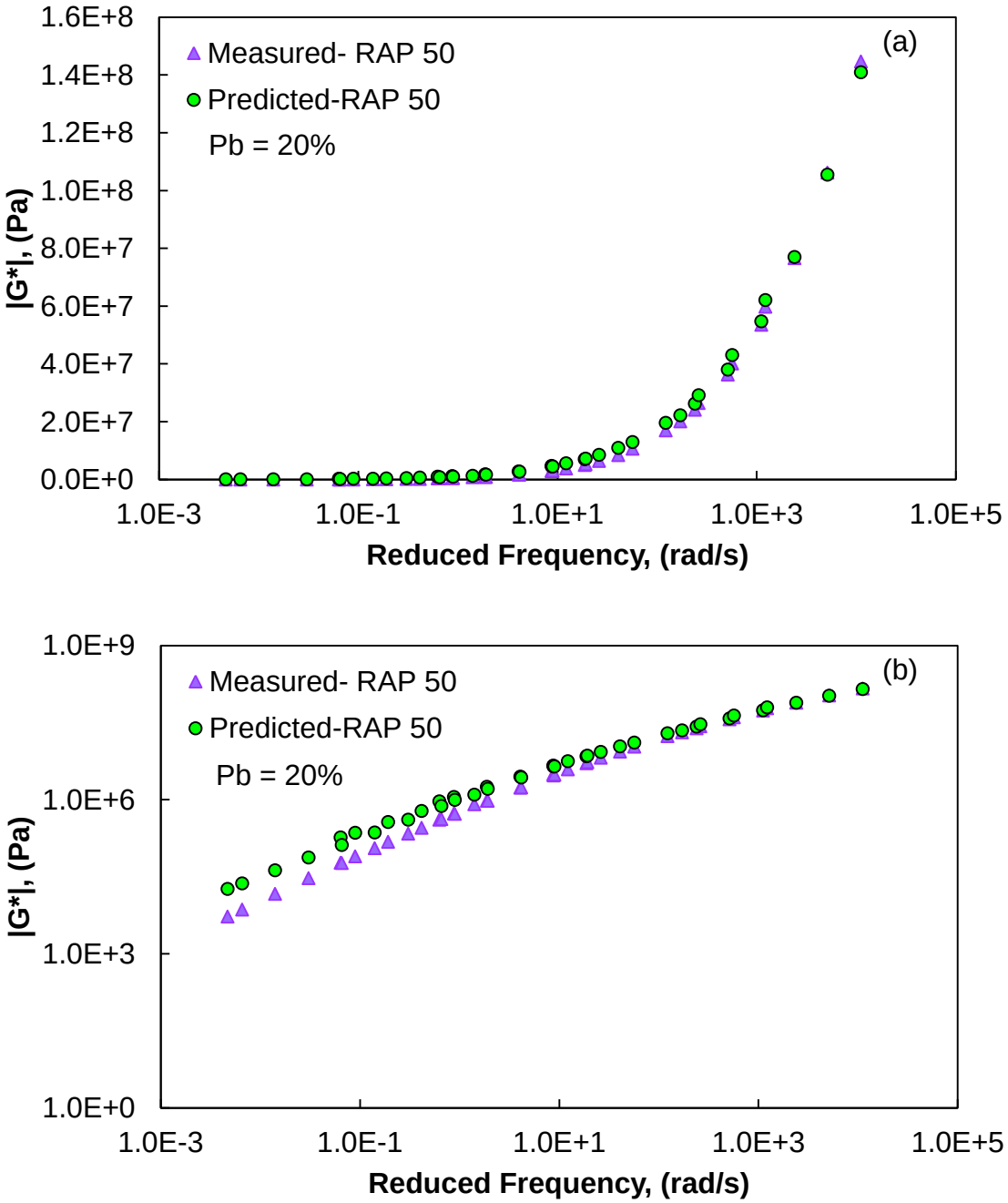

Figure 4-49: Predictions for RAP 50 at Pb = 20% Using Herve and Zaoui model: (a) semi-log scale; (b) log-log scale.

4.4.3.6 RAP 100

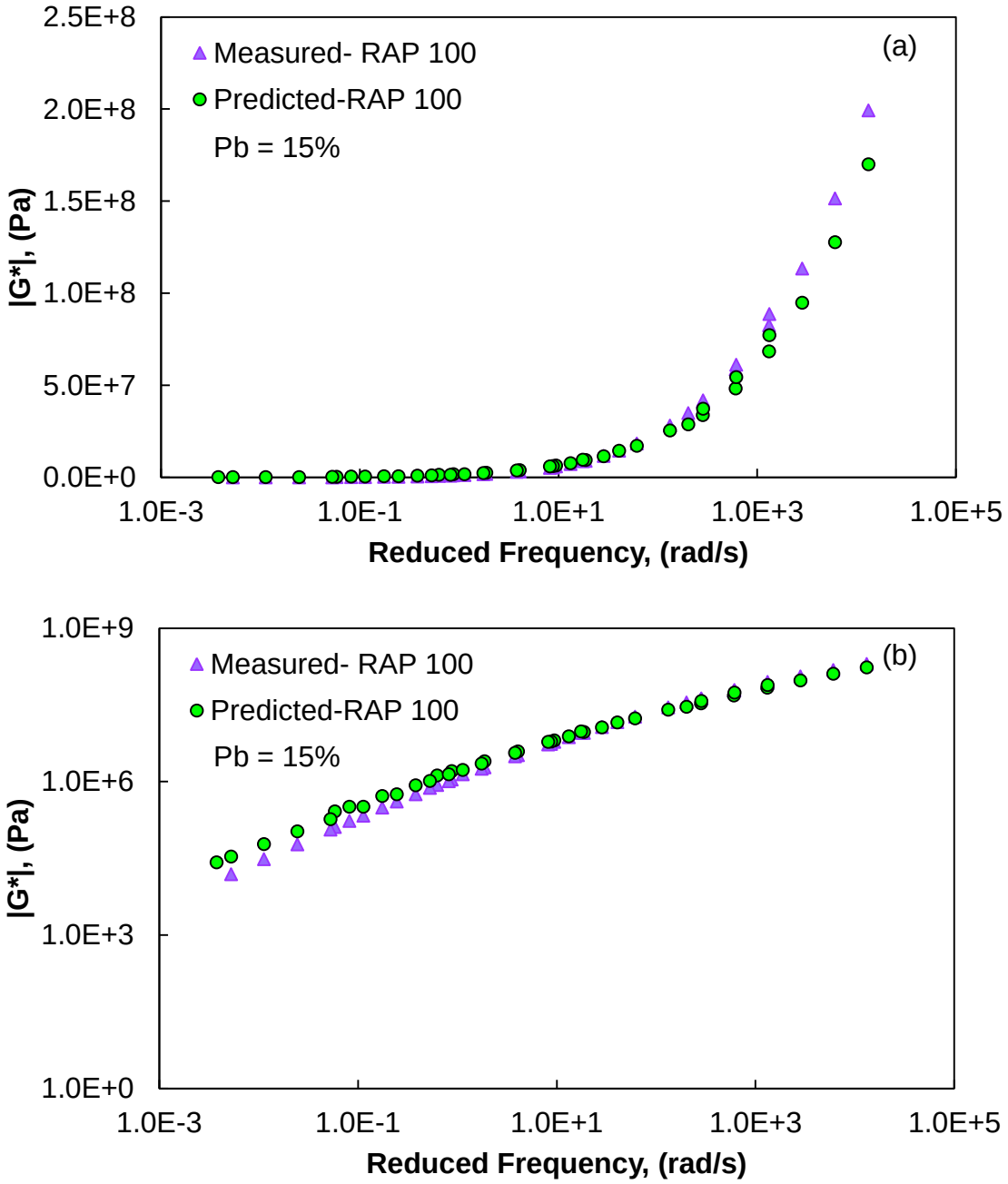

Figure 4-50: Predictions for RAP 100 at Pb = 15% Using Herve and Zaoui model: (a) semi-log scale; (b) log-log scale.

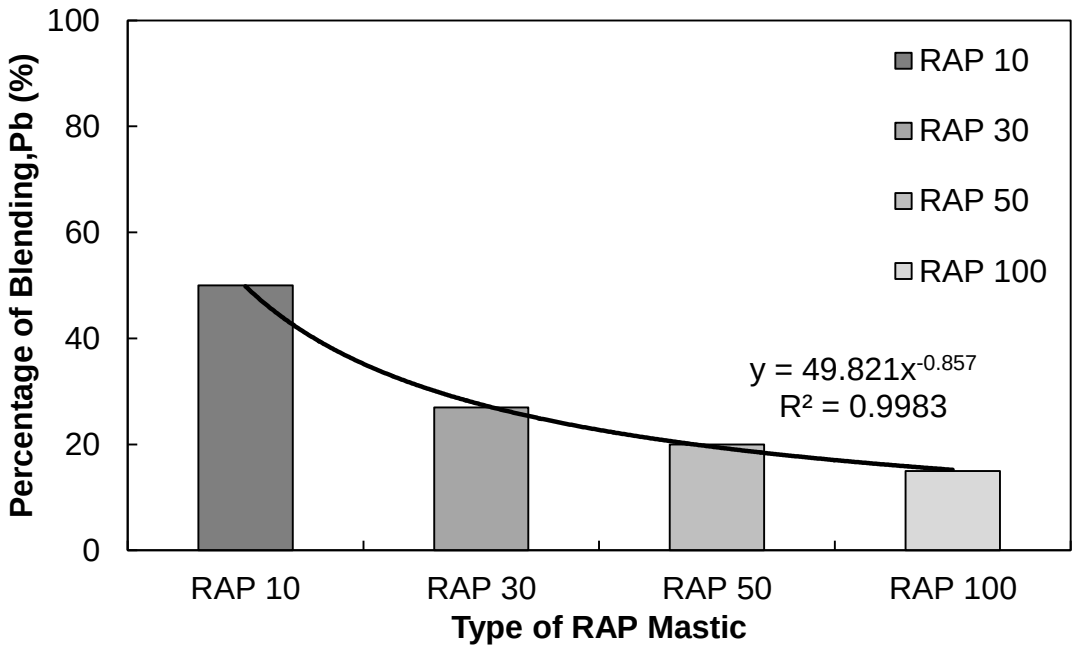

Figure 4-51: Variation of Blending for Different RAP Mastic Dosages.

Chapter 5 Summary and Conclusions

5.1 Summary and Conclusions

The main objective of the present study was to compare and model the mastic level structure of un-modified and RAP modified asphalt concretes using multiple phase micro mechanical models. Better understanding of the mastic level structures of these materials provides more insight into physicochemical interactions which contribute significantly to the performance of these mixtures.

In line with the above objective, mastics both RAP modified and un-modified were prepared at a filler content of 27%. The material matrix consisted of virgin binder, RAP binder, virgin mastic, recovered aggregate mastic and four different RAP dosages, 10%, 30%, 50% and 100% RAP. Virgin mastic represents the unmodified mastic case in the matrix. Recovered aggregate mastic (RAM) was conceptualized to represent the mastic that is formed due to the presence of uncoated particles in the RAP filler. RAP 10, RAP 30, RAP 50 represent low, medium and high RAP dosages. RAP 100 was included in the study to see the effect of full aggregate replacement. Also it provides an insight into how the blending progresses.

Rheological experiments such as, temperature and frequency sweep, strain controlled time sweep, and repeated stress sweep were performed the study materials. The results from the temperature and frequency sweep indicated a clear pattern in modulus, where in dynamic modulus of the mastics increased with increase in RAP dosage. The stiffest material however was the RAP binder. The results from the time sweep tests did not show any clear pattern with regard to the number of cycles to failure

of the mastics, but clear distinction could be made between the results obtained for binder and mastic. All mastics had a lower number of cycles to failure than the virgin binder at all strain levels. Owing to its high stiffness RAP binder failed very early at 2.5% strain level, however at 1.25% strain level it was seen that the material lasted very longer than expected but failed suddenly. It was presumed that the strain level of 1.25% is not high enough to cause the binder to failure within reasonable time. However, at 5% the torque exceeded machine limits so the test could not performed on RB.

Advanced characterization techniques such as simplified viscoelastic continuum damage modelling were applied to characterize the linear and non-linear behavior of the tested binders and mastics. By assessing the linear behavior it was found that a good collapse of the damage characteristic curve among different strain levels could not be achieved. This was primarily due to the existence of non-linearity in binders when tested at high strain levels. Repeated stress sweeps were conducted on the test materials to derive inputs for the non-linear formulation. It was found that the use of non-linear formulation resulted in better collapse in the damage characteristic curves.

Micromechanical models were employed to predict the properties of the composite from the constituents. From the models evaluated it was found that the distance between upper and lower bounds for the predicted modulus generally increased and the difference in stiffness between the constituents increased, thus leading to higher errors of prediction. Also it was found that many of the bound based models, predicted the modulus of asphalt closer to the lower bound. A surrogate method for prediction of modulus for RAP 10, 30 and 50 was developed by expressing them as a blend of VM and

RAP 100. The results obtained through Hashin's model by this method were promising but the predictions cannot be considered entirely acceptable due to its lack of physical insight and also since the errors for virgin and RAM mastics were considerably high. In order to better predict the modulus of the mastic, it was required that the modulus considers the physicochemical interactions at the aggregate surface. Literature has shown physicochemical interactions can be a significant source of stiffening in the mastics.

In order to account for these interactions Herve and Zaoui model was used. The main advantage of the model was that it did not have any limitations on the number of layers that can be present in the composite and this was particularly beneficial for the present study. In order to implement the Herve and Zaoui model it is necessary to first assume a hypothesized blend structure. The model development would then be carried out based on the hypothesis. The implantation of the model was carried out in two stages. The first stage consisted of predicting the modulus of VM and RAM and also their adsorbed and non-adsorbed binder components. In the second stage these were used as inputs among others to implement the hypothesized structure and calculate the composite modulus of RAP mastics. The model predictions showed that reasonably good predictions were obtained at intermediate and low temperatures but the predictions at high temperatures did not match the measured data well. One possible reason for this behavior can be the unexpected high adsorbed modulus of binder for RAM. The blending percentages at which the predictions were carried out showed a consistent trend with increase in RAP percentage. It was observed that percentage of blending reduced with increase in RAP. Thus, the current mix design assumption of 100% blending is not true.

The present study presents a tool to quantify blending between RAP and virgin binders by testing RAP mastics. Based on the observed percentage of blending adjustments can be made to the mix design to incorporate correct amount of asphalt binder. Also based on the present study, quality control tests can be carried out as it provides a way to determine the amount of working binder in the mixtures.

5.2 Future Work

1. Verification of the predicted blending results obtained from Herve and Zaoui model.
2. Scanning electron microscopy of the fatigued faces of the RAP mastics can provide insight into the fatigue behavior, based upon the proximity of the crack to either virgin or RAP particles.

REFERENCES

[1] Copeland, A. *Reclaimed Asphalt Pavement in in Asphalt Mixtures: State of Practice*. Report No. FHWA-HRT-11-021, Federal Highway Administration, McLean, VA, 2011.

[2] Craus, J., I. Ishai, and A. Sides. Some Physico-Chemical Aspects of The Effect and The Role of The Filler in Bituminous Paving Mixtures. *Journal of Association of Asphalt Paving Technologists*, Vol. 47, 1978, pp. 558-587.

[3] Al-Qadi, I.L., S.H. Carpenter, G. Roberts, H. Ozer, Q. Aurangzeb, M. Elseifi, and J. Trepanier. *Determination of Usable Residual Asphalt Binder in RAP*, Research Report No., FHWA-ICT-09-031, Illinois Center for Transportation, Illinois, 2009.

[4] Underwood, B.S. and Y.R. Kim. Microstructure Association Model for Upscaling Prediction of Asphalt Concrete Dynamic Modulus. *ASCE Journal of Materials in Civil Engineering*, Vol. 25, No. 9, 2013, pp. 1153-1161.

[5] McDaniel, R., and R.M. Anderson. *Recommended Use of Reclaimed Asphalt Pavement in the Superpave Mix Design Method*. NCHRP D9-12 Project Report, National Cooperative Highway Research Program, National Research Council, Washington, D.C, 2000.

[6] Bukowski, J.R., *Guidelines for Design of Superpave Mixtures Containing Reclaimed Asphalt Pavement (RAP), Memorandum*, ETG Meeting, FHWA Superpave Mixtures Expert Task Group, San Antonio, TX, 1997.

[7] Federal Highway Administration. *A Study of the Use of Recycled Paving Materials: A Report to the Congress*, Report No. FHWA-RD-93-147, Federal highway Administration, Washington, D.C., 1993.

[8] Huang, S.C., A.T. Pauli, and Q. Qin. Physicochemcial Interactions of RAP Binder Blends. Chapter 27, Proceedings of the International Conference on Asphalt Pavements, Raleigh, NC, 2014.

[9] Li, X., and N. Gibson. Analysis of RAP with Known Source History and Influence on Fatigue Performance. Compendium of Papers, 92nd Annual Meeting of the Transportation Research Board, Washington, D.C., 2013.

[10] Basueny, A., D. Perraton, and A. Carter. Laboratory Study of the Effect of RAP Conditioning on the Mechanical Properties of Hot Mix Asphalt Containing RAP. *Journal of Materials and Structures*, Vol. 47, 2014, pp. 1425-1450.

[11] Loria, L., E.Y. Hajj, P.E. Sebaaly, M. Barton, S. Kass, and T. Liske. Performance Evaluation of Asphalt Mixtures with High Recycled Asphalt Pavement Content. *Transportation Research Record: Journal of the Transportation Research Board*, No. 2208, Washington, D.C., 2011, pp. 72–81.

[12] Shah, A., R.S. McDaniel, A. H. Huber, and V.L. Gallivan. Investigation of Properties of Plant-Produced reclaimed Asphalt Pavement Mixtures. *Transportation Research Record: Journal of the Transportation Research Board*, No. 1998, Washington, D.C., 2007, pp. 103-111.

[13] Huang, B., W.R. Kingery, and Z. Zhang. Laboratory Study of Fatigue Characteristics of HMA Mixtures Containing RAP. Presented at the International Symposium on Design and Construction of Long Lasting Pavements, Auburn, AL. June, 2004

[14] Shu, X., B. Huang, and D. Vukosavljevic. Laboratory Evaluation of Fatigue Characteristics of Recycled Asphalt Mixture. *Journal of Construction and Building Materials*, Vol. 22, 2007, pp. 1323-1330.

[15] Apeagyei, A.K., B.K. Diefenderfer, and S.D. Diefenderfer. Rutting Resistance of Asphalt Concrete Mixtures that contain Recycled Asphalt Pavement. *Transportation Research Record: Journal of the Transportation Research Board*, No. 2208, Washington, D.C., 2011, pp. 9–16.

[16] Hou, T., B.S. Underwood, and Y.R. Kim. Fatigue Performance Prediction of North Carolina Mixtures Using the Simplified Viscoelastic Continuum Damage Model. *Journal of Association of Asphalt Paving Technologists*, Vol. 79, 2010, pp. 35-80.

[17] North Carolina Department of Transportation. *Standard Specifications for Roads and Structures*, North Carolina Department of Transportation, Raleigh, 2012, pp. 6-22.

[18] Oliver, J. W. H. The Influence of Binder in RAP on Recycled Asphalt Properties. *International Journal of Road Materials and Pavement Design*, Vol. 2, No.3, 2001, pp. 311-325.

[19] Stephens, J.E., J. Mahoney, and C. Dippold. *Determination of the PG Binder Grade to Use in a RAP Mix*, Report No. JHR 00-278, Connecticut Department of Transportation , Rocky Hill, CT, 2001.

[20] Huang, B., G. Li, D. Vukosavljevic, X. Shu, and B.K. Egan. Laboratory Ivestigation of Mixing Hot-Mix Asphalt with Recycled Asphalt Pavement.

Transportation Research Record: Journal of the Transportation Research Board, No. 1929, Washington D.C., 2005, pp. 37-45.

[21] Buttlar, W.G., F.E. Rebholz, and W. Nassar. *Detection of Recycled Asphalt Pavement in Bituminous Mixtures*, Illinois Transportation Research Center, Illinois Department of Transportation, project iA-H1, FY 02, Report No. ITRC FR 02-2, 2004.

[22] Lee, K.W., N. Supharath, A. Shukla, C.A. franco, and F.J. Manning. Rheological and Mechanical properties of Blended Asphalts Containing Recycled Asphalt Pavement Binders. *Journal of the Association of Asphalt Paving Technologists*, Vol. 68, 1999, pp. 89-128.

[23] Buttlar, W.G., and E.V. Dave. A Micromechanics-Based Approach for Determining Presence and Amount of Recycled Asphalt Pavement Material in Asphalt Concrete. *Journal of the Association of Asphalt Paving Technologists*, Vol. 74, 2005, pp. 829-884.

[24] Delaporte, B., H. DiBenedetto, P. Chevrot, and G. Gauthier. Linear Viscoelastic Properties of Bituminous Materials: From Binders to Mastics. *Journal of Association of Asphalt Paving Technologists*, Vol. 76, 2007, pp. 445-494.

[25] Anderson, D.A., and W.H. Goetz. Mechanical Behavior and Reinforcement of Mineral Filler-Asphalt Mixtures. *Journal of the Association of Asphalt Paving Technologists*, Vol. 42, 2007, pp 37-66.

[26] Durand, A., J. Morel, O. Sutton, and G. Muller. Investigations on Bitumen/ Polymer/ Filler Interactions and Rheological Properties of Mastics. *Mechanical Tests for Bituminous Materials, RILEM 1997*, 1997, pp. 173-178.

[27] Rigden, P.J. The use of Fillers in Bituminous Road Surfacings. A study of Filler-Binder Systems in Relation to Filler Characteristics. *Journal Society of Chemical Industry*, Vol. 66, 1947, pp. 299-309.

[28] EN 1097-4:2008. Tests for Mechanical and Physical Properties of Aggregate: Part 4 Determination of the Voids of Dry Compacted Filler. CEN. European Committee for Standardization, Brussels, 2008.

[29] Bahia, H.U., A. Faheem, C. Hintz, I. Al-Qadi, G. Reinke, E. Dukatz. *Test Methods and Specification Criteria for Mineral Filler Used in HMA*. NCHRP 9-45 Revised Draft Final Report, National Cooperative Highway Research Program, National Research Council, Washington, D.C., 2010.

[30] Tan, Y., and M. Guo. Interfacial thickness and interaction between asphalt and mineral fillers. *Journal of Materials and Structures*, Vol. 3, 2013, pp. 1-10.

[31] Hesami, E., B. Birgisson, N. Kringos. Numerical and experimental evaluation of the influence of the filler-bitumen interface in mastics. *Journal of Materials and Structures*, Vol. 47, 2014, pp. 1325-1337.

[32] Underwood, B.S. *Multiscale Constitutive Modeling of Asphalt Concrete*. Ph.D. Dissertation, North Carolina State University, Raleigh, NC, 2011.

[33] Arizona Department of Transportation. *Material Testing Manual: Sampling and Testing Procedures*, Arizona Department of Transportation, Intermodal Transportation, Materials Group, 2014.

[34] American Association of State Highway Transportation Officials (AASHTO) (2012). AASHTO T 319: Standard Method of Test for Quantitative Extraction and Recovery of Asphalt Binder from Asphalt Mixtures, *AASHTO*, Washington, D.C.

[35] American Association of State Highway Transportation Officials (AASHTO) (2012). AASHTO T 248: Standard Method of Test for Quantitative Extraction and Recovery of Asphalt Binder from Asphalt Mixtures, *AASHTO*, Washington, D.C.

[36] American Association of State Highway Transportation Officials (AASHTO) (2012). AASHTO T 308: Standard Method of Test for Quantitative Extraction and Recovery of Asphalt Binder from Asphalt Mixtures, *AASHTO*, Washington, D.C.

[37] American Society for Testing and Materials (ASTM) (2012). ASTM D854-10: Standard Test Methods for Specific Gravity of Soil Solids by Water Pycnometer, *ASTM International*, West Conshohocken, PA.

[38] Christensen, R.H. A Critical Evaluation for A Class of Micro-Mechanics Models. *Journal of Mechanics and Physics of Solids*, Vol. 38, No.3, 1990, pp. 379-404.

[39] Einstein, A. Investigations on the Theory of the Brownian Movement. Ed. R. Furth, Transl. A.D. Cowper, 1956, New York: Dover Publications.

[40] Hashin, Z. he Elastic Moduli of Heterogeneous Materials. *Journal of Applied Mechanics*, Vol. 29(1), 1962, pp. 143-150.

[41] Christensen, R.M., and K.H. Lo. Solutions for Effective Shear Properties in Three Phase Sphere and Cylinders. *Journal of Mechanics and Physics of Solids*, Vol. 27(4), 1979, pp. 315-329.

[42] Herve, E., and A. Zaoui. *n*- Layered Inclusion-Based Micromechanical Modelling. *International Journal of Pavement and Science*, Vol. 31(1), 1993, pp. 1-10.

[43] Underwood, B.S., and Y.R. Kim. A Four Phase Micro-Mechanical Model for Asphalt Mastic Modulus, *Mechanics of Materials*, Vol. 75, 2014, pp. 13-33.

[44] Buttlar, W.G., D. Bozkurt, G.G. Al-Khateeb, and A.S. Waldoff. Understanding Asphalt Mastic Behavior Through Micromechanics, *Transportation Research Record, Journal of the Transportation Research Board*, Vol. 1681, 1999, pp. 157-169.

[45] Shashidhar, N., and A. Shenoy. On Using Micromechanical Models to Describe Dynamic Mechanical Behavior of Asphalt Mastics, *Materials and Mechanics*, Vol. 34(10), 2002, pp. 657-669.

[46] Kim, Y.R. *Mechanistic Fatigue Characterization and Damage Modeling of Asphalt Mixtures*. Ph.D. Dissertation, Texas A&M University, College Station, Texas, 2003.

[47] Yin, H.M., W.G. Buttlar, G.H. Paulino, and H. DiBenedetto. Assessment of existing micro-mechanical models for asphalt mastics considering viscoelastic effects, Road Materials and Pavement Design, Vol. 9(1), 2008, pp. 31-57.

[48] Faheem, A.F., and H.U. Bahia. Conceptual Phenomenological Model for Interaction of Asphalt Binders with Mineral Fillers, Journal of Association of Asphalt Paving Technologists, Vol. 78, 2009, pp. 679-720.

[49] Schapery, R.A. *A Simple Collocation Method for Fitting Viscoelastic Models to Experimental Data*, Report GALCIT SM 61-23A, California Institute of Technology, Pasadena,CA., 1961.

[50] Underwood, B.S., and Y.R. Kim. Nonlinear Viscoelastic Analysis of Asphalt Cement and Asphalt Mastics, *International Journal of Pavement Engineering*, 2014, pp.1-20.

[51] DeBruijn, H. The Viscosity of Suspensions of Spherical Particles, *Recueil des Travaux Chimiques des Pays-Bas*, Vol. 61, 1942, pp. 863-874.

[52] Ward, S.G., and R.L. Whitmore. Studies of the Viscosity and Sedimentation of Suspensions Part 1: The Viscosity of Suspension of Spherical Particles, *British Journal of Applied Physics*, Vol. 1(11), 1950, pp. 267-269.

[53] Roscoe, R. The Viscosity of Suspensions of Rigid Spheres, *British Journal of Applied Physics*, Vol. 3(8), 1952, pp.286-290.

[54] Paul, B. Prediction of Elastic Constants of Multiphase Materials, *Transactions of American Metallurgical Society, AIME*, 218, 36, 1960.

[55] Eshelby, J.D. Determination of the Elastic Field of an Ellipsoidal Inclusion, and Related Problems. *Proceedings of the Royal Society of London*, Series A, Vol. 241 (1226), 1957, pp. 376-396.

[56] Hashin, Z., and S. Shtrikman. A Variational Approach to Theory of the Elastic Behavior of Multiphase Materials, *Journal of Mechanics and Physics of Solids*, Vol. 11, 1963, pp. 127-140.

[57] Rad., F.Y. *Estimating Blending Level in Fresh and RAP Binders in Recycles Hot Mix Asphalt*. Master of Science Thesis, University of Wisconsin Madison, 2013.

APPENDIX A

VOLUMETRIC CALCULATIONS FOR RAP MASTICS

The volumetric calculations begin with knowing the percentage filler contribution from each aggregate stockpile i.e. virgin aggregate, fine RAP and coarse RAP aggregate. In the present appendix, aggregate blends for all the blend cases RAP 10, RAP 30, RAP 50 and RAP 100 are shown. However, the volumetric calculations are performed only for RAP 10 as the calculations for the other cases are similar.

Actual aggregate gradations of the stockpiles:

	% Passing		
Sieve Size	Virgin Agg.	Fine RAP	Coarse RAP
1"	100	100.0	100.0
3/4"	91	99.8	98.2
1/2"	83	99.3	89.6
3/8"	76	98.3	77.7
#4	60	73.8	48.8
#8	46	52.7	35.0
#16	32	40.8	27.5
#30	22	31.4	22.2
#50	13	21.3	16.2
#100	8	13.3	10.2
#200	4.9	8.8	6.5

Weighted aggregate percentage for RAP 10:

	% Aggregate		
Sieve Size	Virgin Agg.	Fine RAP	Coarse RAP
1"	90.0	6.7	3.3
3/4"	89.2	7.2	3.6
1/2"	88.6	7.9	3.5
3/8"	88.2	8.5	3.3
#4	89.2	8.1	2.7
#8	89.8	7.6	2.5
#16	88.8	8.4	2.8
#30	87.5	9.3	3.3
#50	85.7	10.4	4.0
#100	85.5	10.5	4.0
#200	84.6	11.2	4.2

Weighted aggregate percentage for RAP 30:

	% Aggregate		
Sieve Size	Virgin Agg.	Fine RAP	Coarse RAP
1"	70.0	20.0	10.0
3/4"	68.1	21.4	10.5
1/2"	66.8	22.8	10.3
3/8"	66.0	24.4	9.6
#4	68.1	24.0	7.9
#8	69.6	22.8	7.6
#16	67.3	24.5	8.3
#30	64.4	26.3	9.3
#50	60.8	28.4	10.8
#100	60.4	28.7	11.0
#200	58.8	30.1	11.2

Weighted aggregate percentage for RAP 50

	% Aggregate		
Sieve Size	Virgin Agg.	Fine RAP	Coarse RAP
1"	50.0	33.3	16.7
3/4"	47.8	35.0	17.2
1/2"	46.4	37.0	16.7
3/8"	45.4	39.1	15.5
#4	47.8	39.2	13.0
#8	49.6	37.9	12.6
#16	46.8	39.7	13.4
#30	43.7	41.6	14.7
#50	39.9	43.5	16.6
#100	39.5	43.8	16.7
#200	37.9	45.3	16.8

Weighted Aggregate percentage for RAP 100

	% Aggregate		
Sieve Size	Virgin Agg.	Fine RAP	Coarse RAP
1"	0.0	66.7	33.3
3/4"	0.0	67.0	33.0
1/2"	0.0	68.9	31.1
3/8"	0.0	71.7	28.3
#4	0.0	75.2	24.8
#8	0.0	75.1	24.9
#16	0.0	74.7	25.3
#30	0.0	73.9	26.1
#50	0.0	72.4	27.6
#100	0.0	72.4	27.6
#200	0.0	73.0	27.0

Volumetric Calculations for RAP 10:

Asphalt content in fine RAP filler = 19.02%

Asphalt content in coarse RAP filler = 18.27%

Asphalt content in blended coarse and fine RAP filler = 18.82%

Effective specific gravity of virgin filler = 2.63

Effective specific gravity of recovered filler = 2.64

Filler blend ratio of RAP 10 :

Virgin Agg.	Fine RAP	Coarse RAP
84.6	11.2	4.2

Assume weight of blended filler i.e. virgin filler plus recovered filler =250 grams

Weight of virgin filler = 250*0.846 = 211.5 grams

Wight of recovered filler = 250-211.5 = 38.5 grams

Correct weight of recovered filler to incorporate RAP binder = $\frac{38.5}{1-0.1882}$ = 47.4 grams

Volume of filler = $\frac{211.5}{2.63}+\frac{38.5}{2.64}=95$ cc

Weight of binder contribution from RAP = 47.4 – 38.5 = 8.9 grams

Total filler volume = 27%

Volume of binder required (inclusive of RAP binder) = $\frac{95}{0.27} - 95 = 256.9\,\text{cc}$

Weight of binder required (inclusive of RAP binder) = 256.9 * 1.03 = 264.6 grams

Mass of virgin binder to be added (exclude RAP binder contribution) = 264.9 – 8.9 = 255.6 grams.

APPENDIX B

CALCULATION OF PERCENTAGE UNCOATED FILLER IN RAP FILLER

Iteration No.	% M_{uc} (Assume)	P_{200} (%) (True)	V_{filler}	Mac	Mc	Muc	% Muc
1	0	8.02	36.72	40.32	59.68	114.22	53.32
2	35	5.22	24.71	54.43	45.57	189.24	65.43
3	77.55	1.80	11.68	74.78	25.22	297.36	74.83
4	75	2.01	12.85	72.67	27.33	286.14	74.10
5	74.1	2.08	13.23	72.01	27.99	282.61	73.86
6	73.8	2.10	13.36	71.77	28.23	281.37	73.78
7	73.78	2.10	13.37	71.76	28.24	281.29	73.77

M_{ac} = Mass of asphalt in RAP filler

M_c = Mass of aggregate which has coating

M_{uc} = Mass of uncoated filler

P_{200} = True filler content of the recovered aggregate blend, if there were no uncoated aggregates then the aggregate blend would have 8.02% filler.

$$P_{200} = (1 - \%M_{uc}) * 8.02$$

V_{filler} = Volume of filler, in mastic calculated by separate volumetric calculations using P_{200}.

Asphalt content of RAP filler = 18.82%

To determine M_{uc}, use the following equation,

$$18.82 = \left(\frac{M_{ac}}{M_{ac} + M_{uc} + M_c} \right) * 100$$

APPENDIX C

CALCULATION OF PERCENTAGE OF VM AND RAP 100 in RAP 10, RAP 30, and RAP 50

1. Using the mastic volumetric calculations, the volume proportions of each of the four constituents, virgin filler, recovered filler, virgin binder, and RAP binder can be calculated.
2. But in order to express them in terms of VM and RAP 100 an assumption has to be made.
3. It is assumed that the ratio of volume of virgin binder to RAP binder in RAP 100 is constant for all blends.
4. So, for RAP 10, RAP 30, and RAP 50 the RAP binder concentration is known. Multiplying this concentration with the constant gives the volume of virgin binder in RAP 100.
5. Subtracting the resulting value from the total virgin binder added, will give the virgin binder concentration in VM.
6. Since concentration of all other components is already known, RAP 10, RAP 30, and RAP 50 can now be expressed in terms of RAP 100 and VM.